SEMINAR ON NUMERICAL, DYNAMICAL AND MESOSCALE METEOROLOGY

by

Professor David Houghton
Department of Meteorology
University of Wisconsin
Madison, Wisconsin

Presented
February 23-March 14, 1980
at
Nanjing University
People's Republic of China

Preliminary Text

Seminar on Numerical, Dynamical and Mesoscale Meteorology

by

Professor David Houghton

Department of Meteorology
University of Wisconsin
Madison, Wisconsin

Presented

February 23 - March 14, 1980

at

Nanjing University

People's Republic of China

Preliminary Text

Preface

In order to facilitate translation of my lectures into Chinese, the proposed text for each 3-hour lecture was prepared one day in advance for the translator to study. As a result, it is possible to share the preliminary text with those interested in the level and content of the scientific communication attempted during my recent visit to the People's Republic of China.

The Chinese are preparing a final version for the lecture proceedings in both English and Chinese which should be available in the near future. Their publication should give more adequate reference to the several hundred slides and nine movies used in the lectures.

The lectures were prepared while in China with very little reference material available and with very limited time. (Total time required for lecture preparation was estimated at 60 hours, 4 hours for each of the fifteen sessions.) I offer this material not as a polished scientific publication but as an item of record for my exchange trip.

One 3-hour session was used for each of the 15 topics listed in the Table of Contents. The exceptions were topic I.A. which took two sessions and topic II.D. and II.E. which were combined into one session.

Support for this lecture series was provided by the People's Republic of China, the University of Wisconsin-Madison, and the Atmospheric Science Division of the National Science Foundation through Grant ATM-7911996.

TABLE of CONTENTS

i. INTRODUCTION

It is a pleasure and privilege for my wife and me to come to your country and the University of Nanjing. We hope that our visit will help to strengthen relations between our two countries. (Wǎu mə̄n shī hwàn wǎu mə̄n de fǎng wèn chyāng jyā chǔng lyǎng gwo rén mín de yǒu yī.) Unfortunately, I do not know the Chinese language and must depend on your interpreters and patience for communication.

This exchange program between the University of Nanjing and the University of Wisconsin is important to me. It provides the opportunity for communication between our countries and universities and also between the meteorologists of both countries. As you already know, the atmosphere is common to all mankind and its understanding requires the sharing of information from the peoples of all countries. We cannot ignore this science because of the important problems of agriculture, energy, air pollution and transportation, to name a few, which are sensitive to the atmospheric conditions.

Our visit has been wonderful so far thanks to the efforts of Mr. Chao Shu Ming who has given us a short tour of some of your country.

I have been interested in the weather for as long as I can remember. A hailstorm when I was five years old is still in my memory. I proceeded directly from secondary school into university studies first at the Pennsylvania State University and then at the University of Washington. It was at the latter place where I received my Ph.D. under the guidance of Professor Fleagle. My study there was on the nonlinear behavior of gravity waves and I developed a numerical model as part of this work.

I have continued with research involving theoretical and numerical meteorology ever since, looking into a wide range of problems according to the resources and interests of others at the two places I have worked: first the National Center for Atmospheric Research in Boulder, Colorado and then at the University of Wisconsin in Madison, Wisconsin.

At Boulder, Colorado, I became involved with the problems of general circulation modeling and thus considered elements of synoptic and global scale meteorology. Boulder is at the edge of the Rocky mountains and there was much interesting mountain related weather including the warm strong downslope winds called the Chinook. At Boulder, these winds sometimes reached 40 meters per second and damage occurred. There was great local interest in understanding

and forecasting these events so my research work expanded to include nonlinear mesoscale modeling of the downslope winds.

At the University of Wisconsin I came into contact with a large effort concerning the analysis of data from meteorological satellites. I thought that this data could provide sufficient information about mesoscale fields in the atmosphere so that the initialization of general mesoscale short-range numerical models might become feasible. Thus some of my recent work has been with satellite data.

My work with general circulation models diminished after I left Colorado, however, because of my teaching, contact with many aspects of numerical modeling continues. Interest in and work with the operational numerical weather prediction has increased for me. Those of us, who felt that a pure scientific approach to modeling was the best way, have come more and more to appreciate the modeling achievements of those in the government agencies. There the daily test is not the scientific exactness of the model design but rather the quality of the model results, namely the forecast.

Before proceeding into the more technical parts of my lectures, I want to share a few things of general interest about the place from where I came.

The Department of Meteorology at the University of Wisconsin is located at Madison, the capital city of the State of Wisconsin. As you can here, we enjoy lakes. The first picture shows the buildings of the center of Madison. From the university we see Lake Mendota. In the late fall when it is still not frozen but the air temperature is far below freezing, interesting fog, clouds and even "steam devils" can occur.

Our Department occupies much of the upper half of the 15 story building, constructed in 1967-1968, which is shown in the picture. We now have two receivers for the geostationary satellites located on the roof, one looking at the 75°W position and the other at the 120°W position.

In the fall of 1978 we celebrated our 30th year as a department. On that occasion, all of the eight persons who have served as chairman attended. The picture shows them all. In order of service they are Profs. Bryson, Suomi, Lettau, Ragotzkie, Horn, Wahl, Johnson and myself. [Discussion of other slides] At the celebration we enjoyed dinner and then a speech from Professor F. Kenneth Hare from Canada. We had many guests. Here Prof. Baum, who was president of the American Meteorological Society at that time, talks with Profs. Suomi and Lettau. Prof. Stearns (who along with Prof. Lettau is working with Dr. Zhang from Nanjing University) is talking with a former student. Numerical modelers

such as Dr. Halem from NASA (center) attended. Finally, I wanted to show you Dr. William Smith who is associated with our department and who was here last year.

I have proposed to present lectures on a wide range of topics concerning numerical modeling, large-scale meteorology and mesoscale meteorology. These cover most of my areas of study for the past 20 years.

I hope to convey to you some of the results of my work and to give an overview of research accomplishments in these areas in my country. I must confess that I have not been able to keep up to date on all of these areas. The literature is too voluminous for that and my teaching and administrative duties have taken much time.

Nevertheless, both you and I have made much effort to come here for these three weeks so it is essential that the material discussed be in your areas of interest and that the level of technical detail be satisfactory. I hope that through discussion, we can make proper adjustments in my presentations to suit you. If more information is desired in a specific topic, I would be glad to look up a few key publications in your library to help out. Please do not hesitate to share with me your desires.

I. NUMERICAL MODELING

Numerical modeling has become a basic tool for study in most areas of meteorology (or the atmospheric sciences). It is nearly impossible for anyone to keep up with all of the advances in the general techniques of modeling. Journal articles in the United States alone which discuss new modeling methods number well over 60 per year. It makes more sense to keep up with the modeling advances in a given area of meteorology of interest.

Computer resources have shown an astounding advance in the 32 years since the first automated electronic computing facility was developed. The slide shows the relative "through put" computing speed for a number of large computer systems compared to the IBM 701 machine in 1953 which could do several thousand operations per second and had a storage capacity of several tens of thousands of words. We now have parallel processing machines that can do upwards to 60 million instructions per second and have core storage of many hundreds of thousands of words in addition to mass storage disk units that can hold millions of words.

It is useful to note the very recent emergence of numerical modeling in our science by giving some key dates in its history.

≈ 1900: deterministic equation for weather prediction (V. Bjerkness)

1922: concept of numerical weather prediction published (Richardson)

1947: simplified equations for large scale motions (Charney, Rossby)

1948: first automated computing facility at Princeton, New Jersey

1950: first successful weather prediction (Charney, Fjortoft von Neumann, Freeman)

1955-58: simplified equations for smaller scale motion (analastic and Boussinesq equations)

1959: first successful model for cumulus convection (Malkus and Witt)

1960: first sea breeze numerical model (Estoque)

1962: successful primitive equation models (Smagorinsky, Lieth, Mintz)

1966: operational forecast primitive equation model (Shuman, Hovermale)

1970 and on: modeling of nearly all atmospheric phenomena.

A. Operational Numerical Weather Prediction

Numerical models of some form have become adopted in many countries of the world. The countries include Canada, Japan, U.S., England, U.S.S.R., Australia, Sweden and, I believe, your country, although I do not know much about your system.

Deterministic numerical prediction has become the basis for most weather forecasting in the U.S. It is a sophisticated system and, as I said before, a system that gives as good forecast results as any of the more rigorously developed research models. With the incorporation of more documented procedures, this system becomes as good as any to illustrate the current "state of the art" techniques in numerical modeling. I propose to discuss it in some detail.

One must bear in mind that it is very difficult to obtain a complete description of the operational models. Changes can be made on the spot to improve results and these may then be described in internal memos. But it may take years to be published in a regular journal by which time the model has been changed again.

An overview of the U.S. system is shown in the slide. It includes five different numerical models plus specialized procedures of primarily a statistical nature to obtain local forecasts which will be discussed later. The five models are all interrelated as shown by the green and red arrows. The next slide shows my most recent information with better data on the length of the forecast and the initialization techniques.

The justification for each model and some basic characteristics are summarized below.

Model Name	Domain Covered	Horizontal Resolution	Number of Layers	Forecast Length	Initialization Technique	Lateral Boundary Conditions
Global	Globe	2½° Latitude/ Longitude	9	12-24 hrs	Optimal Interpolation	None
Barotropic	Most of Northern Hemisphere	381 km	1 (+)	48 hr	Cressman Scheme	Rigid wall
Limited Fine Mesh (LFM)	North America and surrounding oceans	127 km	6	48 hr	Cressman Scheme	From PE
Primitive Equation (PE or Baroclinic)	Most of Northern Hemisphere	191 km	7	84 hr (3½ days)	Hough functions	Rigid wall
Moveable Fine Mesh MFM Nested Grid Model NGM	About ¼ of LFM	60 km	6	48 hr	Interpolation	From PE

The "Global" model is used mainly to provide a uniform "first guess" analysis field for the other models, (at least, uniform for the domain of the other models). The "Barotropic" is a very simple filtered model that runs fast and gives surprisingly good results in many cases. It has remained virtually unchanged for over 20 years. It is also used for extended forecasts. The "LFM" is the general purpose high resolution model. The PE is the general purpose model to cover most of the northern hemisphere and to give input for longer range forecasts. The MFM or NGM is a special purpose model used for severe storm situations such as for hurricanes or tornadoes where extra good resolution is considered helpful.

The models are run twice a day in the order shown. The observational data that get to each model are different and depend on the data available when the model is run. Three different initialization methods are used.

The Cressman method has been used for a long time. It is a weighted linear interpolation approach that determines the correction to a first guess value usually the forecast value from an earlier run. If the correction is denoted by C, then C at the grid point, C_g ,is determined from C at the observation points, C_o , by the formula

$$C_g = A \sum_i a_i (C_o)_i + B \sum_j a_j (C_o)_j \ .....$$

where A and B are constant weighting coefficients determined by the nature or type of observation and "a" is the basic distance weighting function

$$a_n = \frac{R^2 - d_n^2}{R^2 + d_n^2}$$

where d_n is the distance from the grid point to the observation point and R is the maximum distance for obtaining information

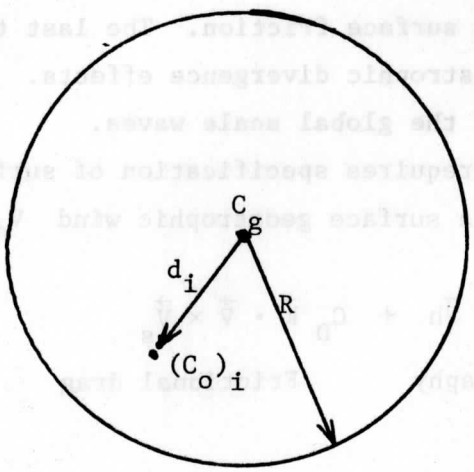

The "Optimal Interpotion" method is similar to the Cressman method except that the weighting functions "a" are determined from an analysis of climatological correlations of values between points according to the method of Gandin in order to minimize a root mean square error. This approach has recently been adopted because it seemed more justifiable than the Cressman approach; however it is not clear that results are that much better.

The Hough function method uses the non-divergent (Rossby) eigenfunction mode for linearized perturbations on a spherical surface with no mean (basic) flow as the structure for the analysis using a least squares fit to the observations. It was hoped that this method would provide more mutually consistent pressure and non-divergent velocity fields. However there is the problem of data from poorly observed areas degrading the final analysis in "data rich" areas.

It is instructive to look at the most simple and most comprehensive models in this prediction system to appreciate the range of physical processes that are now considered.

Description of the "Barotropic" model

This was one of the original quasi-geostrophic model systems used for operational weather prediction. It is still used today because of its quickness and well understood performance characteristics for a range of situations. In some cases it does as well as the more complex models.

The basic dependent variable is the stream function at 500 mb, ψ, which relates directly to the geopotential in the quasigeostrophic system, ϕ, by the equation $\psi = \frac{\phi}{f_o}$ where f_o is a constant Coriolis parameter value.

The governing equation is the "nearly non-divergent" vorticity equation.

$$\frac{\partial}{\partial t} \nabla^2\psi = - m V_\psi \cdot \nabla[(\nabla^2\psi) + f] + f_o \frac{\partial \omega}{\partial p} + H \frac{\partial \psi}{\partial t}$$

where V_ψ is the non-divergent horizontal velocity determined from ψ. The second term on the right represents effects of a net divergence in the troposphere due to topography or surface friction. The last term on the right represents global scale geostrophic divergence effects. It is needed to prevent rapid retrogression of the global scale waves.

The divergence term requires specification of surface vertical motion, ω_s. This is obtained from a surface geostrophic wind V_s using

$$\omega_s \propto \underbrace{V_s \cdot \vec{\nabla} h}_{\text{Topography}} + \underbrace{C_D \vec{k} \cdot \vec{\nabla} \times \vec{V}_s}_{\text{Frictional drag}}$$

V_s is determined from the velocity at 500 mb extrapolated downward using the thermal wind in the 850 - 500 mb layer. This requires that the 850 - 500 mb layer thickness be a predicted parameter which is done by a simple advection equation

$$\frac{\partial}{\partial t}\,(\text{Thickness}) = -\,V_\psi^* \cdot \nabla\,(\text{Thickness})$$

$$\text{where} \qquad V_\psi^* = \frac{3}{4}\,V_\psi \text{ at 500 mb.}$$

Thus in summary the model carries the following:

	Predicted Variables	Extrapolations
200 mb	$\omega = 0$	
500 mb	V_ψ	V_ψ, V_ψ^*
850 mb	$\Delta\phi$	Thermal wind
surface	$\omega = \omega_s$	V_s

The model 48 hour forecast for the northern hemisphere is done in 30 minutes with Δx = 381 km and Δt = 1 hour.

Limited fine mesh (LFM) model

In contrast to the Barotropic model which contains primarily horizontal advection at 500 mb, the LFM incorporates numerous physical processes and has a general three dimensional representation of the atmosphere. It is considered to give the most suitable forecast information for the United States.

The next slide shows the domain of coverage of the LFM. It is embedded in the grid domain covered by the PE model so that the boundary conditions can be specified by the latter as time-dependent functions. Notice that the two grid systems are not oriented in the same direction so that there are essentially no grid points in common. The boundary specification still represents a source of error for the LFM which moves inward over the course of time limiting the length of forecast that can be made. The model is run for 48 hours by which time one would expect boundary influences to be present throughout the domain.

The specific 127 km grid is shown for the US area. It is important to keep this in mind when studying the forecasts. The normal tendency is to focus on the small scale features in the forecast. These are the scales for which

the model has the greatest truncation error. Phenomena with a wavelength dimension of four grid spaces or less would be expected to be very poorly forecasted by the model. This applies to precipitation area structure which may be contained within a given state such as the State of Wisconsin.

The vertical coordinate system is based on the so-called sigma system which is a pressure coordinate normalized by pressure at certain reference levels. In general circulation models, the reference level is usually only the surface pressure at the earth; however, in the LFM there are three such levels. These are at the surface of the earth, the tropopause level and the top of the active model at about 100 mb. In this way the coordinates conform to the tropopause and large errors due to cutting across large gradient regions at that level are avoided. As shown on the blackboard, the layer above the tropopause which approximates the stratosphere is divided into two equal layers, and the layer below the tropopause which is the troposphere is divided into three equal layers after specifying a planetary boundary layer at the bottom with a 50 mb thickness. The pressure variables and the sigma vertical motion are defined at these coordinate levels while the horizontal velocity, thermodynamic variables and moisture are specified at the intermediate levels. The upper boundary zone is an artificial adiabatic layer which helps to model static stability for the topmost layer in the stratosphere. Moisture is defined only in the boundary layer and the two lower layers in the troposphere.

The hydrostatic primitive equations are used. The next slide shows in schematic form the basic prognostic equations. The equations of motion include horizontal and vertical advection, Coriolis effects, pressure acceleration and friction, but only friction at the earth's surface. The first law of thermodynamics is used with horizontal and vertical advection, compression effects, a limited degree of surface heat flux and the diabatic effects of condensation, radiation and convective condensation. The condensation and convective processes apply only to the lowest three layers in the model. The hydrological cycle includes horizontal and vertical transports of moisture, condensation and precipitation and a limited amount of moisture flux from the surface. The key terms which embody the important questions of parameterization are underlined. It is the parameterized effects which provide a major challenge to any model improvement and which remain one of the important distinguishing features for any numerical model for synoptic scale meteorology.

The next diagram shows a slightly more complete description of the model equations. Note that x and y are not east and north but are the two directions in the polar stereographic coordinate system used in the model. Thus both

components of velocity occur with the Coriolis parameter factor due to map scale factor changes in both the x and y coordinate directions. Also note that the pressure term is really two terms because the coordinates are not of constant pressure. The fifth prognostic equation, which was not shown before, is for mass continuity. Here the basic dependent variable is the mass between two adjacent sigma coordinate surfaces.

Along with the 5 prognostic equations are a number of diagnostic relationships needed to complete the specification of all dependent variables as the model integration proceeds. These include the vertical velocity and a pressure "Exner" function, π. The hydrostatic relation, $\frac{\partial \phi}{\partial \sigma} = - C_p \theta \frac{\partial \pi}{\partial \sigma}$, is used to determine the geopotential heights of the sigma coordinate surfaces.

As noted before, a number of physical processes are represented by parameterization methods of varying degrees of sophistication. The detailed formulation may appear to lack a valid physical basis; however, in association with the total numerical model they have been judged to contribute positively to the forecasts.

1) Small scale turbulence

   There is no small scale turbulence effect in the free atmosphere modeled explicitly. The numerical scheme itself provides considerable diffusion of the variables.

2) Planetary boundary layer

   With the lowest level of model velocity and temperature being 25 mb above the surface ($\approx$ 250 meters), it is clear that the representation of boundary layer processes must be very minimal.

   Surface friction is modeled using a surface stress computed using a drag coefficient, C_D, and the wind at the first level: $\tau = - \rho C_D |\vec{V}| \vec{V}$. The value of C_D is variable and depends on whether the lower boundary is water or land. It ranges in value from 15×10^{-4} to 95×10^{-4}.

   Sensible heat flux is present due to two model characteristics. One is for the situation of cold air over the warm ocean. In that case the heat flux is made proportional to the difference between potential temperature at the first level and the sea surface temperature. The other is in the short wave radiation calculation which automatically uses 10% of the energy reaching the lower boundary to heat the boundary layer if it is over land and without snow.

Moisture flux from the lower boundary occurs only over water and then only by imposition of the constraint that the boundary layer relative humidity cannot go below 30%.

3) Radiation

Both short wave and long wave radiation effects are included and I will describe these separately. First, for the short wave component. Heating due to absorption by water vapor in the lower three layers of the model is included. The path length is a function of solar zenith angle which is determined from the latitude, time of day, and the time of year. Reflection from clouds can reduce the downward solar radiation intensity with a cloud defined as being present if the relative humidity is greater than or equal to 60%. The amount of reduction depends on which layer the cloud is in being 100%, 75%, and 50% for the 1st, 2nd, and 3rd layers respectively. Of the radiative flux reaching the earth's surface over land 90% is reflected to space and the remaining 10% goes directly to heat the boundary layer, if the surface is not snow or ice covered. Thus the earth is assigned zero heat storage capacity. A schematic of the short wave radiation processes is shown on the blackboard.

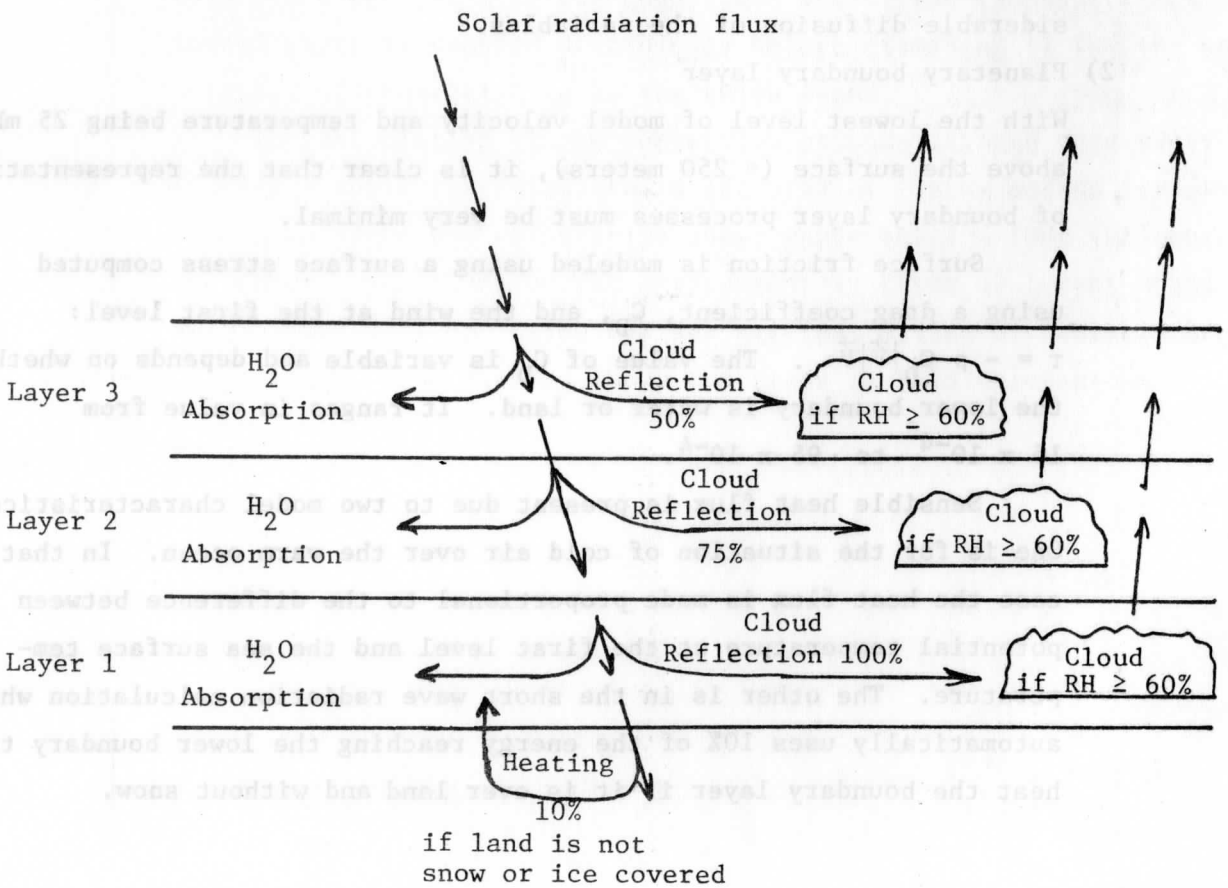

For the long wave component, all layers are cooled at the rate of 1.44°C/day unless the layer is in or under a cloud again defined as existing if the relative humidity is greater than or equal to 60%. An additional cooling rate of 2.4°C/day is specified for the boundary layer if there is snow cover with a clear sky and the sun elevation angle is less than 10°. Snow cover is a specified parameter in the initial state.

4) Precipitation process

The large scale precipitation is calculated explicitly by examining the magnitudes of the mixing ratio variable and requiring condensation when values exceed a critical value (currently 85% of the saturation value) and requiring evaporation of precipitation falling through a layer if the relative humidity is less than this critical value of 85%. In order to handle the fact that moisture is defined only in the lower three layers, moisture is not allowed to be advected into the fourth layer. As shown in the diagram the procedure is straightforward according to physical reasoning. Latent heating or cooling of the layers is consistent with the net change of phase.

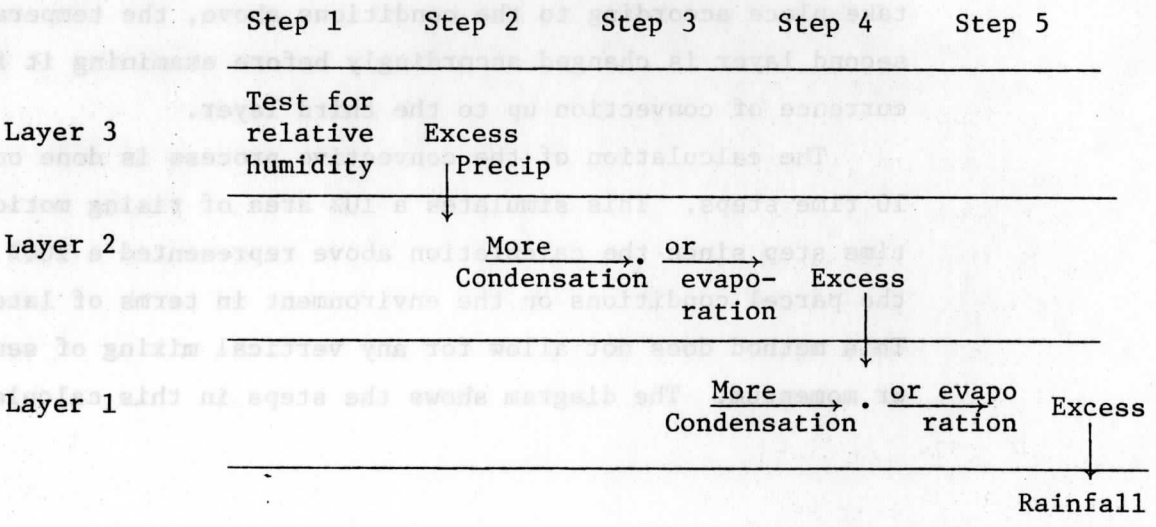

The convective scale precipitation part of the model has recently been changed. I will attempt to describe the new version. The parcel ascent method is used for each of the three lower layers examining the conditions in the parcel if raised to the mid level of the next higher layer. This parcel lifting is done only if four conditions are met:

a) There is moisture convergence in the layer of origin.

b) The relative humidity exceeds 85% in the layer of origin.

c) The lifted condensation level is below the mid point of the next higher layer

d) The parcel temperature exceeds the environment temperature by more than 0.1°C at the next higher level.

If all of these conditions are met, the water vapor in excess of 85% of the saturation value is considered to precipitate directly to the surface. The water vapor content in the layer of origin is depleted by the amount of the rainfall and the latent heat released is used to increase the temperature of the upper layer of the two considered.

The model first considers the lowest layer. If convection does take place according to the conditions above, the temperature of the second layer is changed accordingly before examining it for the occurrence of convection up to the third layer.

The calculation of the convective process is done once every 10 time steps. This simulates a 10% area of rising motion for every time step since the calculation above represented a 100% influence of the parcel conditions on the environment in terms of latent heating. This method does not allow for any vertical mixing of sensible heat or momentum. The diagram shows the steps in this calculation.

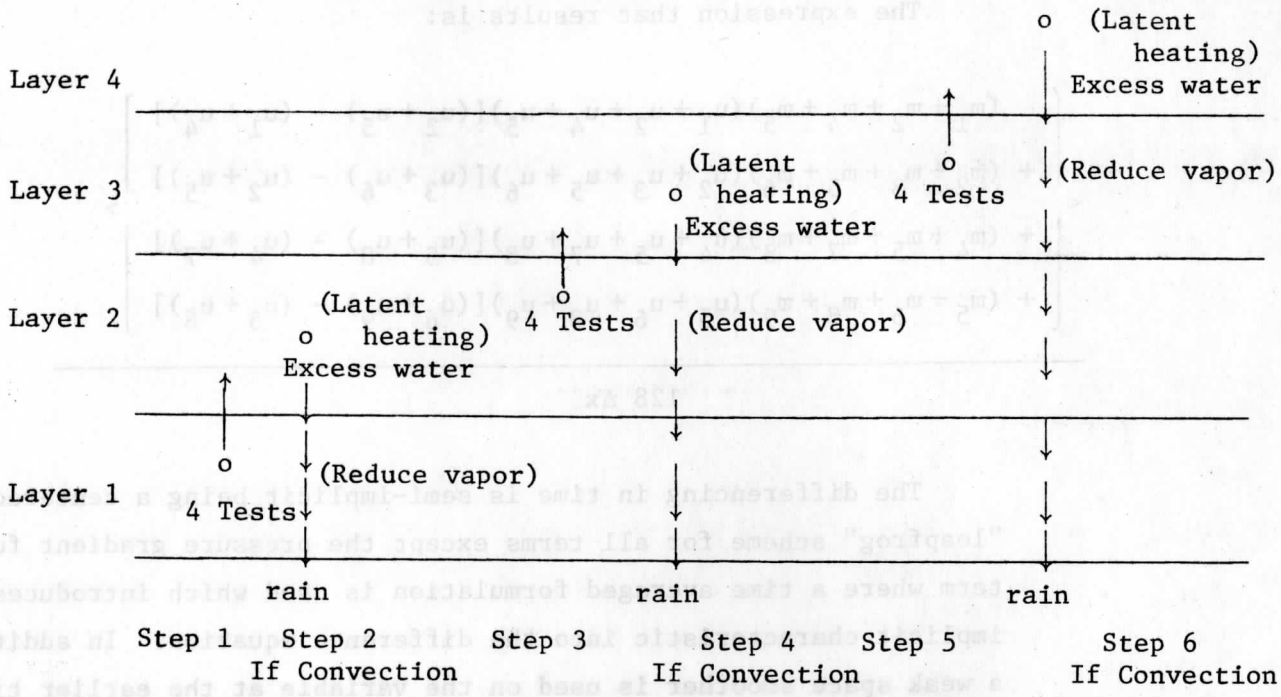

The finite difference method used in space follows the so called "Shuman" averaging scheme. This includes much averaging which is not considered elegant by the mathematicians. It does give a numerical diffusion which dampens the smaller scale features and controls non-linear instability. The advection terms are not formulated so that conservative or quadratic conservative differencing methods can be applied.

To demonstrate the method, the finite difference formulation is written for a single term in full detail. We can look at the horizontal advection term, $mu \frac{\partial u}{\partial x}$ as evaluated at point 5 in the grid array shown.

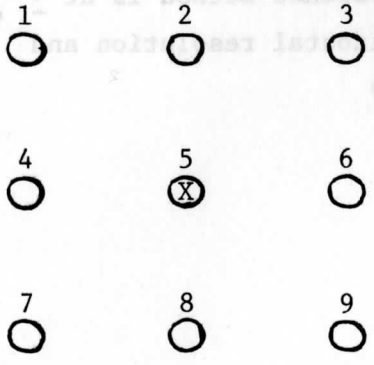

The expression that results is:

$$\frac{\left\langle \begin{array}{l} (m_1+m_2+m_4+m_5)(u_1+u_2+u_4+u_5)[(u_2+u_5)-(u_1+u_4)] \\ +(m_2+m_3+m_5+m_6)(u_2+u_3+u_5+u_6)[(u_3+u_6)-(u_2+u_5)] \\ +(m_4+m_5+m_7+m_8)(u_4+u_5+u_7+u_8)[(u_5+u_8)-(u_4+u_7)] \\ +(m_5+m_6+m_8+m_9)(u_5+u_6+u_8+u_9)[(u_6+u_9)-(u_5+u_8)] \end{array} \right\rangle}{128\,\Delta x}$$

The differencing in time is semi-implicit being a centered "leapfrog" scheme for all terms except the pressure gradient force term where a time averaged formulation is used which introduces an implicit characteristic into the difference equation. In addition a weak space smoother is used on the variable at the earlier time level in the time differenced term. This can be best illustrated by writing the scheme for a simple equation, $\frac{\partial u}{\partial t} = A + P$, where A represents all the terms in the equation of motion except for the time derivative and the pressure gradient force and P represents the pressure gradient force term. The scheme is written:

$$\frac{u^{\tau+1} - \bar{\bar{u}}^{\tau-1}}{2\Delta t} = A^{\tau} + \frac{P^{\tau+1} + 2P^{\tau} + P^{\tau-1}}{4}$$

where τ refers to the time level and the dashed line refers to the weak space smoother. The time averaging in the pressure gradient term allows linear computational stability to be retained for a time step of 6 minutes with the 127 km grid (actually less than 100 km at low latitudes). (A normal condition for such stability with an explicit finite difference method is $\Delta t \leq \frac{\Delta x}{c}$ where Δt is the time step, Δx is the horizontal resolution and c is a maximum speed of signal propagation.)

The operational numerical prediction system also includes a number of mathematical manipulations which are applied to the model forecast fields before they are presented to the forecasters and other users. It turns out that these are essential to get realistic patterns. These manipulations also mean that the final variables are not completely consistent with each other and thus the data is not so useful for quantitative diagnostic studies. In the research models it is possible to take more care to preserve this quality of the output data.

There are four basic manipulations:

1) Vertical interpolation from the sigma coordinate system of the model to the standard pressure levels at which the forecasters are accustomed to viewing the data. Because the variables are not all at the same levels in the model, the interpolation errors are different for different variables.
2) Horizontal space smoothing of all the variables to reduce the amplitudes of the smaller scale features. The smoothers eliminate all of the 2-grid increment scale features and over 50% of the amplitude of the 4-grid increment features.
3) Time averaging of the vertical motion field so that the value outputted represents the two-hour average ending at output time.
4) Filtering of features in the geopotential fields due to large scale gravity waves that develop in the LFM model from the boundary constraints. This is accomplished by computing a balanced 500 mb ϕ field from the 500 mb streamfunction, ψ, of the velocity field using the balance equation.

$$\nabla^2\phi = f\nabla^2\psi + \frac{\partial f}{\partial y}\frac{\partial \psi}{\partial y} - 2J(u_\psi, v_\psi)$$

This correction in the 500 mb ϕ field is then applied equally to the geopotential fields at all other levels so that thickness (or temperature) fields are not affected by this filtering process.

To demonstrate the effect of these output processing procedures especially the space smoother, we can look at samples of surface pressure and low level wind fields before and after the output manipulations are performed. It is evident that the model itself contains large oscillations with a 2-grid-increment wavelength. Apparently these oscillations do not seriously distort larger scale features or result in nonlinear instabilities.

Some aspects of model performance will be discussed in later lectures.

Some references are:

Shuman and Hovermale, 1968. An operational six-layer primitive equation model.
J. of Applied Meteorology, 7, 525-547.

Gerrity, Jr. J., 1977. The LFM Model - 1976: A documentation. NOAA Technical Memorandum NWS NMC 60. NMC Washington, D.C. 68 pp.

B. General Circulation Models

It is in this area that research concerning modelling techniques has the longest history. Following the successful operation of a primitive equation general circulation model in 1962, considerable effort has continued on improving these models from all points of view. Currently general circulation models represent the most sophisticated numerical models in meteorology. Nevertheless as I had mentioned before, the accuracy of these models when applied to standard weather prediction situations has not been any better than the results from the operational weather prediction models discussed before.

Global numerical models exist in a number of countries of the world today. These include Canada, England, The United States and Australia. In the United States, a number of institutions now have active programs in the general circulation that use numerical models. These include:

1. Geophysical Fluid Dynamics Laboratory (GFDL) at Princeton, N.J.
2. National Center for Atmospheric Research (NCAR) at Boulder, Colo.
3. National Aeronautics and Space Administration (NASA) at Washington, D.C.
4. University of California at Los Angeles (UCLA)
5. University of Oregon at Corvalles, Oregon.

Despite 18 years of effort, primitive equation general circulation models are still not fully perfected. The sources of error remaining are considered to be in several areas as summarized on the board.

Rough estimate of sources of error in general circulation models today.

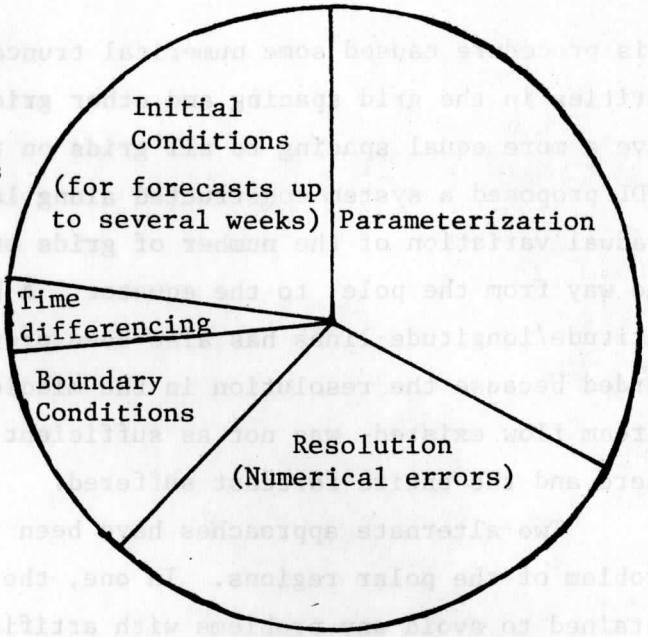

The relative size of each sector is not to be taken seriously. However, it is significant that there are several important areas where more work is needed. The need for accurate initial conditions is only for short term forecasts up to perhaps two weeks.

In this lecture today I would like to summarize some of the advances that have been made in numerical modeling in connection with general circulation studies, then give a very brief overview of several models, and then end up focusing on some of the accomplishments and deficiencies in the model simulations.

Advances in numerical techniques

If a latitude-longitude grid system is used to cover the earth, the east-west separation between grid points becomes very small near the north and south poles because of the convergence of the longitude lines. This increases the possibility of linear computational stability because satisfying the condition on the time step mentioned before, $\Delta t \leq \frac{\Delta x}{c}$, requires smaller and smaller time steps. Several methods have been used to handle this problem.

One approach has been to reduce the number of grid positions on a latitude circle as the poles are approached. In the 5° latitude/longitude version of the NCAR model the change in grid interval was done only poleward of 60° latitude and the number of grid points around a latitude circle was prescribed as follows:

60°	-----	72 points
65°	-----	60 points
70°	-----	48 points
75°	-----	36 points
80°	-----	24 points
85°	-----	12 points
90°	-----	1 point

This procedure caused some numerical truncation problems due to the irregularities in the grid spacing and other grid systems were proposed intended to give a more equal spacing to all grids on the sphere. Kurihara in 1965 at GFDL proposed a system constructed along latitude/longitude lines which had a gradual variation of the number of grids on a latitude circle extending all the way from the pole to the equator. A hexagonal grid which did not follow latitude/longitude lines has also been proposed. These approaches were discarded because the resolution in the middle latitudes, where the strong jet stream flow existed, was not as sufficient compared to the resolution elsewhere and the entire forecast suffered.

Two alternate approaches have been introduced recently to handle the problem of the polar regions. In one, the total latitude/longitude grid is retained to avoid any problems with artificial inhomogeneities in spacing; however, efficient Fourier filtering methods along latitude lines is used to completely eliminate the smaller scale oscillations in the polar regions including those which will numerically amplify when the criterion, $\Delta t \leq \frac{\Delta x}{c}$, is violated. Thus the time step that can be used is that which can be determined by the grid spacing at lower latitudes.

The second approach has been to adopt a Galerkin or spectral approach to modeling. In this case the model does not depend on a grid system in the horizontal and the orthogonal functions used to represent the solution do not have any singularities or irregularities in the polar regions.

Another important development with grid systems has been the design of staggered systems. This has allowed not only for more efficient finite difference formulations but it has also permitted conservative and quadratic conservative schemes to be developed which will be discussed shortly.

The basic advantage of efficiency can be demonstrated by considering the finite difference model for the simple equation system which describes a linear gravity wave in water with mean depth, H:

$$\frac{\partial u}{\partial t} = - g \frac{\partial h}{\partial x}$$

$$\frac{\partial h}{\partial t} = - H \frac{\partial u}{\partial x}$$

where u is the perturbation horizontal velocity

g is the acceleration of gravity and

h is the deviation in fluid depth from the mean depth, H.

Assume that this equation system is solved by a centered difference system which will be stable for sufficiently small Δt.

$$u_m^{n+1} = u_m^{n-1} - \frac{g\Delta t}{\Delta x}(h_{m+1}^n - h_{m-1}^n)$$

$$h_m^{n+1} = h_m^{n-1} - \frac{H\Delta t}{\Delta x}(u_{m+1}^n - u_{m-1}^n)$$

where the superscript refers to the time level and the subscript refers to the position in the x direction. Knowing the values of h and u at time levels, n and n-1, is sufficient for computing the values at the later time n+1 and the progression in time can be depicted as shown:

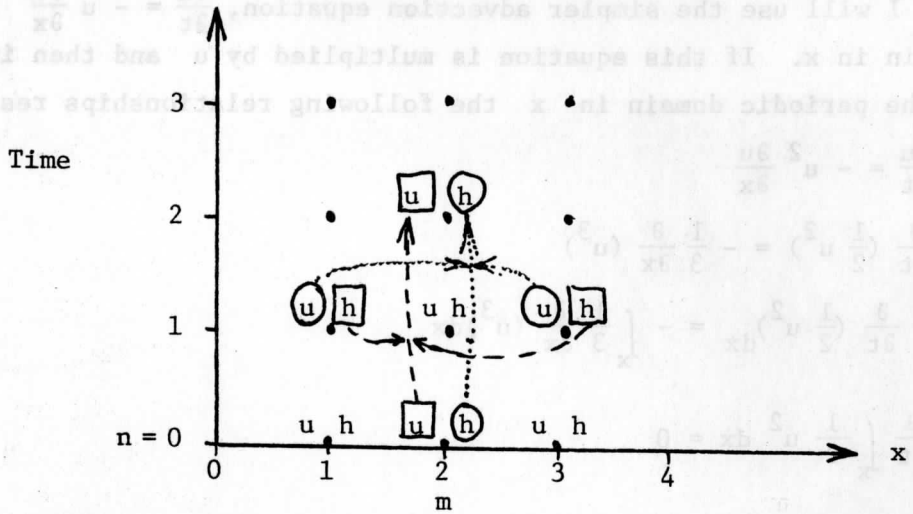

The value of h at the time level 2 is derived from h at time level 0 and the two values of u at time level 1 which are enclosed by circles. In the same way the new value of u at time level 2 is derived from the variables enclosed by squares. By inspection it is evident that identical values will be obtained if variables are defined only at alternate points as shown:

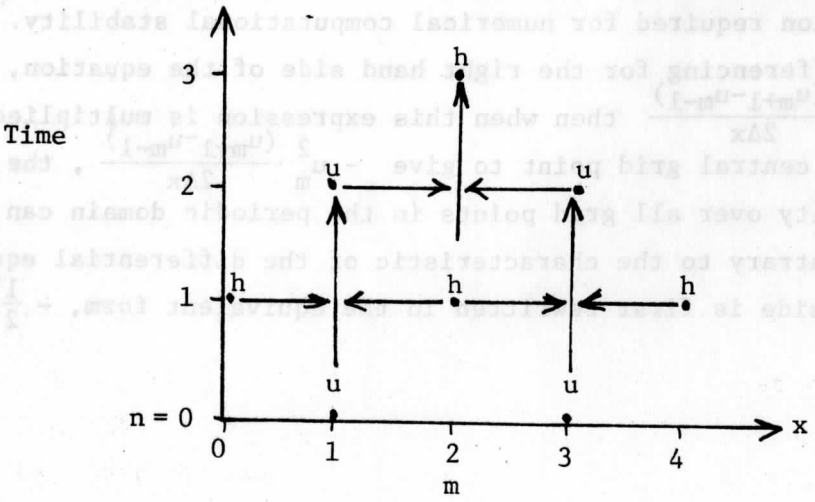

The truncation error in the solution is the same even though the spacing between data points appears to be greater. This shows an effective use of grid staggering.

Since general circulation models were being designed to run for long periods of time, it was important that the finite difference equations would satisfy the same type of integral constraints as the partial differential equations did for quadratic quantities (such as the kinetic energy when only advection processes are operating). This provides some assurance against nonlinear instability as well as maintaining physically meaningful conservation conditions.

Professor Arakawa at UCLA did some very innovated work in this area. He first considered the vorticity equation. In order to demonstrate the principle I will use the simpler advection equation, $\frac{\partial u}{\partial t} = - u \frac{\partial u}{\partial x}$ in a periodic domain in x. If this equation is multiplied by u and then integrated over the periodic domain in x the following relationships result:

$$u \frac{\partial u}{\partial t} = - u^2 \frac{\partial u}{\partial x}$$

$$\frac{\partial}{\partial t} \left(\frac{1}{2} u^2\right) = - \frac{1}{3} \frac{\partial}{\partial x} (u^3)$$

$$\int_x \frac{\partial}{\partial t} \left(\frac{1}{2} u^2\right)_{dx} = - \int_x \frac{1}{3} \frac{\partial}{\partial x} (u^3) dx$$

$$\frac{\partial}{\partial t} \int_x \frac{1}{2} u^2 \, dx = 0$$

Thus it can be shown for the differential equation that in a periodic domain (or also one where u is zero at both boundaries) the integrated quadratic function for kinetic energy, $\int_x \frac{1}{2} u^2 dx$ must remain constant in time.

The problem is to have the finite difference version of this equation satisfy the same constraint. Since u^2 is positive definite, requiring it to be bounded also puts an upper bound on the magnitude of u itself which is the same condition required for numerical computational stability.

If space differencing for the right hand side of the equation, $u \frac{\partial u}{\partial x}$ is given by $- u_m \frac{(u_{m+1} - u_{m-1})}{2\Delta x}$ then when this expression is multiplied by the value of u at the central grid point to give $- u_m^2 \frac{(u_{m+1} - u_{m-1})}{2\Delta x}$, the summation of this quantity over all grid points in the periodic domain can be shown not to be zero (contrary to the characteristic of the differential equation). If the right hand side is first rewritten in the equivalent form, $- \frac{1}{2} \frac{\partial}{\partial x} (u^2)$,

and then expressed as $-\frac{1}{2}\frac{(u^2_{m+1}-u^2_{m-1})}{2\Delta x}$ for finite differences, the summation of this quantity after multiplication by the value of u at the central grid point, $-\frac{1}{2}u_m\frac{(u^2_{m+1}-u^2_{m-1})}{2\Delta x}$, is still not zero for the periodic space domain. Arakawa showed that by first expanding the advection term into several parts before taking the finite differences, the quadratic constraint could be satisfied. For this simple equation the corresponding expansion would be:

$$\frac{\partial u}{\partial t} = -u\frac{\partial u}{\partial x} = -\frac{1}{3}u\frac{\partial u}{\partial x} - \frac{1}{3}\frac{\partial}{\partial x}(u^2)$$

$$\frac{\partial u}{\partial t} = -\frac{1}{3}u_m\frac{(u_{m+1}-u_{m-1})}{2\Delta x} - \frac{1}{3}\frac{(u^2_{m+1}-u^2_{m-1})}{2\Delta x}$$

It was this type of sophisticated thinking that has been applied to the finite differencing in some of the general circulation models.

Spectral methods have become an important numerical method for general circulation modeling. In this approach to modeling, the horizontal structure of the dependent variables is represented by a finite summation of orthogonal functions in which case the dependent variables become the amplitude factors for these functions instead of the total value of the dependent variable at specific points in space. This formulation becomes very complicated in the mathematical representation and I will not attempt to give many details here.

The orthogonal functions commonly used for general circulation models are called surface spherical harmonics. These have a structure given by $e^{im\lambda}P^m_n(\theta)$ where $P^m_n(\theta)$ is a Legendre polynomial which gives the structure in the north-south direction. Here

- e is the exponential function
- m is the east-west wavenumber
- λ is longitude
- n is related to the number of nodal points in the north-south direction
- θ is latitude

Thus, for instance, the velocity component $u(x,y)$ or $u(\lambda,\theta)$ would be represented by $\sum_m \sum_n \hat{u}(m,n)\, e^{im\lambda}P^m_n(\theta)$ where m and n are integers of a limited range and $\hat{u}(m,n)$ are the amplitude coefficients which become the dependent variables for the model.

The advantages of this method for general circulation modeling are numerous

1) The space finite differencing problems near the poles are avoided
2) Horizontal derivatives for each harmonic are determined exactly

3) The growth of smaller scale features due to unrealistic nonlinear interactions can be controlled separately from the larger scales because the various scales are separately represented in the model.

The spectral approach would have long ago become the common practice for all general circulation models except that there were several drawbacks to the method:

1) In order to have enough harmonics to represent the range of space scales in the general circulation, the number of calculations needed to represent the nonlinear advection terms becomes prohibitive.
2) Local phenomena such as precipitation and the associated latent heating required knowing the total magnitude of the dependent variable which necessitates a frequent recombination of all the harmonic components.

The development of a fast technique to transform between a variable field and its harmonic components made it possible to reconsider the use of spectral models. This is the so-called "fast Fourier transform method". Now at the current time there are a number of good resolution general circulation models being developed according to the "semispectral" approach. In this method at each time step, linear terms including those with first and second derivatives are evaluated using the harmonic function representation and the nonlinear and local effects terms such as condensation are evaluated using the total variable representation. In this way the advantages of both the harmonic and finite difference approaches are combined and the computational requirements are no greater than the standard finite difference models because of the fast Fourier transform technique.

Time does not permit a discussion of the numerous studies in the parameterization of various processes for general circulation models that have been done. Considerable work has been done in planetary boundary layer processes, moist convection, turbulence and radiative transfer. Discussion of each could be the topic of an entire course. As noted before, parameterization remains an important problem. Many experiments have shown a profound change in the average conditions in a model simulation due to a seemingly small change in a parameterization procedure. It is hoped that studies of smaller scale aspects of meteorology done for other reasons will assist in improving the parameterization formulations in general circulation models.

Overview of current models

A few characteristics of the general circulation models at NCAR, NASA and GFDL are given below. These initials refer to institutions listed before. All use the primitive equations.

NCAR model

Coordinates: horizontal, 5° by 5° or 2 1/2 by 2 1/2 degree latitude longitude grid with skipping near the poles

vertical, height coordinate system with 6 layers evenly spaced

Planetary boundary layer: Drag and bulk aerodynamic laws for stress, heat and moisture fluxes

Parameterization: dry and moist convection, radiation and sub-grid scale turbulence.

NASA model

Coordinates: horizontal, 5° longitude, 4° latitude grid vertical, sigma coordinates in pressure with 9 levels

Planetary boundary layer: Stability dependent eddy coefficient for momentum, heat and moisture fluxes.

Parameterization: dry and moist convection, radiation and sub-grid scale turbulence (vertical only)

GFDL model

Coordinates: horizontal, 5° by 5° latitude/longitude grid with no skipping near the poles, with Fourier filtering along latitude lines. Vertical, sigma coordinates in pressure with 9 levels and better resolution near the lower boundary.

Planetary boundary layer: surface drag and bulk aerodynamic formulas with some stability dependence

Parameterization: dry and moist convection, radiation (assuming climatological cloud cover instead of predicted cloud cover), and sub-grid scale turbulence.

Many other things can be said about these models. Above, I merely wanted to demonstrate that even for some of the basic points, there remains some important differences, especially in the parameterization formulations.

Numerous papers have been written describing specific features that have been simulated by the general circulation models. It is clear that they have been successful in many aspects.

Here I want to show using model output made years ago that these models have had some degree of realism even with their earlier versions.

a. Movie output of NCAR 6-level model

In this movie we see the surface pressure fields and areas of large scale upward motion (shown by fuzzy clouds) for a constant-season January simulation and then a constant-season July simulation. Although the details and quantitative aspects are poor, the model shows the west to east motions in the middle latitudes, extratropical cyclone development in the middle latitudes. The July simulation at first appears reasonable in having weaker systems but soon we see all transients dying out and a super active tropical convergence zone. This movie was made to show optimism in the possibilities for general circulation models.

b. Movie output of NCAR 2-level model

Although this movie was made at an even earlier date, it was able to demonstrate some basic features of the general circulation. The movie starts from an initial state of rest with an isothermal atmosphere and then allows a solar heating distribution for January to persist. There are four interesting dynamical events simulated.

1) Gradual enhancement of the middle latitude westerlies as implied by the increasing equator to pole temperature differences.
2) Development of global scale stationary waves due to continent ocean contrasts.
3) Outbreak of baroclinic instability at around day 30 due to sufficiently large vertical wind shears again implied by the latitudinal temperature gradient. Smaller scale transient waves form.
4) Negative feedback from baroclinic waves to reduce the zonally averaged temperature gradients and to establish an equilibrium state with zonal flow, standing waves, and transient waves superimposed.

In simulations from most general circulation models there are a few persistent errors that are noted.

1) Lack of temperature equilibrium especially in the stratosphere. This led to a zonally averaged jet flow that is too strong.
2) The jet stream maximum is usually too close to the upper boundary. The upper boundary is generally too close to the active tropopause level and it has a strong effect on conditions there.
3) The eddy component magnitudes are suppressed compared to those observed in the atmosphere. Overall eddy kinetic energy levels are anywhere from one half to three quarters of the observed values.

4) Transient activity as evidenced in the surface positions of extra-tropical cyclones is too far towards the pole in the northern hemisphere.

The following four slides demonstrate these points.

References:

Haltiner, G.J., *Numerical Weather Prediction*, John Wiley, 1971.

Haltiner and Williams, 1975, Some recent advances in numerical weather prediction, Monthly Weather Review, 103, 571-590.

Chang et al.: General circulation models of the atmosphere. Methods in Computational Physics, 1977.

(Also GARP Publication Series No. 17. Volumes I and II Numerical Methods used in Atmospheric Models. WMO/ICSU Geneva, Aug. 1976 and Sept. 1979.

C. Mesoscale Numerical Models

As mentioned before, numerical modeling studies have been extended to a wide range of atmospheric phenomena at scales smaller than the synoptic scale. Many of these are at the mesoscale which can be loosely defined for the discussion here as having horizontal dimensions ranging from 1 to 500 km, vertical dimension from 1 to 10 km and a time scale ranging from tens of minutes up to a day. Phenomena modeled include: orographic flow, sea breeze, fronts, hurricanes and typhoons, gravity waves, moist convection and planetary boundary layer processes.

An important limitation to most of these studies has been the lack of verification data. Only recently with the improvement in remote sensing techniques and aircraft observations has it become possible to consider adequate verification analyses. Some phenomena such as the sea breeze have a major effect on conditions at the earth's surface and verification in terms of surface parameters has been possible. Nevertheless it is frequently not possible to properly analyze and improve such models without considering the full three dimensional aspects.

In general, mesoscale modeling is far less advanced than the large scale modeling. In many situations the parameterization formulations are even more important than for the large scale and the theory for such processes is frequently not available. Many of the meteorological problems facing mankind involve the mesoscale phenomena and mesoscale characteristics of the atmosphere, so there is a great need to continue to work actively in this area of modeling.

In this lecture I hope to summarize some of the recent advances in mesoscale modeling and to describe the range of simplifications that have been tried in order to obtain results from the numerical modeling approach.

Under the assumption that resolution alone has been an important limitation in model performance and under the assumption that many mesoscale features derive an important forcing from synoptic-scale conditions, attempts have been made to simulate the mesoscale phenomena at the larger end of the scale range by merely adding more grid points to existing primitive models for synoptic and global scale meteorology.

In the area of operational numerical weather prediction the horizontal resolution used to be 381 km for all the models. Then a limited area half mesh model of 191 km was introduced. Recently the hemispheric model resolution was reduced from 381 to 191 km and the limited area model was specified with a 127 km grid. More recently the 60 km moveable fine mesh model has been introduced. The remarkable fact is that very little change was made in the physics and parameterization formulations when the resolution increases were made. They are all similar to what I described for the LFM model.

Presumably the limiting factors to this approach are the inadequacies in the equation formulation and the lack of mesoscale observation for proper initialization.

In the last few years, several research groups in the United States have begun to develop models intended to give general mesoscale forecasts for the tropospheric condition with a focus on precipitation forecasting. These groups include the Pennsylvania State University, Drexel University and NCAR, and NASA. The fundamental equations for these are still the hydrostatic primitive equations however there are a number of differences from the models discussed before especially in the parameterization.

Drexel University and NCAR Regional Mesoscale Model

To provide an example, I will discuss briefly the formulation of this model focusing on the differences from the LFM model instead of the complete formulation.

In its final form the high resolution portion of the model will cover about half the area of the US using a latitude-longitude grid with a spacing of approximately 35 km. Boundary conditions are specified by a larger scale model.

In the vertical, a height coordinate system is used normalized by the height of the lower boundary to give a sigma coordinate system in height

(Compared to pressure for the LFM). The layers extend up to 16.5 km (approximately 100 mb) and are unevenly spaced to give better resolution in the planetary boundary area below 3 km. All variables are defined at each level. There are 15 levels where the dependent variables are defined compared to 6 for the LFM at heights shown:

Coordinate heights (for lower boundary at sea level)
16.5 km
15.0
13.5
12.0
10.5
9.0
7.5
6.0
4.5
3.0
2.0
1.25
750 m
375 m
25 m
0 m

The basic Governing equations are similar to the LFM model with prognostic equations for horizontal velocity, temperature, and water vapor. There is a diagnostic equation for the vertical motion and the hydrostatic equation is used to compute pressure at the height levels. Because of the coordinate system, pressure at the upper boundary becomes a prognostic variable. The prognostic equations also include relationships to determine cloud drop and precipitation drop water concentrations. These will be discussed in the section on rainfall determination.

Parameterization formulations are summarized.

a) Small scale turbulence effects in the free atmosphere are modeled explicitly by an eddy diffusion formulation using $K \frac{\partial^2}{\partial z^2}$ operator for vertical diffusion and a $K(\frac{\partial^4}{\partial x^4} + \frac{\partial^4}{\partial y^4})$ operator for horizontal diffusion. This diffusion acts on the temperature, moisture, and horizontal momentum fields.

b) For the planetary boundary layer, both a transition and surface boundary domain are modeled. The transition layer extends from the 25 m level to 1.25 km level and has a variable eddy diffusion coefficient for vertical mixing ranging from the constant value of 1 m^2 sec^{-1} used in upper levels to the value determined in the surface layer at 25 m height from Monin-Oboukhov similarity theory.

In the surface layer the surface heat and moisture fluxes are currently prescribed variables. Drag effects on the velocity at 25 m height are determined by assuming the velocity to be zero at the earth's surface and using Monin-Oboukhov similarity theory.

c) No radiation effects are included. The model is designed to run no longer than 24 hours so this approximation may not be too serious.

d) Precipitation forecasting is the part of the model where major improvements are attempted over the large scale models such as the LFM. This section also includes a more elaborate model for subgrid scale moist convection since the hope was to model severe convective storm situations.

Large scale water vapor, cloud liquid water content and precipitation liquid water content are all modeled explicitly and change according to advection effects and the conversion effects shown on the blackboard.

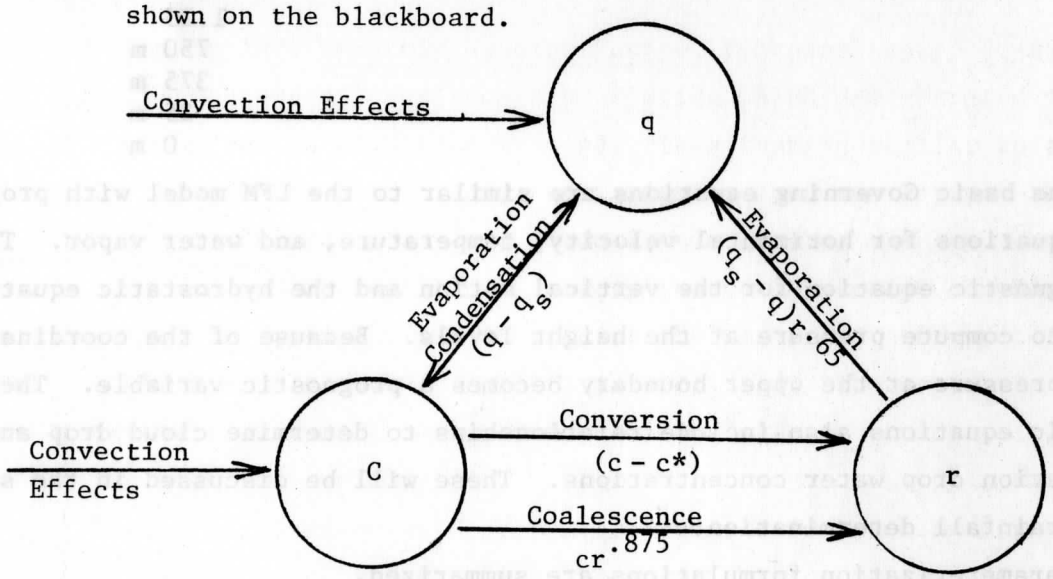

here q is the water vapor

q_s is the saturation value of q

c is the cloud drop water content

c* is a threshold value of c. (If c is less than c* there is no conversion from cloud drops to precipitation. If c exceeds this value then there is a conversion.)

r is the precipitation liquid water content

The magnitudes of water vapor and cloud drop water content are also affected by convection effects as denoted by the arrows coming in from the left. The large scale precipitation liquid water is allowed to fall downward relative to the air at a specified terminal velocity at the same time it is being influenced by all the processes just described. That which reaches the ground is then the predicted rainfall.

Sub-grid scale moist convective motion effects are determined by a one dimensional nonhydrostatic steady state convective plume model. Six variables describing parcel conditions are computed for the parcel rising in the steady convective plume

1) Vertical motion
2) Temperature
3) Water vapor
4) Cloud drop water
5) Precipitation water content
6) Radius of the parcel (radius at cloud base is prescribed)

The vertical motion is determined by the nonhydrostatic equation of motion including buoyancy computed by comparing the virtual temperature with the environment, entrainment and drag due to falling precipitation. Temperature is determined from moist adiabatic relationships with entrainment effects included. Conversions from cloud drops to precipitation drops are determined by the relationships used for the large scale situation. The key factor in the calculation is the fractional area of upward motion at cloud base. This parameter is adjusted until the total pressure difference from the top to the bottom of the plume is the same as in the environment outside the plume according to a simple hydrostatic relationship in both columns. A subsidence warming of the environment is assumed.

The rainfall determined from this calculation is added to that obtained from the large scale calculation. Large scale changes in water vapor and cloud drop water content and temperature are determined by appropriate area average over both the updrafts and environment.

This concludes the brief description of a representative regional scale model. The detail is not important here. What is important is the degree of complexity currently being attempted in such models. An early reference to this particular model is a 1976 paper by Perkey starting on page 1513 in the Monthly Weather Review.

The performance of this or any other regional mesoscale model has not been outstanding to date. Relatively few runs with the model have been made and the verification has not been complete due to the lack of observational data. The next few slides show the results of one test calculation for May 20, 1977 in the central U.S. The first shows a grid spacing which is actually slightly larger than the 35 km used. The second shows the synoptic situation that existed at the initial time including the distribution of precipitation

as determined by radar. The third shows the observed precipitation 6 hours later. The squall line in the north has weakened; the precipitation towards the west and south has increased. The high resolution model covered the area outlined in green. The next slide shows a comparison of two versions of its prediction (using slightly difference initial states) to the observations. As you can see, there is some sense to the results but we have a long way to go.

The remaining mesoscale modeling approaches described are examples where major simplifications have been made in the model design in order to make a numerical approach feasible.

Pielke in 1974 (Monthly Weather Review, February issue) constructed a model for the sea breeze condition over Florida which demonstrated the usefulness of limiting scales of motion modeled. In a fashion similar to the perturbation approach, he partitioned the variables into two parts: the synoptic scale and the mesoscale. Thus for example, $u = u_s + u_M$, where u_s refers to the synoptic scale component and u_M refers to the mesoscale component. Then the equations were derived to predict the mesoscale component for the case when the synoptic scale component is specified. The mesoscale component was not required to remain small, and nonlinear effects remained in the equations.

Using this approach, errors due to finite difference modeling of the advection process were reduced since the major portion of that process was linear. An example of model results is shown in the next two slides. The first shows the development of the sea breeze circulation at low levels starting with a situation with only synoptic scale flow and then gradually imposing a land-ocean temperature difference. The second slide shows a comparison of the predicted vertical motion fields with the precipitation observed by radar. The results correspond closely. This approach is best for situations where the synoptic scale conditions are quite uniform.

The planetary boundary layer model developed by the National Weather Service in the U.S. is a good example of reducing the domain to be modeled. Here the complete dynamical relationships are retained in the boundary layer but conditions are specified at the 1.6 km top level from another model. Good resolution is possible in the vertical because of the small vertical extent. The simplification is similar to the limited horizontal domain model. In this case the propagation of errors down from the upper boundary are less obvious than those which come in from lateral boundaries because of the small magnitudes

of vertical advection near the earth's surface.

If a model with a reduction of the number of independent variables can be considered relevant to a physical situation, this simplification usually greatly simplifies the numerical procedures. For instance with an analastic equation model, a vorticity equation can be used if the model is two dimensional (x and z).

Linearization allows for more precise control of the numerical approximation and for the possibility of comparison of solutions to analytical solutions of the differential equations.

Model for vertical propagation of gravity waves

As an example of the modeling that has been achieved using the last two simplifications mentioned, I wish to briefly discuss a model that I developed and tested by which some simple but not trivial situations for the vertical propagation of gravity waves were simulated which could be compared to theoretical solutions.

This was the most satisfying model that I ever worked with since I was able to clearly observe the type of accuracy in the solution provided by the finite difference equations. It is good sometimes to look at mesoscale models which have this kind of success since so frequently we deal with models which are too complicated to allow full understanding of the results. Some scientists question the general feasibility of the modeling of mesoscale situations by using dynamical deterministic prediction equations.

This was a model to simulate the propagation of gravity and sound waves in a two-dimensional vertical plane. The equations to predict these waves were linearized about a specified mean horizontal velocity, density, pressure and temperature distribution. The basic processes for horizontal and vertical acceleration, continuity of mass and the first law of thermodynamics were included. Since the dynamics included local compression and nonhydrostatic vertical accelerations, both sound waves and internal gravity waves were included. Coriolis effects were ignored. A description of this model is published on page 339 of the February 1969 issue of the Journal of Computational Physics.

The governing equations are shown in the slide. Since no filtering approximations were introduced there are prognostic relationships for all of the four dependent variables:

u* horizontal velocity

w* vertical velocity

ρ^* density

p* pressure

An important additional simplification made was to assume a periodicity of specified wavelength in the x direction and to assume a weighting by the square root of the mean density, $\sqrt{\rho_o}$. For example, $u^* = \frac{1}{\sqrt{\rho_o}} u\, e^{ikx}$. This latter transformation removed large variations in perturbation amplitudes due to the vertical variation of mean density alone.

The equations for the coefficients of the periodic functions are shown in the next slide. It is these which are solved by numerical methods. Here I will discuss the design and accuracy of results. In a later lecture there will be more discussion of the range of results produced in this modeling study.

For an isothermal basic state with no mean flow, the dispersion equation which governs the relationship between the frequency of oscillation, the wave dimensions, and the buoyancy and compression factors can be written:

$$\omega^4 - \omega^2[1.4\ RT_o(k^2 + \ell^2) + \frac{1.96\ g^2}{5.6\ RT_o}] + 0.4\ g^2k^2 = 0$$

where ω is the frequency of oscillation

R is the specific gas constant

g is the acceleration of gravity

k is the horizontal wave number

ℓ is the vertical wave number

T_o is the mean temperature

This equation has three unknowns, ω, k and ℓ. By specifying any two of them the third is determined. In the numerical model ω and k were prescribed and the vertical wavelength observed was then compared with that from this theoretical relationship.

A very accurate numerical model was developed. This was possible because a grid staggering in both space (height) and time, the large number of grid points that could be used in the vertical, and the lack of any differential diagnostic relationships all made it possible to handle boundary and resolution problems in the best way possible.

The model domain extended up to 100 km for the region with no viscosity effects in the model. Then a large number of layers were added above that level where a gradually imposed linear damping term for the velocity components was used to remove energy from upward moving waves and prevent artificial reflection from the upper boundary. The staggered grid system is shown in the next diagram. Only the vertical motion was defined at the lower boundary which

avoided the need for any special finite differencing in any of the equations since vertical motion at the lower boundary was a specified condition and the one by which wave motion was introduced to the atmosphere.

The effective performance of this upper boundary formulation is shown in the next diagram. Here we see a vertically propagating sound wave entering and then dissipating in the upper viscous zone with no noticeable reflection back from the upper boundary. This type of upper boundary condition is the best for atmospheric models. However, in most models it is far too expensive in computer time to add such extra layers at the top of a model.

The next diagram shows a comparison of the numerical model results to a theoretical solution for the same sound wave test shown before. Even though the method of forcing the model has introduced small scale oscillations, the solutions agree very closely.

The next figure shows a test for an internal gravity wave situation where the lower boundary is forced with a constant frequency oscillation. With that frequency a wave with vertical wavelength of 17.516 km and a constant amplitude is expected. After 6 hours these characteristics are very closely approximated in the region with no viscosity and the oscillation amplitude decreases smoothly in the viscous zone with no evidence of reflection. The correlation product for vertical and horizontal velocity components is expected to be constant with height in this situation.

The model was tested on another case where a theoretical solution existed. This is for the situation where the mean flow increases linearly with height. At the level where the horizontal mean flow velocity equals the horizontal phase speed of the gravity waves, a so-called "critical level" exists which acts to block the upward propagation of the gravity waves. As this level is approached, theory predicts that the vertical wavelength and the vertical velocity should vary (decrease) as the square root of the distance to the critical level while the amplitude of the horizontal velocity should increase according to the inverse of the square root of the distance to the critical level with the correlation product, $\overline{uw}$, remaining constant. The next figure shows the model solution in this case where the critical level is at a height of 56.6 km.

This model was subsequently applied to the problem of describing the mesoscale structure in the upper atmosphere which will be discussed in a later lecture.

In conclusion, I have tried to show a wide range of approaches that have been made for modeling mesoscale phenomena. The applicability of such modeling to general weather forecasting seems obvious but much more work with model formulation and initial data specification is required to make this a reality.

D. Initialization

The process of initialization is vital to using numerical prediction models for synoptic and mesoscale forecasting. Inconsistencies in the nature of observational data with the formulation of a numerical model can mean that carefully analyzed data will result in large errors and spurious components in the model forecast.

A model for an initial value forecast problem requires specification of all of the prognostic variables at every grid point where the variables are defined. There are many interrelated steps in the procedure to accomplish this satisfactorily. These are outlined in the diagram.

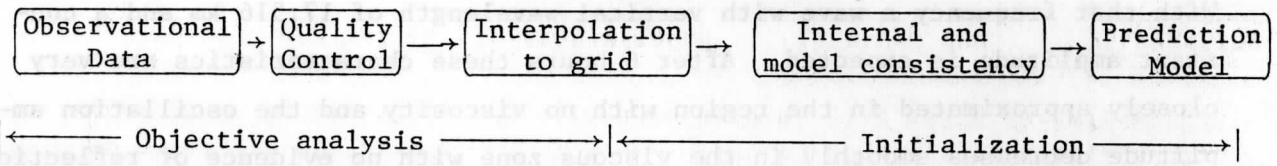

With earlier models the process could be considered in series as shown by the arrows. Objective analysis was the first procedure and initialization was the second. With more recent work, it has become evident that it is important for the prediction model to be used to properly accomplish the earlier steps so that the process becomes a fully interrelated one.

In the lecture today, I wish to discuss several theoretical and practical aspects for this problem. As will be shown, there remain many serious problems in this area.

Objective analysis

Objective analysis may be defined as the procedure to determine regular grid point values of a variable from given observed values, usually at irregularly spaced positions, by a reproduceable method. There are three important functions of this analysis. The first is interpolation to the grid positions. The second is to eliminate gross errors in the observations and the third is to smooth. The smoothing is to reduce the amplitude of features that are poorly resolved by the observing system and poorly handled by the numerical model.

Two basic mathematical approaches are polynomial interpolation and optimal or weighted linear interpolation. The polynomial interpolation requires specifying the coefficients in the polynomial of the form $F = \sum_n a_n x^n$ using the values of F at the data points x_o and then using the polynomial to find the value of F at the grid positions x_g. It would seem that the best strategy would be to fit the highest order polynomial possible to the data points and to make it match the observational values exactly as shown. However, this approach has great computational complexity, is difficult to apply in boundary regions, tends to emphasize small scale oscillations, and disregards the fact that the observational values themselves contain errors.

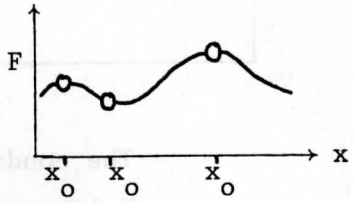

A more reasonable approach is to use a lower order polynomial and to specify its coefficients according to a least equares fit. Here we must find the a_n so that

$$\sum_{\substack{\text{data}\\\text{points}}} [F_{observed}(x_o) - F_{polynomial}(x_o)]^2$$

is a minimum where x_o are the observation points.

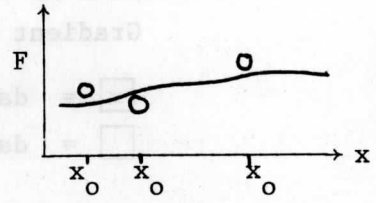

Recent work with this type of interpolation has introduced fitting according to "spline theory". (Refer to an article by Fritsch in the May 1971 Monthly Weather Review, p. 379) and this is referred to in many studies today. In this method a polynomial is fitted to the data according to both magnitude and gradient constraints. Cubic splines are commonly used and for them the method is described.

Assume the cubic form to be $F = a_3x^3 + a_2x^2 + a_1x + a_o$. Fit cubic curves over successive intervals of 3 data points requiring a matching of magnitudes and gradients at each intersection as shown to give a continuous curve, also continuous in the first derivative, which goes through alternate data points. For each cubic function there are four unknowns and four conditions to be met so the procedure is determinate.

The magnitude to be specified is the magnitude at the data point itself. The gradient value to be matched is the slope at the end data point determined by a quadratic curve fitted to three adjacent data points with the grid position in question in the middle.

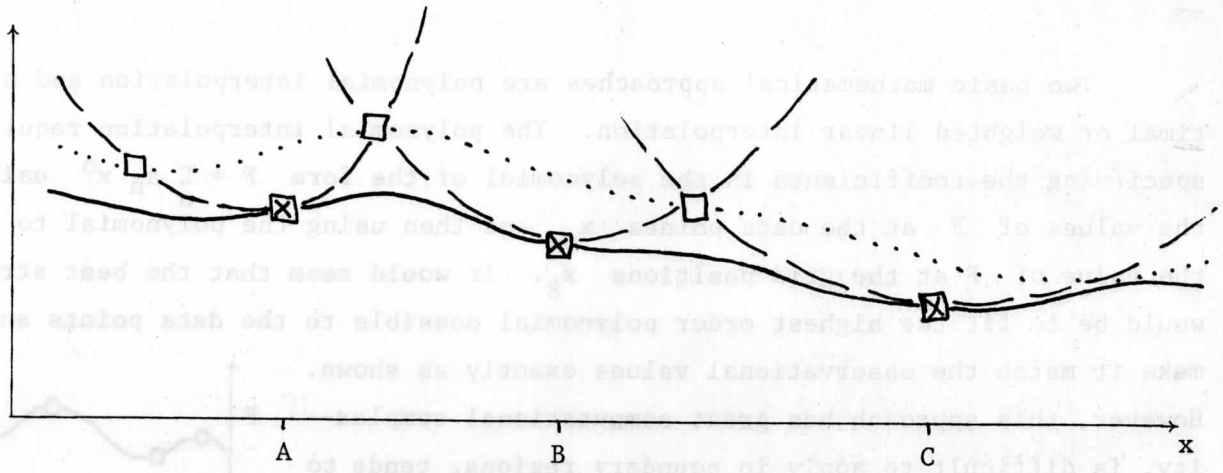

The conditions on the cubic from A to B.

Value at A = $F(x_A)$

Value at B = $F(x_B)$

Gradient at A = slope of dashed curve at x_A

Gradient at B = slope of dashed curve at x_B

[x] = data points for first curve

[ ] = data points for second curve

The curve is fitted to the alternate points, A, B and C by this method. Then another curve, shown in a dotted line is fit to the other set of data points. Then the data point values are adjusted to the midpoint between the two curves and the procedure is repeated. According to the theory of splines, the result will minimize the curvature in the final curve which gives the smoothness desired in objectively analyzed fields.

The optimal or weighted linear interpolation approaches were described briefly in the lecture on operational numerical prediction models and they use the formula $F_{grid} = \sum_n a_n F_{observed}$, where the weighting functions are obtained by empirical or error-minimizing techniques.

It is sometimes difficult to determine which objective analysis method is best for a given situation. In cases of mesoscale data sets where the grid spacing is very irregular, results can be quite sensitive to the method. As an example I would like to show the results of an objective analysis test with mesoscale satellite wind data. Four analysis procedures were used:

1) Least squares first degree polynomial fitting method developed by Mancuso and Endlich
2) Least square fitting of quadratic polynomial used at the Madison campus computing center MACC without any parameters derived using meteorological information

3) Optimal interpolation method using exponential form weighting functions with coefficients as determined by the method of Gandin

4) A Cressman type weighted linear interpolation scheme adopted to the mesoscale by Barnes.

These were used to interpolate the satellite wind values to a grid and then divergence was computed from the grid point values. The slide shows the observational data. Note that regions B and D have sparser data coverage than elsewhere. The next slide shows the velocity divergence values determined by each of the four methods. Note that the optimal interpolation results have more smaller scale structure than the other results and all of the methods differ in the regions B and D. For reference note that magnitudes are in the range of 5 to 10 x 10^{-5} sec^{-1}. The next diagram shows the difference between the Barnes results and the others with a contour interval of 2.5 x 10^{-5} sec^{-1}. This shows that the difference in the values between the methods is nearly the same as the magnitudes in some places.

Reference:

Houghton, Lee and Chang, 1979: Numerical model initialization with subsynoptic scale satellite wind data. Preprint Volume, 4th Conference on Numerical Weather Prediction, October 1979, Silver Spring, Maryland, pp. 16-23.

Another approach to analysis is to use information about the structures of the solution expected in the model which will include the relationship between different variables and then to determine the magnitudes of these eigenfunctions or structure functions to best fit the observations. By this means the relationship between the two variables should be consistent with each other according to a physical phenomenon. This method was used employing the Hough functions for one of the operational numerical prediction models.

To illustrate this method, consider initializing the linearized gravity wave system mentioned in an earlier lecture. $\frac{\partial u}{\partial t} = - g \frac{\partial h}{\partial x}$

The eigenfunctions can be found by first assuming periodic functions in time and space with frequency and wavenumber of ω and k. $\frac{\partial h}{\partial t} = - H \frac{\partial u}{\partial x}$

$u = \hat{u}\, e^{i(kx-\omega t)}$; $h = \hat{h}\, e^{i(kx-\omega t)}$.

The equations become $\omega\hat{u} = kg\,\hat{h}$ and $\omega\hat{h} = kH\,\hat{u}$

where the $\hat{u}$ and $\hat{h}$ are coefficients of the periodic functions. Solution of the system requires that

an eigenvalue equation be satisfied,

$$\omega^2 = k^2\ gH \quad \text{or} \quad \omega = \pm \sqrt{gH}\ k$$

Substituting these values of the frequency ω back into the equations yields the eigenfunctions $\hat{u} = \sqrt{\frac{g}{H}}\ \hat{h}$ for the wave moving in the +x direction and $\hat{u} = -\sqrt{\frac{g}{H}}\ \hat{h}$ for the wave moving in the -x direction. These define the co-existing velocity and height field structures which if used as the basis for the u and h fields by a least squares fit will insure that the initial analysis is compatible with the physical phenomena. Of course, this is an example which has been simplified to the trivial level.

The fact that two dynamically related variables such as the velocity and pressure can be used to specify a single structure entity raises the question which should be given more weight in the analysis because the observational values might not agree with each other in the same manner as in the eigenfunction or other simple relationship such as the geostrophic equations.

The problem was studied for the case of synoptic scale motions by considering adjustment theory. Consider a simple one layer linearized fluid model with variations only in the y direction, no mean motions and constant Coriolis parameter:

$$\frac{\partial u}{\partial t} - fv = 0$$

$$\frac{\partial v}{\partial t} + fu + \frac{\partial \phi}{\partial y} = 0$$

$$\frac{\partial \phi}{\partial t} + gH\ \frac{\partial v}{\partial y} = 0$$

where u is the zonal velocity

v is the meridional velocity

f is the Coriolis parameter

ϕ is the perturbation geopotential

g is the acceleration of gravity

H is the mean depth

If periodic solutions in y and t of the form $e^{i\ell y - i\omega t}$ are assumed, there are three solutions for the frequency: $\omega = 0$ for a steady state model and $\omega = \pm\sqrt{\ell^2 gH + f^2}$ for gravity inertial wave modes. The steady state solution for this model is $v = 0$ and $u = -\frac{1}{f}\ \frac{\partial \phi}{\partial y}$ or $\psi = \frac{\phi}{f}$ where ψ is the streamfunction. The steady state here is intended to represent the large scale or quasigeostrophic conditions in a more general situation.

Time evolution is governed by the constraint of conservation of potential vorticity, $[\frac{\partial u}{\partial y} + \frac{f\phi}{gH}]$ which can be derived by eliminating v from the equations.

Thus the initial and final states of the model can be equated as follows:

$$\left[\frac{\partial^2\psi}{\partial y^2} - \frac{f\phi}{gH}\right]_{\text{initial}} = \left[\frac{\partial^2\psi}{\partial y^2} - \frac{f\phi}{gH}\right]_{\text{final}}$$

For the final state we can assume that the gravity inertial waves have propagated away leaving only the steady mode as shown for which $\phi = f\ \psi$.

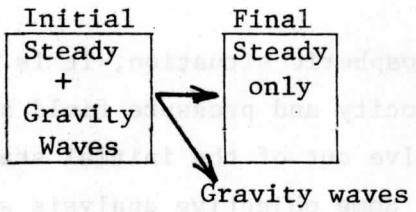

Making this substitution on the right hand side and introducing the subscript s for steady and i for initial gives

$$\frac{\partial^2\psi_i}{\partial y^2} - \frac{f\phi_i}{gH} = \frac{\partial^2\psi_s}{\partial y^2} - \frac{f^2}{gH}\ \psi_s$$

Now assume that the variables are periodic in the y direction with wavenumber ℓ so that $\psi = \hat{\psi}\ e^{i\ell y}$

$$\phi = \hat{\phi}\ e^{i\ell y}$$

Then the relationship simplifies to

$$-\ell^2\hat{\psi}_i - \frac{f\hat{\phi}_i}{gH} = -\ell^2\hat{\psi}_s - \frac{f^2}{gH}\hat{\psi}_s$$

and we can solve this for the single variable, $\hat{\psi}_s$, to describe the final state:

$$\hat{\psi}_s = \frac{\ell^2\hat{\psi}_i + \frac{f^2}{gH}\left(\frac{\hat{\phi}_i}{f}\right)}{\ell^2 + \frac{f^2}{gH}}$$

The factor $\frac{\sqrt{gH}}{f}$ is the Rossby Radius of Deformation for which we define a wavenumber, λ. $\left[\lambda = \frac{f}{\sqrt{gH}}\right]$.

Then

$$\hat{\psi}_s = \frac{\ell^2\hat{\psi}_i + \lambda^2\left(\frac{\hat{\phi}_i}{f}\right)}{\ell^2 + \lambda^2}$$

This equation gives the relative contributions of the initially prescribed velocity and pressure fields to the final steady or adjusted state. This relationships shows that for the small scale features where $\ell >> \lambda$

$$\hat{\psi}_s \approx \frac{\ell^2\hat{\psi}_i}{\ell^2+\lambda^2} \approx \hat{\psi}_i$$

so that the final state depends mainly on the initial specification of velocity and not on the initial pressure field.

For the large scale situation where $\ell << \lambda$

$$\hat{\psi} \approx \frac{\lambda^2 \frac{\hat{\phi}_i}{f}}{\ell^2+\lambda^2} \approx \frac{\hat{\phi}_i}{f}$$

the situation is reversed and the initial pressure specification is the important variable.

Generalizing this result to the atmospheric situation, it is seen that the relative importance of the initial velocity and pressure field specifications to the synoptic scale state which will evolve out of the initial state vary and depend on the scale of the phenomena. Some objective analysis schemes have been proposed which change the weighting given to the observations in this manner.

Reference:

Houghton and Washington, 1969: On global initialization of the primitive equations: Part 1. Journal of Applied Meteorology, 8, 726-737.

The diagnostic method is the original approach to achieving consistency among the variables in an initial data set. Relationships such as the hydrostatic, geostrophic and balance equations were applied as constraints to the data fields. For the primitive equation model, the hydrostatic constraint is consistent: however the geostrophic or balance relationship between velocity and pressure is not consistent with the prediction equations and the intent to remove gravity inertial waves from the early forecast period of the model is not fully achieved. The geostrophic and balance relationships remove most or all of the initial horizontal divergence even that associated with the synoptic scale motions and thus distort the larger scale phenomena.

Diagnostic initialization of a realistic large scale vertical motion field has been attempted using a so called "omega" equation consistent with either the quasi-geostrophic or balanced model. For the quasi-geostrophic system

$$\nabla^2\sigma\omega - f^2 \frac{\partial^2\omega}{\partial p^2} = f_o \frac{\partial}{\partial p} [V_g \cdot \nabla(\zeta_g + f)] + \frac{R}{p} \nabla^2 (V_g \cdot \nabla T)$$

However, the forecasts have been generally no more satisfactory than with a zero initial vertical velocity. The following characteristics where noted in a study I did with the NCAR general circulation model. I looked at the

computed vertical motion and surface pressure in a region near an important baroclinic disturbance for initializations with and without a diagnostically determined vertical motion. Results were as follows

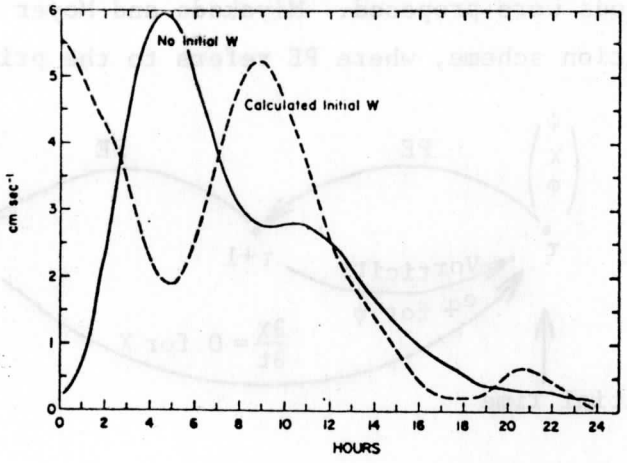

Comparison of the vertical velocity (cm sec^{-1}) at 40N, 140E for the first 24-hr period. Solid line shows the vertical velocity with no initial divergence; dashed line with initial divergence.

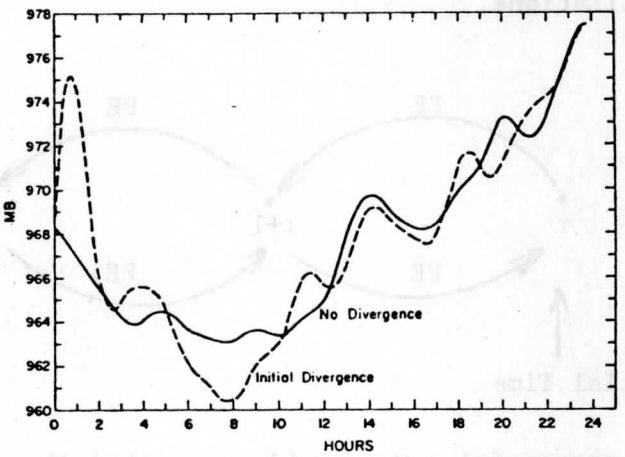

Comparison of the surface pressure (mb) at 40N, 140E for the first 24-hr period. Solid line illustrates behavior of pressure with no initial divergence; dashed line with initial divergence.

The gravity wave activity appears to be as large or larger in the forecasts where an attempt is made to insert an initial vertical motion field from quasi-geostrophic theory. Currently the initial vertical motion in the LFM model is the 12 hr forecast value from a previous run. No attempt is made to determine it from the observations at initialization time.

Reference:

Houghton, Baumhefner and Washington, 1971: On global initialization of the primitive equations Part II. The divergence component of the horizontal wind. Journal of Applied Meteorology, 10, 626-634.

Most recent work in initialization has been concerned with methods to use the prognostic relationships of the forecast model itself to obtain an initial state for this model. In this way it was hoped that there would be more consistency between the initial conditions and the forecast model.

Several methods were proposed. Miyakoda and Moyer at GFDL considered the following iteration scheme, where PE refers to the primitive equations

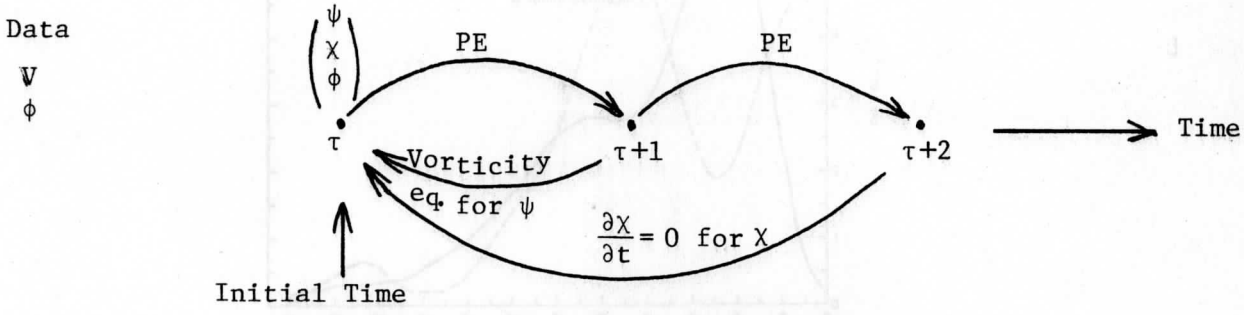

Nitta and Hovermale tried using the complete forecast equations on the forward and backward steps with a time differencing method that was designed to damp high frequency oscillations.

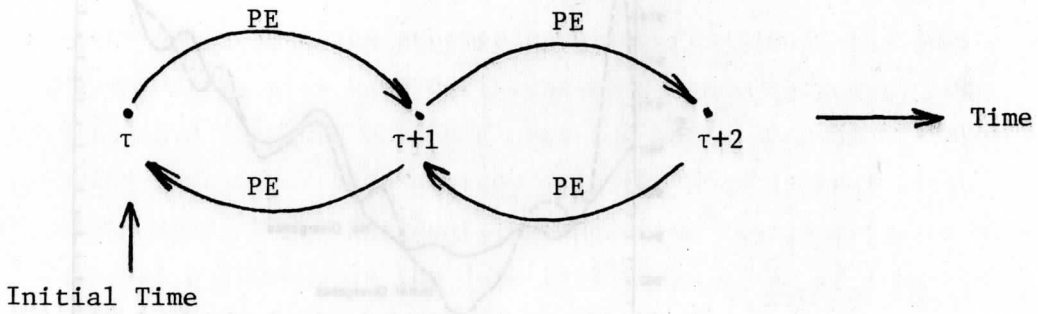

Neither method was successful. One problem was that the diabatic processes could not be properly included.

Recently a method called the "nudging" method has been proposed. Here an artificial term is added to the appropriate equations for a short interval of time to sway the value of the variable towards an observed value. The term is of the form, for example, in the equation of motion

$$\frac{\partial u}{\partial t} = A + K(u-u_o)$$

where A refers to all of the standard physical effects.

With the advent of more frequent observations at non-standard times, initialization involving the prognostic model equations has become more focused on techniques that allow the model to move ahead in time as the information is

added. This is referred to as four dimensional data assimilation. There are two basic strategies called intermittent and continuous data assimilation, respectively.

In the intermittent method the asynchronous observation are merged and inserted into the model at a single time. Observations off the standard time may be projected to the standard time by simple displacement techniques to correct for the time difference. The advantage of grouping the data together is that cross checking of data is possible and filtering and smoothing of the data can be done before insertion. The final system looks very much like the operational weather prediction system where the feedback of the model forecast into the initialization calculation for the new data provides some influence of the model prognostic equations on the initialization

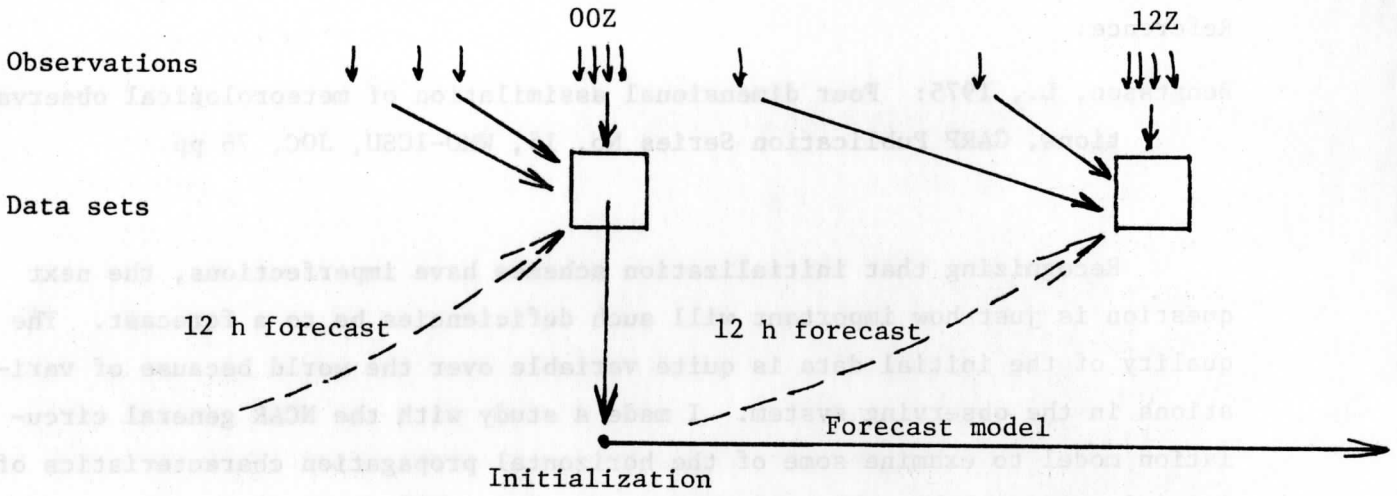

In the continuous assimilation method, the observations are inserted directly into a model to maintain a model based "data bank". At specified times a forecast can then be made starting with the information in this data bank. There are numerous problems. There is lack of quality control of the input data. The noise level grows in the model because of the small scale of the input data at any given time. A strongly damping model numerical scheme is required in order to control the noise level. This means the data bank becomes strongly dependent on the characteristics in the model. The method has not been found to be practical for most situations yet. It works as shown:

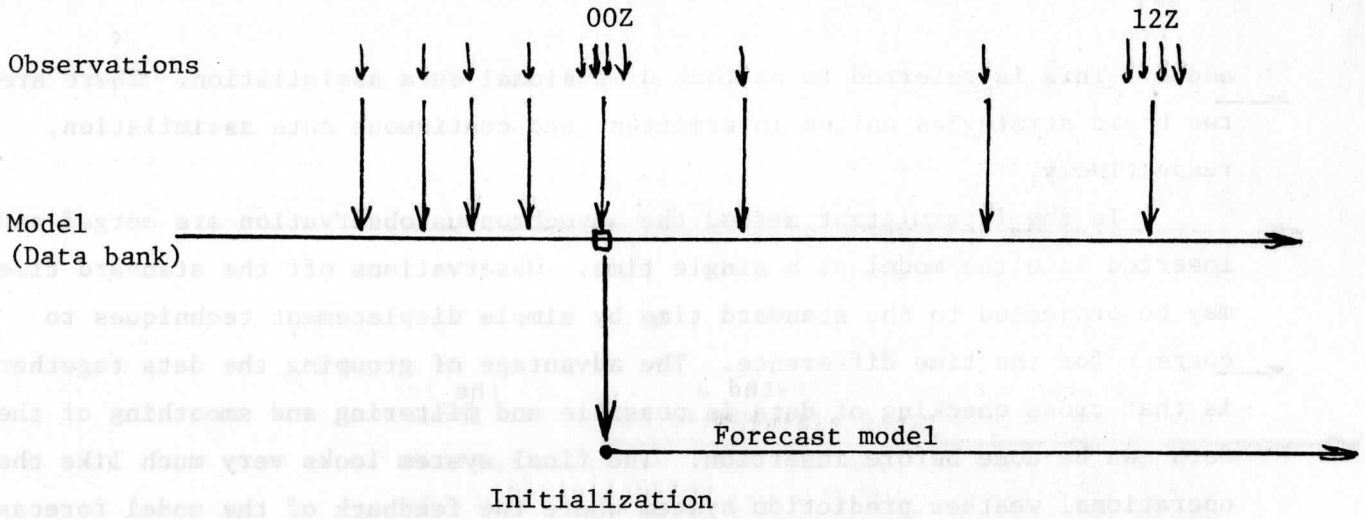

Reference:

Bengtsson, L., 1975: Four dimensional assimilation of meteorological observations, GARP Publication Series No. 15, WMO-ICSU, JOC, 76 pp.

Recognizing that initialization schemes have imperfections, the next question is just how important will such deficiencies be to a forecast. The quality of the initial data is quite variable over the world because of variations in the observing system. I made a study with the NCAR general circulation model to examine some of the horizontal propagation characteristics of initial errors. This was published in the July 1972 issue of J. of Atmospheric Science, p. 816.

Data from 1200 GMT for December 6, 1967 was used to initialize a 5° x 5° version of the NCAR general circulation model. Then 5 day forecasts for this situation with and without the inclusion of a specified error field in the initial data were compared. The differences in the forecasts could be related directly to the error in the initial condition since all other aspects of the model experiments were identical.

The error was placed in the northern Pacific Ocean and covered a circular area with a radius of 2000 km. Three different central latitudes were used in three separate experiments to show the differences between propagation characteristics due to the position of the middle latitude jet stream relative to the error region. The propagation of error effects from the North Pacific is a very practical question for forecasting in the United States since the observations that are available for the Pacific Ocean area are often deficient.

The error was prescribed in the temperature, pressure and velocity fields with internal consistency in terms of the hydrostatic and geostrophic relations imposed. This was to make sure that a significant portion of the error was into the synoptic scale component of motion.

The next two slides show the middle tropospheric pressure and velocity fields at the beginning and end of the forecast period. The central position of the three error fields tested are shown by the letters A, B, and C. The first slide shows that Case A was north of the local position of the jet stream and the other two were south of it. Relative to the zonally averaged zonal flow component, Case A was to the north of the jet maximum, Case B was along the axis and Case C was to the south. The vertical structure resembles somewhat that for baroclinic disturbances as shown in the diagram.

The results of the three cases are shown separately in the diagrams in terms of both the pressure and velocity vector difference magnitudes. For Case A, the effects remain primarily north of the jet axis for the five day period. There is some influence noted in the tropical region in the velocity field after 5 days. There is a remarkable persistence of the error at the initial location. In Case B, the error does not spread across the polar region into the Eastern Hemisphere as much. The eastward propagation rate along the jet stream ranges from 10 to 20 m sec^{-1} which is approximately the vertically averaged zonal velocity magnitude in the polar jet stream region. More of the error shows up in the tropical regions than in Case A and a little even gets into the middle latitudes of the Southern Hemisphere. As in Case A there is a remarkable persistence of error in the original position. This has implications for the initialization method using a model forecast as the first guess. It means that an error in a given initial data field can persist and show up in subsequent initial data fields. In Case C, the error remains almost entirely in the tropical and subtropical regions where it has spread around the globe after 5 days.

Examining the globally averaged root mean square difference statistics shows the growth of these quantities (which are associated with predictability experiments) have with a doubling time in the order of 7 days. This is greater than the doubling time associated with predictability studies using very small initial perturbations. The velocity difference map in Case B at a higher level shows that errors are larger there than at the mid tropospheric levels.

Even after running the forecast experiments for 7 days, it was noted that some parts of the Northern Hemisphere particularly in the region of

Siberia did not have much difference in the solutions. This would imply that the initial conditions in the North Pacific are not crucial for a forecast up to 7 days in Siberia.

It is useful to know what areas must have good observations in order to make a forecast at a given location for a specified length of time (the so-called "domain of dependence" using mathematician's terminology). This would help alert the forecaster to the expected quality of a forecast from information about the quality of the initial data set.

It is generally agreed that a two week forecast in most places would require initial data of reasonable quality from all over the world. It is interesting to note, however, that currently the U.S. Weather Service provides forecasts out to 10 and 1/2 days using only northern Hemispheric data. These requirements for longer range forecasting should encourage a cooperating spirit among countries of the world, at least, for the meteorological data.

In summary, initialization is a vital problem for synoptic and mesoscale prediction models. There is no one standard procedure which is accepted as the best method even for the synoptic scale. The accomplishments are very preliminary for the mesoscale. New forms of data, unclear behavior characteristics of the models, and the lack of diagnostic relationships make general mesoscale model initialization a real challenge to the meteorologist.

E. Recent Technical Advances (SSEC-McIDAS)

I want to digress somewhat from my lectures on scientific matters, and in particular problems in numerical modelling, in order to talk about some recent technical advances in the handling and display of meteorological data that have taken place in our country. The technical advances have opened many new possibilities for operational forecasting and research activity. It is hard enough for the researcher and teacher to keep up with advances in science. It is impossible for us to keep up with technology which is flooding our institutions with new data and new ways to study and understand it.

I showed two movies made at NCAR from general circulation model output. These represent the forerunners of a technology that is emphasizing the visual and pictoral methods of studying data. Those movies were made directly from a 35 mm filmstrip produced on the NCAR computer system. The digital numerical model output was used to specify the drawing of contour lines on a cathode ray tube (CRT) device which is the same as a TV screen. Other program subroutines added the plotting of labels. Then the picture was automatically photographed.

This output method can be used for any form of output from the computer including the standard printed numbers. This increases the rate of output from the computer by well over a factor of 100 from the usual printer method. The microfilm is also more compact since one small reel of film about 5 inches or 12 cm in diameter holds all of the data printed on 2000 computer print out pages, which would make a pile over 25 cm high.

Of course there is still the problem for the scientist to have the time to look at all this information. That is where the use of automatically made plots and graphs becomes essential. The video computer output allows us to see in an easy manner the fourth dimension in our scientific problems, namely time. This capability was important for me to be able to understand the details of evolution in some of my modeling studies. I will be showing more of this type of computer output in later lectures.

Computers are becoming more versatile and omnipresent in American society. They are now used for more than basic mathematical calculations and data processing in institutions. National reservation systems in hotels and for trains, airplanes, and busses now use computers. A key point is that they are being integrated with communication systems. The same is happening in meteorology. Our National Weather Service is now installing a national data transmission and handling network that uses computer systems at each station. This is called AFOS which I believe stands for Automated Field Observing System. It is intended that this will replace our system of teletype and facsimile machines. It means that persons at local weather stations will be able to rapidly access the data they want to see without having to scan many sheets of paper.

The University of Wisconsin has been a leader in the development of computerized data processing systems for meteorology. One of the usual exhibits for anyone visiting the meteorological group at Wisconsin is this computer system. It has been developed in the Space Science and Engineering Center under the direction of Prof. Suomi. It was initially needed to handle the large amounts of data that the satellite systems were providing. Soon the advantages for handling all of the types of data in meteorology became apparent.

The system is referred to as McIDAS with the initials standing for "Man computer Interactive Data Access System". Prof. Suomi purposely wrote the word "computer" without a capital letter to emphasize that it was the man and not the computer that was the master of the system. It consists of six minicomputers. Two of these are devoted to managing the enormous amount of data and are called "data base managers". The other four support the processing and

display activities of numerous terminal stations. The stations have television screens and control keyboards. The diagram shows a schematic plan of the system.

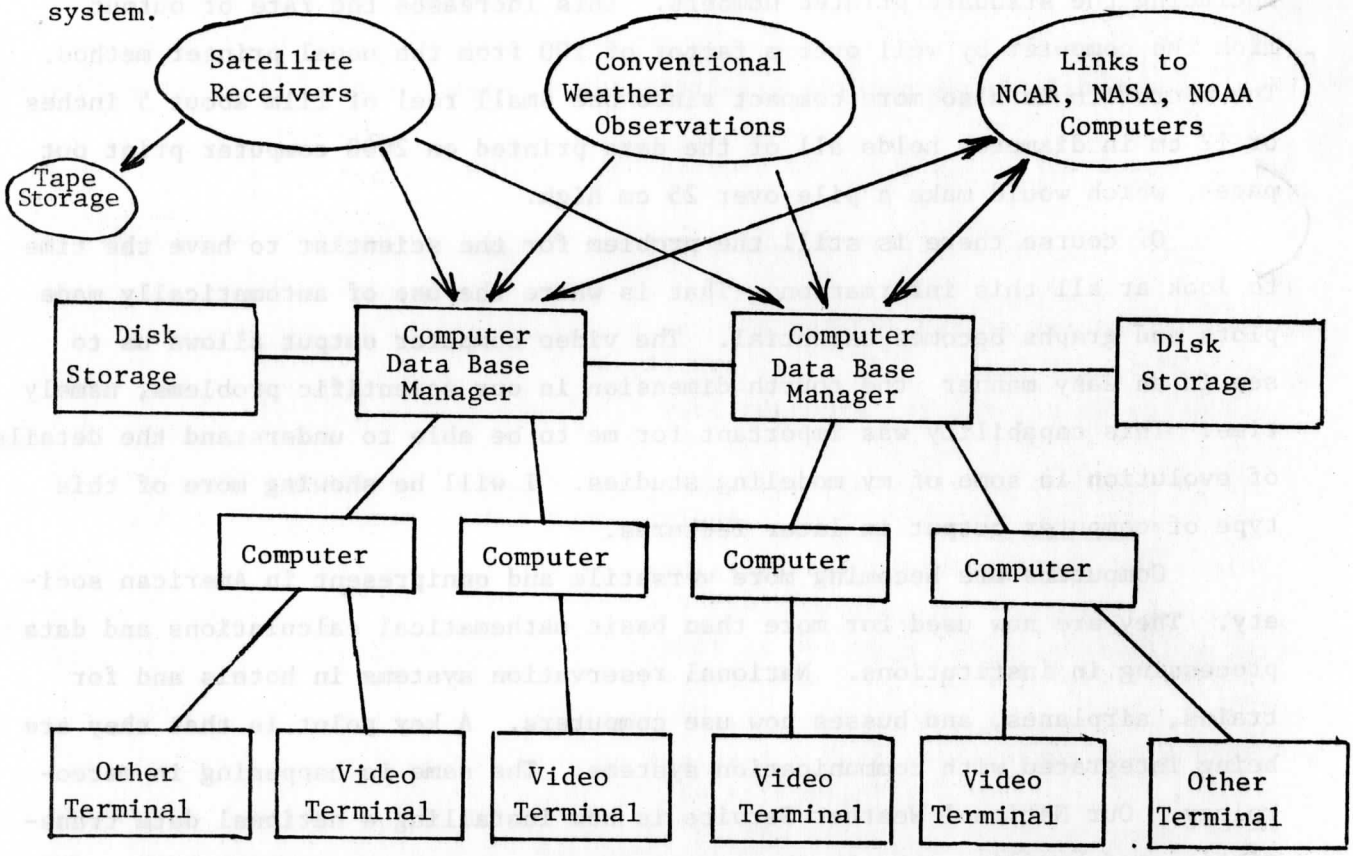

This diagram is intended only to be a schematic, so that the details of the connecting lines and the number of terminals are not to be taken seriously. By the time I return to Wisconsin we should also have direct communication links to the major computer systems at NCAR, NASA and the National Weather Service of NOAA.

In the spirit of this lecture topic, I now wish to show a larger than usual number of visual displays to explain the system and its capabilities. These slides and movie are that same ones used at the first national presentation of our system made at the American Meteorological Society annual meeting in Tuscon, Arizona in January of 1977 by Tom Whittaker.

Slide depiction by number

1. This is to represent where we stand now with weather maps on paper with hand drawn fronts.
2. The data room in the Meteorology Department is equipped with machines of the conventional system. Teletypewriters provide listings of local observation taken on an hourly basis and synoptic data gathered every 12 hours.

Also numerous forecast messages are received. The machine in the back is a facsimile which produces weather maps according to information fed in at the main offices in Washington, D.C. and vicinity.

3. A close-up of the surface weather chart produced by the facsimile machine. This form of information is what we and our students have been used to for many years.
4. New forms of data from the satellite systems have been added to our available information. Here we see one of the many visible images from the geosynchronous satellites received daily. Storm systems and surface features such as the Great Lakes are easily distinguished.
5. Techniques of accurate navigation for these pictures makes it possible to overlay geographic markers.
6. Information of other atmospheric variables can then also be superimposed on the picture.
7. The satellite information in the McIDAS system at Wisconsin is received by antennas on top of our building. We now have two antennas and can receive information simultaneously from both of the geosynchronous satellites that view the U.S.
8. Here is a close-up view of one of the antennas. I believe it is approximately 20 feet (6.5 m) in diameter.
9. The satellite data is transmitted to this demodulating receiving unit on the 6th floor.
10. There it is read onto slant 9-track tape systems for storage.
11. The data is also placed on file in one of these disk storage units.
12. This is a close-up of one of the disk storage units. The rapidly spinning memory unit makes all of the data for one TV image available in a short time so that the TV image can be produced with little delay.
13. The other end of the McIDAS system is the terminal. Many are equipped with television screens so that the operator (scientist user) can view the data in pictorial form.
14. Here is a close-up of the terminal system. The TV screen, the control keyboard, and a monitor TV which can display some data and which shows the control messages.
15. The geosynchronous satellite can see about one third of the total surface of the earth.
16. Accurate navigation allows the placement of a grid on the image.
17. The data base maintained in the computer system allows for the organizing of the data in many ways in contrast to the printer which provides it in a list according to a specified order of stations.
18. The McIDAS system stores hourly reports from up to 1100 stations for 100 hours. Thus it is possible to have lists produced immediately for the conditions at a single station such as shown here for Madison.
19. It is also possible to produce listings for all stations that have a certain kind of weather condition. Here are shown all stations in the Midwestern United States reporting snow showers. Any of the meteorological parameters could be used as the basis for making such lists.

20. The system can show plots of all stations reporting a certain type of weather.

21. It is possible to receive all these lists and plots on paper so it can be saved by using a printer output.

22. Here hourly station data is automatically printed along with geographical boundary information.

23. Here are the 24 hour surface temperature pressure change (in tenths of mb) reports.

24. Here is a listing of surface equivalent potential temperature data for the entire U.S.

25. Here are the surface temperature reports for the region around Tuscon, Arizona (where the AMS meeting was held).

26. The printer can also immediately make contours for the fields being displayed.

27. Or it can show regularly spaced values for the variable produced by an objective analysis of the observations.

28. We have TV terminal screens in several of our classrooms so that weather data can be displayed for class discussions.

29. The computer system can show a number of analyses forms and derived variables such as moisture advection magnitudes in pictorial form. Here a surface streamline analysis is shown.

30. Multiple parameters may also be analyzed. Here the isotach field has been superimposed in yellow on top of the streamlines.

31. The analysis can look at a smaller region if more detail is needed.

32. The temperature in °C is shown for the same area.

33. Here the derived quantity, temperature advection, in °C per day is shown over top of the streamline field.

34. It is possible to show several maps side by side.

35. Satellite data for a specified region is displayed complete with geographical boundaries.

36. Surface temperature data in °C is shown over the satellite data. It is contoured which quickly points out gross data errors. Here a 65°C temperature for Pittsburgh makes an easily noticed pattern in the contours allowing quick detection and then elimination or correction of the data value.

37. Temperature data in °C is plotted on top of the satellite data.

38. Another parameter is plotted over the satellite cloud data.

39. Here is an expansion of one region of the previous satellite picture with surface wind data shown on top.

40. Finally for reference is the starting point for this discussion.

- -

The description of the McIDAS system would not be complete without showing the system in action. The movie to be shown next was taken directly from the terminal TV screen while certain displays were being made. In it you can see several analyses being made at once demonstrating the time sharing nature of the computer system. (Show movie.)

The system has been expanded to include the upper air radiosonde and rawinsonde information. Soon dial-up telephone links will make it possible to receive and display radar data.

This display system also has application to numerical model studies. Soon we hope to be able to display numerical model output in this system. Then it will be possible to show in rapid sequence the model output as a function of time and thereby show the characteristics of evolution as was done in the NCAR computer movies.

To carry this technology even further, the video display in color allows for the possibility for stereoscopic presentations so that the eye can see the depth or height difference of the plotted information. Recently I had the opportunity to see the video display system at NASA. There by looking through a special set of glasses, the wind vectors from a model output grid were displayed and the higher level winds appeared above the low level ones. With the same system I viewed simultaneously the pictures of the same clouds as seen from two different satellites.

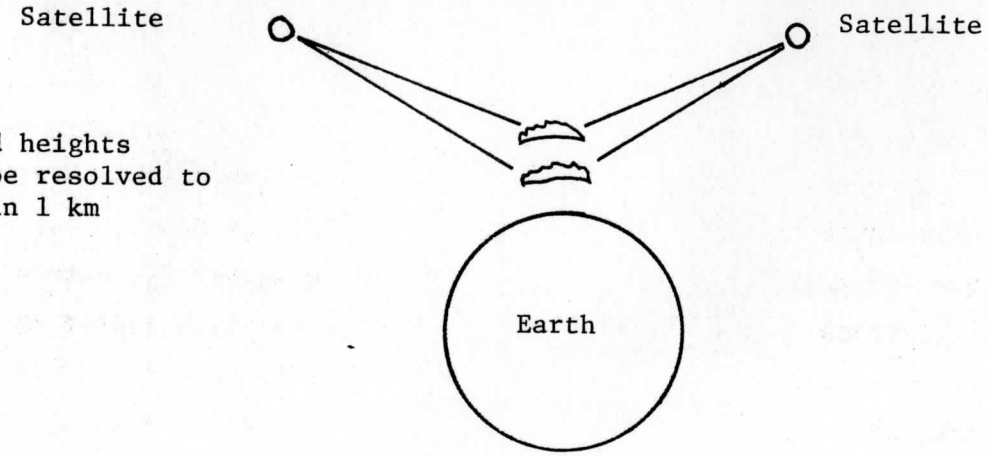

By the appropriate allignment of the images, it was possible to see a true stereo effect so that the high clouds appeared above the low ones.

Thus it seems that the technology will be able to give us everything except the scientific understanding itself. It is a very exciting time but the temptation to be led astray by the glamor is great. Scientific understanding does not come so easily.

Reference:

Proceedings on a workshop on video display applications in meteorology held at the University of Wisconsin in the summer of 1977. Published by Space Science and Engineering Center at the University of Wisconsin.

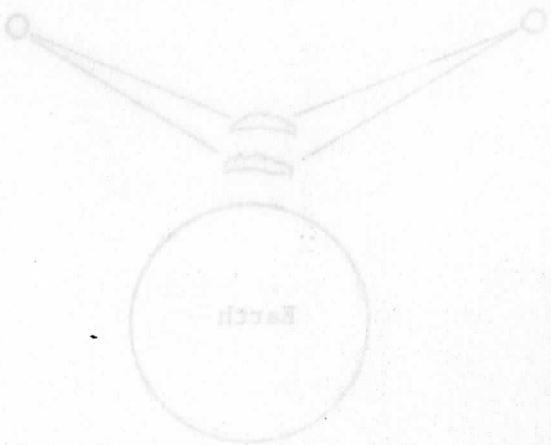

II. DYNAMICS OF LARGE SCALE MOTIONS

A. Basic Observations and Dynamics

An extensive routine observation system for synoptic scale meteorology has been established in many parts of the world. For many years, this was based on the data collected by radiosonde soundings which provided information on the wind, temperature and moisture from the surface up into the lower stratosphere. The observations were taken mainly over land areas because that is where the data had the most justification for many applications and because ocean (ship) based systems were very expensive.

The growing interest in improving forecasts especially by using numerical prediction models and for periods of several days or more has required a more uniform data from over the world. In my lecture on initialization, I showed how the forecast in one area could be greatly affected by initial data specification elsewhere. For forecasts of several days, I demonstrated how the initial data from the Pacific Ocean area could affect the patterns over the United States. Studies of the general circulation and global scale waves also require a more uniform observing system.

The figure shows the radiosonde and rawinsonde observing network. China and Japan, Central Europe and the United States have the best coverage. The Atlantic and Pacific Ocean areas are very poor. The Southern Hemisphere, being almost all water covered, is very poor. The tropical region has little coverage over the ocean areas except for the island based network in the Western Pacific.

Thw World Meteorological Organization has been working for many years to improve observing network. Recently, a special effort was made to provide a total global coverage for the observations for a one year period. This program is referred to as the First "Global Atmospheric Research Program" Global Experiment, terminology shortened to First GARP Global Experiment and then to FGGE. A massive array of satellites, aircraft, ocean surface buoys, and ship based rawinsonde observations were used to augment the existing system and to fill in the poor data areas. The special observing program has just ended and the processing and analysis of the data is underway.

Satellite data

Satellite based observing systems have provided us with an entirely new viewpoint of the atmosphere. Polar orbiting satellites began taking observations in 1960 and those placed at a higher altitude to make them geosynchronous (stationary with respect to a point on the earth's surface) have been making

observations since 1966. A geosynchronous satellite can see about one third of the earth's surface at one time and thus more uniform and complete data coverage is possible.

Professor Suomi at the University of Wisconsin has been leading an effort to develop remote sensing systems for the satellites and to find ways to extract information from the data. Many other faculty at Wisconsin, including myself, have become interested in studies to improve our utilization of this new form of data.

Satellite data can be used to estimate many of the atmospheric variables. Perhaps when Dr. Smith was visiting your country last year, he described some of the possibilities. I will list a few. Short wave or visible radiation gives information on the albedo of the earth-atmosphere system and includes cloud positions. Many new insights about the behavior of the atmosphere have resulted from this cloud data which was never before available. Long wave or infrared radiation sensed by the satellite gives information on temperatures at the earth surface, cloud surfaces and other areas in the atmosphere which emits such radiation. By selecting certain wavelength ranges for this sensing, it is possible to obtain vertical temperature structure data for the atmosphere in cloud-free areas. Sensing at the microwave range promises to give useful information on the water vapor and liquid water content of the atmosphere so that someday rainfall rate determinations might be possible. Special information such as the sun glint (reflected visible light) from the sea surface is being analyzed for possible information about low level winds. Finally, the fact that the geosynchronous satellites remain fixed in position makes it possible to accurately determine the motions of clouds and other features observed by the satellite. To the extent these motions correspond to air flow, valuable information about the wind fields can be obtained. A more exotic type meteorological observation by satellites is for the occurrence of lightning discharges at night. This information has been used for studies of convective activity.

To demonstrate the range of information received from the geosynchronous satellite, I will show a few images produced by the most sophisticated system put up so far, the METEOSAT, which was developed by the European nations. The first slide shows the visible image for February 8, 1978. The center position is at zero degrees longitude on the equator. The reflection from the desert surface and dust over Northern Africa appears whitish. Tropical and extra-tropical cloud structures are evident. Both the low level and high level clouds

show up well. The next slide shows the infrared image for the same time. The dark areas are regions where the infrared intensity is the greatest. The high clouds, which are cold, show up as white. The hot Saharan desert, being the hottest region, shows up as black. It is possible to distinguish low clouds from high clouds because the low ones appear dark. The next slide shows a water-vapor sensing infrared wavelength image. This is a new observing capability for geosynchronous satellites. This wavelength is most sensitive to water vapor in the upper troposphere as well as the clouds. The water vapor information is more continuous in nature than the cloud data and it is possible to see considerable structure in the North Atlantic area. It also complements the cloud data filling in between the cloud areas.

The two circular structures on either side of the Atlantic Ocean at 15°S in the water vapor prompted a bet between Prof. Suomi and myself as to whether or not both were cyclonic circulations or whether one was cyclonic and the other anticyclonic. They looked more similar in this image in contrast to the other two images. In order to resolve the issue, we obtained upper tropospheric wind field analyses at 250 and 500 mb. As the next figure shows, the circulation in the two areas is of the opposite sign, so Suomi won the bet.

Reference: Bulletin of The American Meteorological Society, 1978, p. 1614.

During the FGGE program there were five geosynchronous satellites viewing the earth spaced around the equator so that coverage was complete. I am not sure of the exact longitudes but they were approximately 0°, 75°W, 120° or 135°W, 140°E and 70°E.

Since a geosynchronous satellite sees out to about 75° in longitude or latitude from the sub satellite point the images overlapped considerably in the tropical regions and coverage was complete to about 60°N and 60°S. Quantitative determinations of motions from the cloud images is not possible for distances exceeding about 50° latitude or longitude from the sub-satellite point. Thus the overlap in data is not as much as indicated above.

Being able to view the motions of the clouds from the geosynchronous satellites has been one of the most exciting new forms of data made available. The time lapse pictures have provided new insights about all scales of motion in the atmosphere. In some cases the complexity of motions such as the thin jet streaks seen streaming from the tropical areas into the middle latitudes

has confused previous simple concepts of atmospheric circulation and dynamics. Conceptual models of smooth wave type flows and Hadley circulations now have to be revised to account for streak and vortex type structures.

I was fortunate to be able to bring with me a time lapse movie of images obtained by the Japanese geosynchronous satellite located over the equator at 140°E. This had been supplied to the Space Science and Engineering Center by a scientist from the Japanese Meteorological agency. With it, the dramatic nature of motions over and east of China can be shown. It covers the circular area from approximately 65°E to 145°W along the equator and from 75°S to 75°N along the 140°E longitude. China appears in the upper left hand quadrant of the image. Infrared images at 30 min intervals are shown which are continuous from day to night. The nine month period from April 1978 to December 1978 is presented.

I do not know how many of you have ever had the chance to view such global scale information before. There are so many things to notice that I propose showing the movie twice. I believe it is well worth the time. Features to look for include the westward moving tropical disturbances and typhoons, the intertropical convergence zone activity, extratropical cyclone development, convective activity when cold Siberian outbreaks push over the warm Pacific waters, irregularities in the flow coming off the Tibetan plateau and the diurnal temperature oscillation in the Australian deserts.

I have only seen this film once myself and wait to see it again before making too many comments.

(Show movie and add comments as it proceeds.)

Global scale motions

The previous discussion about satellite data suggest that the time may not be far off when the description of the general circulation will be complete enough to allow comprehensive studies of the global scale waves. The global component of motion is strongly influenced by topography and sensible and latent heating effects.

Nevertheless, the analyses of observations that have been made over the past 20 years in connection with operational numerical weather prediction have already provided some description of the longer term and quasi-stationary flow components in the Northern Hemisphere. In this lecture, I will present some of the data. Discussion of some of the dynamics of the forced wave motions will be included in the next lecture.

A movie made by NCAR in 1974 of 500 mb height analyses provides a unique opportunity to show some of the characteristics of the global scale motions. The movie consists of three parts:

1) Sequence of twice daily maps from August 1, 1969 to July 30, 1970 for 500 mb heights in a polar projection. This shows the evolution of both the slowly varying forced components and the more rapidly varying short wave components.
2) Sequence of time-filtered analyses for the 5 year period from July 1, 1966 to June 30, 1971. A 17 point low-pass filter was applied to 2-day averaged maps which nearly completely removed fluctuations with periods shorter than 10 days with little effect on those with periods greater than 20 days.
3) Sequence for the high frequency fluctuations superimposed upon the time-smoothed analyses shown in part two for the same dates as in the first part, August 1, 1969 to July 30, 1970.

Again as with the satellite movie, there is much to look at and it is very helpful to show the film twice in order to better appreciate its content. Some of the features to look for are the following:

(Much of this descriptive material is taken from NCAR Technical Note, NCAR-TN-STR-94 printed January 1974 by NCAR, "Observed Long-Period Fluctuations in 500 mb Heights -- Supplementary Text to NCAR Films J-4 and J-6".)

Sequence 1:

At all seasons, the polar vortex is distorted by wavelike undulations and by closed highs and lows which have their own vortical circulations. Some of these features tend to recur in particular geographical regions. For example, during the winter season there is usually a broad trough extending from the coast of China, eastward over Japan and into the Central Pacific. The westerly jet is usually quite strong and quite far south at these longitudes.

The atmosphere exhibits a great deal of complicated time variability with the waves and circulations constantly changing in position and intensity. It is apparent that most of the day-to-day fluctuations are related to the eastward propagation of small scale waves with wavelengths ranging from 2,000 to 10,000 km. These appear to be advected by the "steering flow" upon which they are superimposed. In some cases, it is possible to follow a particular short wave ridge or trough for a week or longer.

Sequence 2:

In this sequence only the low-frequency components are present and some characteristics of the "steering flow" for the smaller scale waves may be observed. The flow patterns are somewhat larger in scale than those in Sequence 1; however, it is clear that the patterns contain more than just the ultralong waves. The fluctuations do not show any marked tendency for eastward phase propagation. In fact westward or retrograde movement is quite common. Shifts and splits in the jet appear to be associated with developing features that radiate southward from the pole.

Global scale features such as transient waves and zonal flow are quite prominent. Changes in the position, orientation and intensity of the associated jet stream take place nearly simultaneously over wide ranges of longitude. Jets are easily identified as dark regions of compressed isolines. Except for obvious seasonal changes there is little evidence that certain favored patterns tend to be established at regular intervals. An intermittency of similar patterns is noted.

Sequence 3:

A steering of the high frequency component by the low frequency component is evident. However, since there is no real spectral gap in the time domain, the interaction between the two frequency components is not simply that the low frequency one advects the high frequency one. The growth and decay of the high frequency components as well as their motion are influenced by such interrelations.

(Show and discuss movie.)

I have shown much material today based upon real observations. Having such information does not mean that we understand it or that research to understand it will be easy. Much more basic research into the important nonlinear interactions and the basic forcing mechanisms due to radiation, convection and lower boundary for large scale motion is needed. These studies will require careful numerical studies and plenty of insight into the dynamics.

B. Effects of Sea Surface Temperature Conditions on the large-scale motions.

In this lecture, I wish to discuss in detail a series of studies that I and colleagues have done in the last 10 years concerning the effects of sea surface temperature conditions on the large-scale motions. These studies used the general circulation model at NCAR and represented one of the many applications that general circulation models have had for research in the atmospheric

sciences.

Many of the points discussed here today appear in three publications:

Houghton, Kutzbach, McClintock, Suchman, 1974. Response of a general circulation model to a sea temperature perturbation. J. Atmospheric Sciences, 31, 857-868.

Kutzbach, Chervin, Houghton, 1977. Response of the NCAR general circulation model to prescribed changes in ocean surface temperature, Part I. Mid-Latitude Changes. J. of Atmospheric Sciences, 34, 1200-1213.

Chervin, Kutzbach, Houghton, Gallimore, 1980. Response of the NCAR general circulation model to prescribed changes in ocean surface temperature, Part II: Mid-latitude and sub-tropical changes. J. of Atmospheric Sciences. 37, (to be published in February issue).

In these studies many practical problems concerning the use of general circulation models had to be handled. Some of these issues will be discussed here. It should become quite clear that although producing a model that works and which makes reasonable simulations is a major task, it is even more of a task to have the model provide sound scientific advances.

The NCAR general circulation model, like any general circulation model, has deficiencies in its simulation of the atmosphere. The nature of these deficiencies became more and more apparent as the scientific study progressed. Careful experimental design was important to minimize the effect of the errors on the conclusions. Without having an understanding of basic dynamics, it would have been very difficult to accomplish as much with this research. It is important that strong education in basic synoptics and dynamics be continued and that we not depend on the numerical models to handle all of our future problems in meteorology by themselves.

I began these studies with a general interest in understanding the larger scale motions of the atmosphere. The time-averaged characteristics of these motions are important for determining the anomalous weather situations that may persist for several weeks, a season or even longer. Variability and anomalous conditions are topics of climate that have very direct application to problems of agriculture and energy.

For these large scales and longer time periods, forcing mechanisms play an important role. The primary forcing factors for the atmosphere include topography, radiative heating and cooling, surface heat flux, and latent heat release in the atmosphere, which is related to surface moisture flux

characteristics. There has been much research done to compare the relative effects of surface heating to the mountain or topography effect.

My original interest was in the problem of the effects of air pollution on climate characteristics. It soon became apparent that this would be a relatively small effect in the model and that before meaningful studies could be made, understanding the model response to more basic forcing processes would be essential.

The influence of the ocean surface conditions on the atmosphere is large. Ocean-atmospheric interaction on time scales of months to years is considered an essential element for any large scale climate study model. Numerous theoretical and observational studies have been made to investigate the relationships between the atmospheric and oceanic conditions.

For the studies here, the effect of the ocean on the atmosphere was considered. This is only one half of the interaction cycle but understanding this half would logically help to understand the entire interacting system. In particular, the research focused on the effect of sea surface temperature conditions on the monthly-averaged conditions in the general circulation for the wintertime season. There were several reasons for this focus:

a) The time scale for study was one readily obtained in the general circulation models. Computer simulations have been made for periods as long as 9 years with these models. However, the need to make many individual simulations for proper experimental design meant that a several month simulation was the longest that could be considered.

b) The time scale for atmospheric response to prescribed sea surface conditions would be at least several weeks based on dynamical reasoning, thus time periods less than one month would not be meaningful.

c) Data were available in monthly averaged form from observational studies that ineluded comparing atmospheric conditions in January with oceanic conditions for the previous month of December.

d) At the time when these studies began only the wintertime simulations with the NCAR general circulation model were good at all.

Study for the North Atlantic Sector and Europe

The first model experiments were for examining the effect of prescribed sea surface temperature anomalies in the North Atlantic Ocean with observed responses in surface pressure over Europe. This was a situation for which an

extensive observational analysis had been made. Ratcliffe and Murray in England had examined 80 of observational data to determine correlations between December sea surface temperatures to surface pressure over Europe. They had classified the years according to the sea surface temperature (SST) anomaly patterns. Of these 80 years, 13 had conditions when SST conditions were close to the 80 year average. These defined the reference or control situation. Thirteen of the 80 years were characterized by warmer than normal SST with temperature deviations reaching an average maximum of 2°C in the Western part of the North Atlantic. Nine of the years were representative of SST considerably colder than normal. For each set of years, the corresponding surface pressure data from Europe was averaged and anomalies of surface pressure from normal conditions were determined.

Thus, the North Atlantic area had a good set of verification statistics available and this was considered then to be the most essential requirement for a model experiment. The effect of the ocean on the atmosphere in the middle latitudes would certainly involve the extratropical cyclone systems. I showed earlier, that the characteristics of extratropical cyclone position and movement was one of the significantly deficient aspects of a general circulation model simulation. The maximum SST anomalies tended to be at the 35° - 45° latitude. This is where a major occurrence of cyclone storm centers exist in the atmosphere observations. However, in the control case the model was shown to have very few storm centers at these latitudes. Thus there was reason to expect problems in the model simulation.

I will show the results for the warmer than normal SST case based upon a single general circulation model calculation. The anomaly was prescribed in the model at the initial time starting from an isothermal state of rest. After 30 days the model was assumed to have reached some degree of equilibrium averaged so the monthly averaged state was computed from the day 31 to day 60 period. It was this average which was compared to the observations.

The first slide reviews the characteristics of the model in simulating the extratropical cyclones. The observed maximum of cyclone activity near New Foundland, Canada was the area where the warmest SST anomaly conditions were in the observations. The next slide shows the basic results in terms of surface pressure anomalies. Surface pressure was the one variable for which verification data existed. The maps on the left hand side showed some encouraging aspects to the model simulation. Pressures over the central Atlantic and into western Europe were lower than normal while those over Greenland and Northern

Europe were higher than normal. The implied reduction in the westerly flow over central Europe was the feature that Ratcliffe and Murray had found in their original study. It was simulated in the model results.

We could have stopped here, published the results, and have claimed a success for general circulation models. However, it quickly became clear that the solutions presented more questions than answers and there were a long list of major questions that had to be answered before any scientific advances could be claimed.

The first problem became apparent when we allowed the model to run for a longer period and then looked at the average conditions. For day 51 to day 80 as shown in the figure on the right side, the results for sea surface pressure changed drastically. Pressures remained below normal over the central Atlantic, but value and the sign of the pressure anomaly changed over southern and northern Europe and Greenland. The results now were opposite to the verification data over Europe and the experiment looked like a failure.

To make matters worse, there were other difficulties noticed. When the anomaly in SST was inserted at 20 days instead of at the initial time, the results for the 31-60 and 51-80 day periods were changed again. Furthermore, when looking at the pressure anomalies over the entire world as shown in the next slide, there were larger effects in regions other than the North Atlantic Sector. There was no obvious dynamical reasoning that could explain these other changes.

Thus the entire question of model response to imposed forcing conditions had to be reconsidered and new experimental methods formulated. Questions included

a) The importance of model deficiencies to the meaning of intermodel comparisons.

b) The importance of initial conditions.

c) Time scale to achieve statistical stationarity and equilibrium in a constant-season general circulation model.

d) The sensitivity of model solutions to any imposed effects.

e) Determining the general significance (statistical or physical) of any model change results.

Studies on Determining the Significance of model responses

A number of approaches were used to give better understanding of the general significance for general circulation model responses. At this point attention turned to experiments that were being made with the effects of SST changes in the Pacific Ocean area.

The model response to a situation where SST was increased over the eastern Pacific and decreased over the western Pacific was investigated. Two additional calculations were made besides the one intended to represent actual observed SST changes. In one the magnitude of the SST anomaly was multiplied by three. It was hoped that this would improve the "signal to noise" ratio in the model without introducing new nonlinear effects in the signal which would cause new deficiencies in the signal. In the second experiment, no SST anomaly was introduced, however, a small random type forcing effect was introduced to the model at an earlier time. This experiment was intended to show the spatial characteristics of the natural variability in the model which represents noise for the SST anomaly studies.

Then two additional manipulations were made with the model results. In one, all of the model change fields were normalized by (divided by) the standard deviations for variations in these variables. This natural variability was determined by examining an ensemble of five realizations of the control case which were intended to represent a set of independent cases. The second manipulation was to consider a longer term average in the solution.

All of these analyses were intended to give more information about the signal and noise characteristics in the model responses and to help in distinguishing the signal component. The next four slides show the results. They demonstrate that there is success in this approach for analysis of general circulation model results.

Examining theoretical solutions was another method considered for better understanding the model results. Some analytical solutions have been made for forced atmospheric waves. For example Döös in a 1962 study (Tellus, p. 133) investigated separately the influences of vertical variations in sensible heating, the zonal wind profile, and friction on the planetary flow, using linear model solutions. For the most realistic choice of model parameters (his model 1a) he obtained a surface trough directly over a positive surface air temperature maximum which in turn was located about 30° longitude to the east of the region of maximum surface heating. The pressure trough tilted westward with height so that at a height of 500 mb a ridge was only 30° to the east of the surface air temperature maximum.

Other types of numerical prediction models can also provide independent information on solutions expected due to forcing. Egger in a paper (for which I do not have the reference here) found some solutions for flow in a channel where a forcing effect was introduced at the center. He also applied this

linear model to the North Atlantic case discussed earlier. The next three slides illustrate these theoretical solutions.

Studies to further improve the understanding of GCM output

A basic approach to improve our understanding of the model solutions involves a complete three dimensional analyses of the results and looking at many of the dependent variable at the same time. In this approach there is no hope to compare some of the fields with verification data. However, internal consistency and correspondence with dynamic principles can be evaluated and this helps to determine significant aspects of the model simulations.

To demonstrate this approach, I will present material from the second paper referred to at the beginning of the lecture. In this study the model response to a SST in the middle latitude belt of the Pacific Ocean area was considered. The basic SST anomalies imposed had warmer than normal temperatures in the eastern Pacific and colder than normal temperatures in the western Pacific. This was a "dipole" pattern. It was used instead of an anomaly of a single sign because it corresponded better to the forcing that Döös used in his theoretical model and because it was an anomaly pattern that had been used in other studies.

The basic SST anomaly pattern is shown in the next slide. It shows a maximum amplitude of 4°C which is larger than expected for an average anomaly condition, but perhaps which might be observed in a single year. For this study, the basic SST anomaly magnitudes were multiplied by three. Such anomalies are referred to as "super anomalies". This adjustment was considered essential for demonstrating the capabilities of the diagnostic analyses. In some cases, it was evident that the abnormally large nonlinear effects introduced some unrealistic features. The analyses shown here are the type that should be made when more realistic models are available and when experimental design capabilities allow for better evaluation of the response due to realistic SST boundary forcing.

It is useful first to look at the simulation accuracy of the control case. The next slide shows the simulated 6 km pressure field, the sea level pressure and the storm track for a 30 day period. The areas where the SST anomalies are to be imposed are shown for reference. These simulations are not particularly realistic. The 6 km pressure field is perhaps not too bad, but the surface pressure fails to show an adequate Aleutian Low. Storms do not move across the central Pacific as much as observed.

The next slide shows the changes in the solutions for pressure, vertical velocity and temperature in the monthly-averaged state due to the SST changes. By viewing these fields at the same time, it is possible to see some important details of the dynamical structure of the response. In particular, the direct thermal circulation and the westward tilt with height of the structure is noted. The westward tilt with height is even more clearly shown in the cross-section diagrams.

Examining the effect of the SST anomalies on the tracks and intensity of the extratropical cyclones as shown in the next diagram helps to distinguish between the model response for different cases. By comparing these patterns to the control case and with each other, it is possible to get some feeling for the relative importance of baroclinic processes to latent and sensible heating. A change of storm activity at the edges of the anomaly patterns suggests a baroclinic effect, and changes directly over the anomaly centers suggests local diabatic effects. Understanding the details of the mechanisms that relate the lower boundary forcing to the time averaged response is important.

The global scale response is also of interest. The next slide shows the northern Hemisphere response in the 6 km pressure field, a variable which shows a pronounced signature of response far distant from the forcing area. This effect makes sense in terms of the dynamics. It is important to determine how significant the distant responses are. In the next diagram, the pressure field response is normalized by the January standard deviations in this variable due to natural fluctuations in the model. In this case values of the ratio of 3, 4, and 5 are statistically significant at the 10%, 5% and 2 1/2% confidence levels, respectively, according to the two-sided "t" test. Thus some responses away from the forcing area appear to be significant, even in the case where the SST anomaly values are not three times the realistic value. Although I do not have a slide to show it here, a similar analysis for the 6 km pressure in the North Atlantic case presented earlier showed that responses over the North Atlantic forcing area were significant, but not those anywhere over Europe.

It is encouraging to note that there is some similarity between results for the anomaly and "super anomaly" cases where the values are multiplied by three. This implies that it might be possible to determine some characteristics due to realistic forcing effects by examining results of greatly enhanced forcing effects where the signal is easier to distinguish from the noise.

A third study has just been completed on this topic. It is probably the last one that I will be involved with for a while. In the study we attempted

to clarify the relative roles of the warm and cold SST anomalies and to consider differences in response that might be expected for a mid-latitude forcing compared to one in subtropical latitudes.

We compared model solutions for three cases:

a) Dipole anomaly structure in the middle latitudes as used in the previous study.

b) Single sign anomaly in the middle latitudes corresponding to the warm anomaly part only in the dipole structure.

c) A single warm anomaly pattern at lower latitudes, centered at 27 1/2°N instead of 42 1/2°N.

It was anticipated that changes in the zonal flow in the forcing area, the magnitude of the Coriolis parameter and the increased magnitude in latent energy changes in the lower latitude case would be important factors. Additional methods to analyze for transient extratropical cyclone activity were also examined.

The results can best be described while we look at the slides. In the first the specifics of the SST anomaly patterns are shown. Only the "super anomaly" magnitudes were used. The next three slides show a comparison between the three experiments for the three variables

a) 9 km pressure changes

b) surface pressure changes

c) precipitation rate

The similarity between the results of the first two cases for all three parameters suggests that either the warm anomaly side of the dipole was the important one or that the horizontal scale of the anomaly fields was such that similar east-west wavelength fields were effected in both cases so the only difference would be expected in the magnitude and not the horizontal structure of the response.

The third case differed significantly from the other two. The surface pressure field does not show a large positive change downstream from the forcing area and the effects on precipitation rate are more localized. It appears that the relationship to the middle latitude zonally averaged jet stream flow might be a factor.

The three cases were also compared for parameters describing the extratropical cyclone activity. In the first diagram, these characteristics are shown for the control case. Note that the parameter $\overline{w'\theta'}$ at 3 km corresponds closely the storm track centers where $\overline{\quad}$ is a time average and ' refers to a deviation from the time average. This justifies use of the covariance

parameter to discuss transient cyclone behavior. It is a more continuous and more easily obtained parameter and one which is better suited to taking differences than storm center data.

The next three slides show the transient cyclone effects in the three cases. Again the third case shows less tendency for effects to extend in the east-west direction.

Vertical cross sections along the appropriate latitudes in each case for pressure, vertical motion, temperature and latent heating rates due to condensation document further the similarity of the first two cases and the differences between them and the last case. Notice that in the subtropical case, the pressure anomaly does not show a tilted pattern, the temperature anomaly extends to greater heights and there is more change in the low level condensational heating.

In an effort to isolate the role of some of the main factors on the model response, a simple quasigeostrophic channel model was used to simulate the conditions in the general circulation experiments -- in particular the horizontal advection due to the jet stream, the Coriolis parameter and the heating due to the anomaly field. Results from this simple model were compared to the previous experiment using a variable that both provided, namely the high and low level pressure fields along a latitude line. Height of a pressure surface was the actual variable used. The comparison focused on the second and third cases.

The slides show the comparison. The solid lines show the general circulation model results and the dashed lines show the two-level quasigeostrophic model results. The simple model was not able to show all the difference between the two cases in terms of the downstream response. Some additional effects were introduced into the simple model to try to obtain the downstream surface ridge noted in the general circulation model results in the middle latitudes. This was partially successful as shown in the next slide when an artificial cooling was introduced downstream of the SST warm anomaly to simulate the effects of reduced latent heat release due to the upper level ridging. The simple model was useful to help understand some of the results of the more complete general circulation model.

I have gone into great detail to describe this series of studies because they show well some of the practical problems faced when an attempt is made to use general circulation models for studies of large scale motions. Even though, the results may not have been directly applicable to understanding of the real

atmosphere and forecasting it, the study was justified for many reasons:

a) Techniques for model analysis were developed which can be applied to more accurate models when they become available.

b) Understanding of internally consistent dynamics for large scale motions was increased.

c) A more clear picture of deficiencies in a particular general circulation model was obtained. This should be of value for improving this and other models and documenting the improvements achieved in such models.

d) Last, but not least, it is hoped that some understanding relevant to the actual atmospheric situation was gained.

C. Diagnostic Analyses and Studies

The diagnostic methods such as shown for the sea surface temperature effect studies are becoming more and more important for work with numerical models and with observational data. Obtaining a model simulation or an observational data set can be a very major project. However, it is the diagnostic analyses and studies are usually necessary to find the new scientific insights.

It has become possible to consider many new types of diagnostic analyses because of the more complete data sets that models provide and because of the development of sophistical data handling systems such as McIDAS. It is important that the diagnostics extract the relevant information from the data and help to indicate how a model or a data collection system can be improved.

Diagnostic methods range from examination of fields for the basic variables and their time evolution to the determination of very complex derived variables. The complex variables may represent the characteristics of an entire field or dynamical process with few numbers. But they can be hard to understand. The basic-variable fields may be easy to comprehend, but show very little about the total system. In most cases a compromise has to be made between these two approaches.

In this lecture, I will not review all of the diagnostic approaches that are considered. Instead I will describe two in which I have been interested that represent relatively new methods. The first concerns an analysis procedure suited to understanding the properties of a general circulation model or observational data set relevant to the regional aspects of the mean state. The second method is intended to help improve our understanding of synoptic-scale prediction models.

Diagnostic approach designed for regional mean state studies

The first method is discussed in a paper that should be submitted for publication soon after I return to the United States. It was developed recognizing the need for diagnostics that would be appropriate for study of the forced global scale wave circulations in the atmosphere and the implications of these for local mean state characteristics. The basic concept is the "time domain" approach for model diagnostics as a substitute for the "space domain" method. A common method for the description of the general circulation has been a "space domain" or "mixed space and time domain" decomposition of the variables. Thus, for instance, the variable is split into its zonally averaged component and the deviation from this zonal average or the eddy component.

$$u = [u] + u^*$$

Then all of the statistics refer to zonally averaged quantities and eddy component quantities. This method captures the important and basic latitudinal variations in the atmosphere. It gives a depiction which is consistent with large scale instability theories which considers the properties of eddies superimposed on a basic zonal flow. Many representations of the energetic cycles in the atmosphere are based on the space-domain components and their time averages.

A major problem in this method is to understand the dynamics of the eddy component and to determine the implications of statistics involving the eddy component for conditions at a given location. The eddy component contains waves where baroclinic conversions are the important mechanism and waves where the basic model forcing such as the sea surface temperature conditions are important. A partial resolution to this problem is to do a scale decomposition along latitude lines. This helps to separate the larger-scale forced modes from the smaller-scale baroclinic or "free" modes. With such a decomposition, the number of variables increases and the number of interrelations to be considered increases.

A more direct approach to separating the motions involving different physical processes is the use of "time domain" decomposition. In this case a variable u is split into its time averaged component and the deviation from the time average, or transient, component:

$$u = \bar{u} + u'$$

There are, at least, three possible advantages to this approach.

a) Since the modes forced by the basic stationary forcing functions would tend to be nearly steady except for seasonal changes and the baroclinic

or free modes propagate, a simple division according to the basic physics can result. Of course, there are important nonlinear interactions between these two components since transients of all space and time scales are observed as has been shown in the NCAR movie on the 500 mb height field evolution.

b) Another advantage is that the statistics apply to budget equations for a local region. Thus if there is an interest in examining the reasons why the month of April was particularly dry or warm in China, analyses based on time domain statistics could be used directly.

c) A third advantage is that the quality of the statistics depends entirely on the quality of the local observations. Poorer observations in some distant ocean area would not affect the transient component statistics in the same manner that the eddy component statistics could be affected.

In this study time-domain covariance statistics were computed for a number of NCAR general circulation experiments. These and their zonal averages were compared to an equivalent set derived from real observations. It was intended to demonstrate the method and not to make a complete description of the factors affecting the mean state. In addition, the study showed more about the nature of model deficiencies, the effects of model resolution and the characteristics of interannual variability.

Data from an ensemble of 5 separate general circulation model "realizations" at a resolution of 5° latitude by 5° longitude and 4 realizations from a 2 1/2° latitude by 2 1/2° longitude model for constant January conditions were compared with each other and with observational data analyzed by Oort at GFDL. (Refer to his paper in the February 1978 issue of Monthly Weather Review.) The observations were for the five Januaries in the period 1969-1973.

Steady and transient vertically averaged meridional flux statistics were determined for the u component of momentum, sensible heat, and moisture. The purpose of using vertically-averaged quantities was to minimize the effects of the different vertical coordinate systems used in the NCAR model and for the observations. It was also felt that vertically averaged data would be useful for regional mean state studies, so this form of data compaction was tested for its suitability.

Ensemble means of the statistics for the set of individual January months and the standard deviations from these means were determined. This reduced the sensitivity of the results to individual model cases and to year to year fluctuations in the observations and provided some very crude estimates and comparisons

for interannual variability.

Most of the discussion of the results is for the meridional fluxes of the u-component momentum. The total, steady, and transient components were all computed. These are of the form $\overline{vu}$, $\overline{\bar{v}\bar{u}}$ and $\overline{v'u'}$ respectively. The first figure compares the three components for the 2.5° model and 5.0° model simulations and the observational data, where all data has been zonally averaged. The solid lines show the total flux component, the long dashed line is the steady component and the short dashed line is the transient component.

Important differences are seen between the three. The transient component has larger magnitudes than the steady component in much of the Northern Hemisphere, but the reverse is true in both model results. Neither model simulates well the region of negative fluxes north of 50° N. In the Southern Hemisphere simulation of the steady component is particularly poor for both models. Finally, resolution related differences are more pronounced in the steady and total fluxes than the transient flux. This last result is different from that for the eddy component of kinetic energy which, as I showed in an earlier lecture, was strongly dependent on model resolution.

In the next figures the spatial distributions for these flux statistics are shown. The regional patterns of the three cases show differences far more major than for the zonally averaged values. Note for example the patterns over the SW United States, the North Atlantic and the SW and central regions of Asia. Important model deficiencies in terms of phase as well as magnitudes are apparent. The patterns for the steady component compare similarly as those for the total flux. The transient component results shown in the next figure reveal extreme model deficiencies. Note for instance the region off the east coast of North America.

It is evident that these flux parameters are very sensitive indicators of model performance. It is also clear that important differences exist on a regional basis which are not shown with zonal averages and which would not be shown in the space domain covariance statistics of the zonally averaged and eddy components. It is much easier to discuss the effects of the forcing mechanisms on the results when the horizontal distributions are shown.

The study also provided some interesting comparisons for the interannual variability. The next figure shows the zonally averaged steady and transient flux components with the one standard deviation superimposed. Notice that in general, variability increases towards the north in both the model and the observations. The model has considerably less variability than the observations.

The next two slides show the spatial distribution of the variability statistic. Note the extreme differences between the 2.5° model simulation and the observations. Characteristics in the observational data set alone are of interest. This is one of the first presentations of the spatial variations in interannual variability for the observations. For the transient flux component, only the observational data is worth examination. It shows large variability centers over both the land and ocean as did the steady flux component.

A few results for the heat fluxes are shown. The next diagram shows a comparison of the transient flux component, $\overline{v'T'}$ for the observations in the solid line, the 2.5° model in the long dashed line and the 5° model with the short dashed line. Differences in the Northern Hemisphere are more in the latitude of maximum value rather than the maximum value alone, whereas in the Southern Hemisphere, the differences are more in the magnitudes. The horizontal patterns for the transient heat flux statistic shows important differences in both the latitude and longitude of magnitude maxima. The 2.5° model has a maximum in the North Atlantic which is not observed and the position of the maximum in eastern North America differs considerably from the observations which could have important implications for explaining the average temperature conditions in the eastern part of the United States.

This study has shown some additional methods for diagnosing general circulation model results and large scale observations.

Diagnostic analysis for synoptic scale prediction models

Here, I wish to discuss the problem of evaluating operational numerical model prediction results and to give some ideas for improving the methods used. Some of this material appears in a paper,

Houghton and Irvine, 1976, A case study comparison of the performance of operational prediction models used in the United States. Monthly Weather Review, 104, p. 817.

At the University we have a course where the students perform a large number of quantitative diagnostic studies on forecast data from the weather prediction models. Computer tapes of grid point values are obtained so that many diagnostic approaches can be tried. The results published came from work done in this class for the first specific forecast situation (case study) considered. Since then, other cases have been used including some that had forecast data from the higher resolution prediction models.

A forecaster is interested in the accuracy of predicted variables that are important to the users. These include the precipitation, surface temperature

and wind and the motions in the upper troposphere. For many years, evaluation of the forecasts has involved descriptive and statistical evaluations of the forecast fields for these types of variables. Statistics such as the S_1 Skill score for the 500 mb height fields have been used. The S_1 is a measure of errors in the gradients of the 500 mb geopotential field. It is proportional to,

$$\sum_{\text{grids}} (\nabla\phi_{\text{observed}} - \nabla\phi_{\text{forecast}})^2 .$$

For precipitation, measures such as the Threat Score are used. It is defined at the ratio of the area of a correct precipitation forecast to the area where it was forecasted or observed:

$$T = \frac{A_c}{A_F + A_o - A_c}$$

where A_c is the area of correct forecast of precipitation
A_F is the area of forecasted precipitation
A_o is the area of observed precipitation

Such simple statistics concerned directly the variables of practical interest and can be determined routinely. The qualitative comparisons of fields has included examining the position of upper air trough lines and surface low pressure centers.

The complexity of the current prediction models and of the atmospheric system makes understanding the causes of error as depicted by these simple statistics and descriptions very difficult. In general these diagnostic parameters provide little information for how the numerical models might be improved. In the study discussed here, additional diagnostic methods were considered for evaluating model performance. Variables were considered which would have more direct relevance to the physical processes governing the evolution of the atmospheric state and which would be sensitive to differences in the forecasts.

In the United States, there are three agencies which have general operational prediction models. These are the National Weather Service, The Air Force and the Navy. Their models differ from each other so that a proper intercomparison study could provide some information on the effects of specific parts of the model: especially those which are different. The agencies themselves lack the resources to be able to make complete studies.

The four models are listed and described according to the situation in 1974:

a) NWS PE model -- 6 levels with 381 km horizontal resolution

b) NWS LFM model -- 6 levels with 191 km horizontal resolution

c) Air Force Model -- 6 levels with 381 km grid, and filtered quasigeostrophic equations. Precipitation is predicted using an advection model with velocities from the forecast as prescribed input parameters.

d) Navy model -- 5 levels, primitive equations, 381 km grid.

The forecast situation was the 24 hour period from October 5 to October 6, 1974. In this period of time, a short wave upper level trough moved into the Midwest region of the United States. A weak frontal disturbance associated with it caused significant precipitation.

The forecasts were first evaluated according to the traditional methods. The first slide shows the initial surface pressure field and that at the end of the 24 hour period. A newly formed extratropical cyclone shows up with a central surface pressure of 1016 mb in Wisconsin. The Air Force model did not predict a closed surface center. The Navy Model storm center position shown by X is far to the southwest and has a central pressure of 1013 mb. The NWS PE model results are similar to the Navy with a position at Y and central pressure of 1015 mb. The higher resolution LFM model does best with a predicted center at Z and central pressure of 1015 mb.

General features of the 500 mb height field are compared in the next figure. The forecasts differ with respect to the long-wave trough position shown by the dashed lines. Very little evidence of the short wave feature over Wisconsin is seen in the height field maps.

Precipitation was an important factor in this forecast with over 3 cm occurring in one area. The satellite images in the next two slides emphasize the very small scale of the precipitation area. The first slide shows the visible image about 6 hours into the 24 hour forecast period. The actual precipitation area is more clearly defined in the infrared picture which separates the thick and high extending tops of the convective precipitation system from the nonprecipitating clouds elsewhere.

The 24 hour precipitation forecasts are compared in the next diagram. Note first the observed precipitation with its small scale features. The model predictions vary widely with the LFM correctly simulating the two separate areas in the Upper Midwest area but with the NWS PE model giving more correct magnitudes in the region over Iowa. The filtered Air Force model results are clearly the worst. The Navy model forecast is much less satisfactory than the NWS PE model even though both had about the same forecast for the storm center position.

The analysis of the operationally important parameters shows a wide range in the performance of the prediction models. However, there is no clear indication as to how these various performance measures relate to each other. This was especially evident for the precipitation forecasts.

The data fields were then analyzed by methods intended to focus more on the basic dynamical processes in the model in order to provide a general yet sensitive measure of model conditions. The basis for determining the variables to be used was given by the quasi-geostrophic equations which describe the key processes for large scale motions.

A brief overview of the quasigeostrophic system is given in the next two slides. The first shows this system in a form so that the correspondence to the primitive equations is most easily seen. In the second diagram, the formulation of the governing equations for evolution in the quasigeostrophic system reveals the important and interrelated role played by four variables,

vertical motion

vorticity

vorticity advection

thermal advection

It is these four variables which can be considered fundamental to the large scale dynamical processes.

The first diagnostic analysis was done on the initial data fields used in the prediction models. The next slide shows the initial 500 mb height fields for the four models. Small differences are seen but it is not possible to assess the importance of the difference. In the next diagram, the variables of vorticity, vorticity advection and thermal advection are shown for the three models for which grid point values were available. Now the differences are more apparent. The key difference for the subsequent development of the short wave trough is the small region of positive vorticity advection in northern Kansas in the LFM data. This was much less pronounced in the other model initial data fields which is perhaps an important reason why the LFM model developed the short wave system much sooner than the other models.

An analysis of the forecast fields from the same three models in terms of the dynamically significant variables showed some very interesting differences in model performance. The first slide shows the forecasted 500 mb height field compared to verification data. As noted before there were important differences in the larger scale trough system, and the short wave trough was not evident in any of the forecast fields. The next diagram shows the vertical

motion, vorticity advection and thermal advection fields for the three models and the verification data. Patterns for these variables highlight the activity along the jet stream including the short wave trough. Note that the vorticity advection field for the LFM shows a spurious small scale oscillation. This was indicative of a numerical instability in the model and of subsequent errors to develop in the dependent variables of the model.

These two studies have shown two examples of the types of diagnostic analysis methods that are needed to study the global and synoptic scale processes in numerical models and in the observational data.

D. Seasonal Changes Processes

The final two lecture topics on large-scale motions cover studies that involve very long time scales. Interest in climate and climate change has resulted in greatly expanded research programs in the United States and elsewhere. These programs have covered time scales ranging from seasonal to geologic. An example of each will be covered in today's lecture.

Modeling of climate processes has been tried using statistical schemes, one dimensional thermodynamic models, zonally averaged circulation models, and full three-dimensional general circulation models. Due to the complexity and computer requirements for general circulation models, it has not been realistic to use them for time scales exceeding the annual cycle.

The annual cycle involves changes in the fundamental forcing processes for the atmosphere such as radiation and ocean-atmosphere interaction which are as large as changes in the annual average conditions associated with the ice ages or any climate changes considered important for mankind.

Thus seasonal change research is both practical and relevant scientific research. The time scale of the seasonal cycle is long enough to cover the time scales for the response of the atmosphere to numerous forcing process such as radiative heating and ocean mixed layer surface fluxes. There are, of course, many longer term variations that are observed in the ocean-atmospheric system.

The results that I will present here were obtained by a Ph.D. student, Bette Otto-Bliesner, whom I have been advising and who has just finished her program. A low-order spectral general circulation model was integrated for a five year period and numerous diagnostic analyses were performed on the output. Results were compared to observational data. Special attention was given to temporal variation in the statistics for the model energetics and to the differences between the Northern Hemisphere, Tropical, and Southern Hemisphere

regions. Of particular interest were the asymmetries and rapid shifts in the circulation characteristics due to nonlinear and instability phenomena.

The general circulation primitive equation model contained parameterization for radiation, turbulent diffusion in the horizontal and vertical, precipitation and convective processes, and lower boundary fluxes. It was a global 5-layer semi-spectral model triangularly truncated at wavenumber 10 using the surface spherical harmonics. The triangular truncation is justified on the basis of invariance to coordinate rotation. It means that the component structures permitted in the model become quite unrealistic at the small scale end of the spectrum. In practical terms, the model resolves fairly well the first five zonal harmonics but harmonics from 6 to 10 are very unrealistic. The latter are grouped together in the analysis of the output.

Even though this model contained most of the processes present in the higher resolution general circulation models, it used far less computer time. A semi-implicit time integration scheme, and coarse resolution allowed a time step of 1 1/2 hours to be used. Only 2 1/4 hours of CDC 7600 computer time were required to simulate an entire year. This compares to the requirement of approximately 10 minutes of CDC 7600 computer time to simulate one day with the 5° grid version of the NCAR general circulation model. The ratio for computer requirements is thus about 1 to 30, and simulation of seasonal time scales was practical.

The model was initialized from a state of rest and allowed to develop a circulation for constant January conditions. Certain parameterization specifications were adjusted during this period until a reasonable equilibrium was reached. Then one seasonal cycle was simulated and further checks on model performance made. Finally, the 5 year simulation was made without any additional adjustments in model formulation.

General characteristics of the dependent variables were checked for equilibrium behavior on an annual basis and with observations. Magnitudes of the parameterization effects were individually checked. An important part of the diagnostic analysis dealt with terms in the energetic relationships. The energetic quantities are defined separately for the Northern Hemisphere, tropical and Southern Hemisphere domains with the dividing latitudes between these being at 20° N and 20° S, respectively. The energy quantities are apportioned into zonally-averaged and eddy components, where the eddy is defined as the deviation from the zonally averaged value.

A thorough discussion of the energetic diagnostic for the general circulation would take many lectures. I'll say just enough here so that you can understand presentation of the results. The energy of the general circulation system for each of the latitudinal domains is divided into four parts.

a) Volume integrated zonally averaged available potential energy, A_Z

b) Volume integrated zonally averaged kinetic energy, K_Z

c) Volume integrated eddy available potential energy, A_E

d) Volume integrated eddy kinetic energy, K_E .

Changes in these magnitudes depends on

a) Generation and dissipation

b) Conversions between these four energy forms

c) Transports from adjacent latitudinal domains.

These processes are indicated in schematic form in the diagram:

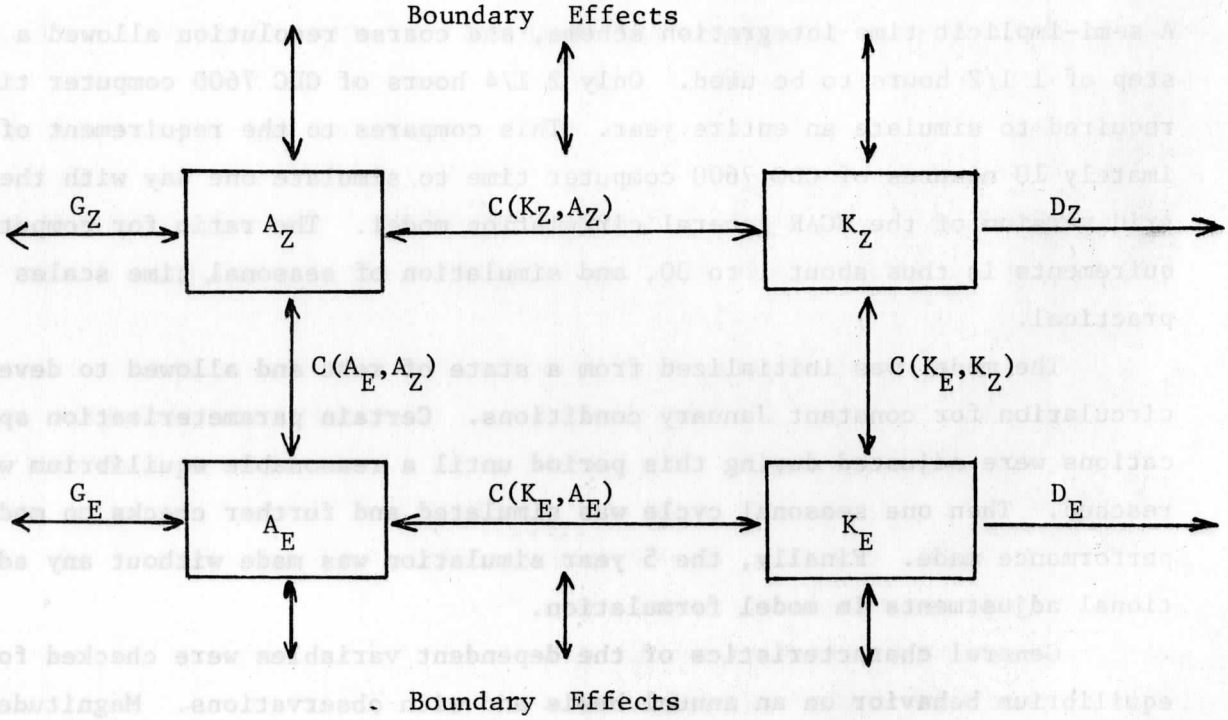

Here the G represent the generation or destruction of potential by diabatic processes. The D refer to frictional dissipation. Boundary effects are noted by the arrows at the top and bottom. The C are the conversion terms. The important baroclinic conversions are the $C(A_E, Z_Z)$ and $C(K_E,A_E)$. The important barotropic conversion is $C(K_E,K_Z)$.

Now let us look at some of the results. The first figures review the basic features of the model including horizontal resolution. In the fourth

slide the features in the topography elevations that can be resolved are shown. Also shown are the continent outlines on a grid point scale consistent with the spectral truncation.

The following diagram shows the time dependent characteristics of the individual parameterized processes. The curve labeled C for condensation also includes vertical heat flux due to convective mixing. Note the delay in the long wave cooling cycle compared to the short wave heating.

The next figure shows the seasonal changes in the zonally averaged values of precipitation and surface temperature. This is perhaps not a useful diagnostic since we are not accustomed to considering the observational data in this form. On the other hand, the wintertime and summertime zonally averaged u component of velocity is a diagnostic variable for which observational values have been determined. The comparison between the model and the observations shows a correspondence that is as good as achieved with some higher resolution general circulation models.

The seasonal variations in the energy quantities show some interesting asymmetries and irregularities in the model results. This is an important result concerning general circulation dynamics since the imposed forcing effects tended to be more regular curves especially the solar heating. Sea surface temperatures were prescribed according to the observed seasonally varying values. The nature of the asymmetries in this forcing effect have not been fully determined.

The next slide shows the behavior of the four basic energy quantities. Time smoothed values are shown with the heavy line. Note in particular the variations in the eddy component. The A_E has a secondary maximum in the summer due to the ocean continent contrasts which exist then as well as in the winter. The K_E shows more rapid build up in the fall than decrease in the spring.

The characteristics of the conversion terms are shown again for the Northern Hemisphere domain. The baroclinic conversion $C(A_E,K_E)$ shows a very non sinusoidal characteristic with nearly constant values for several months in the summer. The generation and destruction terms have a similar assortment of irregularities. Note the rapid shifts in the value of D_E.

The overall characteristics of the energetics of the model are shown for the four seasons and the annual average. The double arrows indicate the most dominant conversions and transfers. The major differences in the processes creating A_E from summer to winter have been shown in some observational studies. For the annual average, the dominant baroclinic effects and values

of the conversion and transfer terms agree quite well with the observations shown in the next figure.

Contrast between the different latitudinal domains is shown by examining the characteristics of the energy component magnitudes and the overall energy cycle. I will not comment too much on these since there is less verification data available than for the Northern Hemisphere.

Since the model is in the spectral formulation, it is a straightforward procedure to examine the results as a function of scale. In the next few slides the details of the winter build up in the energy parameters in the Northern Hemisphere are examined. The first figure shows the interesting oscillations with a period of about one month that occurs just after the equinox. Observations have suggested that this occurs in the atmosphere as the so-called "equinoctal storminess period".

The scale decomposition for this period shows that the K_E variations are most pronounced in the wave number 3 and the "small scale" wave numbers 6-10. The last slide shows properties of the conversion terms which suggest that amplification in both cases resembles a baroclinic instability with energy being derived from the mean flow and not from each other due to a nonlinear interaction.

I have shown just some of the highlights of this research. The study was an initial attempt to do a rigorous analysis of the processes involved in seasonal change. It represents the type of research that is being done currently in this area, and the type which is now possible with deterministic numerical prediction models.

E. Long Term Climate History Studies
(Program of Center for Climatic Research)

At the University of Wisconsin, we have a major research program concerning the climatic conditions for the earth for much longer time scales than the seasonal cycle. This work is being conducted in the Center for Climatic Research under the direction of Professor John Kutzbach. I have chosen to discuss it briefly in this lecture because this type of climate study relates to describing and understanding the same global scale waves that have been observed in the movie of 500 mb height data and modeled in the seasonal cycle research and because this program is one which will have immediate and profound benefits from a joint China-United States research effort.

The basic approach is to study a wide range of climate indicators from the past in order to reconstruct the general circulation patterns. Having data

from an extensive surface area is essential for accomplishing this goal. Only then is it possible to describe the global scale wave features. These features which determine the characteristics of regional climate are important descriptors of the atmospheric response to the main climatic forcing factors. It is hoped that by determining the relationships between the general circulation and the forcing processes from past data, we will have an understanding of the dynamics of climate which could be used to predict future changes.

This climate study is interdisciplinary and requires the cooperation of biologists, limnologists, geologists, chemists, meteorologists and others to properly understand the historical data. Evidence of the past climate must be derived from many sources. Tree ring characteristics, glacial evidence, sea level indicators, animal fossils, lake sediment characteristics, and plant life remains are some of the sources that have been examined.

Middle latitude data is particularly useful since climate variations are more pronounced there than in tropical environment. Significant local changes occur in the historical data. At these latitudes the global scale wave numbers 1, 2, 3, and 4 have large amplitudes and important effects on the climate. Since most data is limited to land areas, a proper definition for these waves is more possible in the Northern than in the Southern Hemisphere. As will be shown, data from China is important. At 40°N, it would be possible to make assessments about wave number 3 characteristics as well as about the zonal flow and wave numbers 1 and 2 if data from your country were combined with that from elsewhere.

Glacial periods represent times with climatic conditions considerably different from at present. Important information can be gained about climate dynamics by understanding the glacial period situation. The changes on plant life were major and can be readily detected in the data. There have been some attempts to simulate the glacial period climates using a general circulation model. However, the lack of observational data precludes being able to assess the results. Studies of the climate changes in the past 3000 years have proven to be feasible. These have provided information on another time scale of variability.

The University of Wisconsin program is doing historical studies for three periods in the past.

a) The Pleistocene glaciation period 18,000 years ago.

b) The last glacial period 12,000 years ago.

c) The recent period from 3,000 years ago to the present.

I will discuss briefly the work on historical data in each area with a series of figures.

The first slide taken from Peterson et al., Journal of Quarternary Research, 1979, pp. 47, shows the location of all sites with paleobotanical and other geological evidence for climates covering the period of 18,000 years ago. The stippled area shows regions covered by glaciers at that time. Vertical strips indicate areas of scattered glaciation. Black points are pollen or other botanical data. The non-black points are geological data such as dated glacial morains, evidence for cryogenic features, depressions of snowlines, or paleo-lake levels. Here it is clear that data from the eastern half of Asia would greatly improve the global coverage. Evidence documenting temperatures cooler than at present has been obtained from many of these points. In some locations the estimates include an actual temperature difference. The next diagram shows estimates of moisture conditions at 18,000 years ago compared to the present. Dark points indicate conditions wetter than now and hollow circles show dryer regions. Changes in the currently dry region of the Southwestern United States are quite prominent.

Pollen records in lake sediments have been useful for mapping changes that were occurring in the period starting 12,000 years ago when the last glacial cover was retreating northward. Pollen counts for spruce, pine, oak and herbs were used to locate regions where each had been growing. The current method for obtaining lake sediment samples is to thrust a metal pipe down into the sediment layer with the pipe so cold from dry ice that a thin layer of the sediment freezes on it. The pipe can then be pulled up and the sample analyzed with the layer patterns intact. Radiocarbon dating is used to determine the age of the sample. The next three slides show results from this approach and are taken from a publication by Bernabo and Webb in Journal of Quarternary Research, 1977, p. 64.

The first slide shows isochrones (in thousands of years) when the spruce pollen count fell to less than 15% of the total. This dated the time when the spruce forests were destroyed by the warming climate. The second figure is an isochrone map showing the northward movement of the boundary between the deciduous forest and the mixed conifer and hardwood forest. The rate of movement is faster in the Appalachian mountain region than further west.

The last figure shows the movement of the forest-prairie boundary as the climate became warmer and dryer from 11,000 to 7,000 years ago. The prairie nearly reached Madison 7,000 years ago then retreated westward again. The warm and dry conditions 7,000 years ago indicate a time of stronger zonal circulation.

Finally a few results for more recent times are shown. Some of these are from papers by Swain in the Journal of Quarternary Research, 1973, p. 383 and 1978 p. 55. The first slide shows the location of lakes in the world which are known to have annually layered sediments. Most of these formed with the retreat of the last glaciers and provide a source of data particularly for the last 3,000 years. Carbon dating is not required. The next slide shows more detail about the lake sites in the United States. The following diagram shows an example of a pollen diagram from a lake in northern Wisconsin. Notice the systematic changes in the white pine and hemlock pollen concentrations, which either started or ended about 1,200 years ago. Estimates of the growing season temperature from a lake in New York State is shown next. It covers the last 2,000 years. The final slide shows a comparison of climatic reconstructions based on glacial activity, tree rings, pollen and soils. The changes do not always show the same relationship.

These are just a few examples of the possibilities for estimating climate parameters from past natural environmental data. As I had said before, cooperative studies to obtain such data in China would be extremely valuable for reconstructing elements of the general circulation patterns over the Northern Hemisphere.

III. MESOSCALE METEOROLOGY

For the last five lectures, I wish to discuss topics in mesoscale meteorology. There are a large number of problems in mesoscale meteorology that are of very practical interest. In comparison to synoptic scale meteorology, progress in mesoscale understanding has been much slower because of poorer observational data, the lack of simple inclusive theories for the phenomena, and the more complicated interactions between scales of motion.

A. Orographic Flow

During my years at NCAR I became interested in explaining the strong downslope winds observed there called the Chinook. I was then a recent Ph.D. graduate in dynamic meteorology and wanted to start with very simple analyses for the phenomena and then gradually add elaborations to better approximate the real physical system. I started with a one layer model and advanced to a two layer model. But then I left NCAR and never did progress any further.

I can still recall the exciting day when the sharp near-discontinuity sometimes observed with the Chinook remained almost stationary in the Boulder, Colorado area for a several hour period. The afternoon began with rather cool and calm conditions at the place where I lived, Point A in the diagram. Then

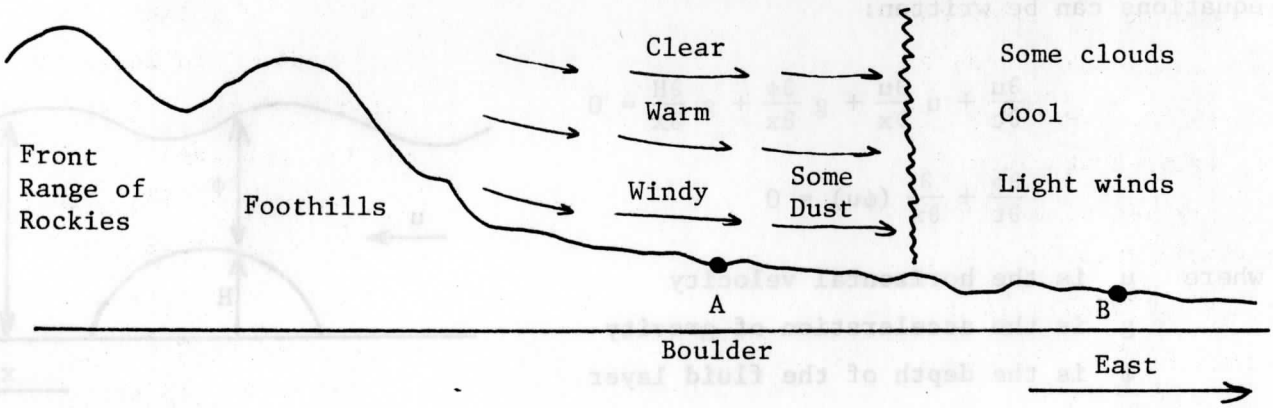

Diagram of Situation

conditions changed rapidly to a strong and gusty west wind from the direction of the mountains and it warmed up. I called a friend who lived 8 km further east at Point B and he confirmed the fact that it was cool with light winds there. I then went by car to Point B passing back into the calm air. From his home it was possible to watch the very slow advance of the dusty air, at a rate much less than the speed of the strong winds.

The general problem of orographic flow already had been studied by numerous linear models for stratified conditions and continuous variables in the vertical coordinate. I decided to use another approach which would emphasize more the near-discontinuous and highly nonlinear low level conditions that I had noticed in the Chinook.

The analogy to shallow, hydrostatic, water flow over an obstacle was made. For this case, there can exist hydraulic jump solutions based on the hydrostatic equations even though conditions at the discontinuity itself are not hydrostatic. Such "jump" features are evident in surf action at the sea shore, as stationary phenomena in a stream bed where the water is moving over rocks, and in the moving tidal bore that propagates twice daily up rivers in some parts of the world. The next three slides show examples of the tidal bore. The first one was observed in New Brunswick, Canada over 10 miles inland from the ocean. The second was observed on the Avon River in England again over 10 miles inland. I had hoped to see the one which is reported in the river estuary near Hangchow while in China but that was not possible. The shallow water flow analogy had been suggested earlier by scientists including, Chao, Chang and Yan at the former Institute of Geophysics and Meteorology in Peking.

A simple one layer model was analyzed for flow over an obstacle or mountain. Results are published in a paper by Kasahara and myself in the Communications on Pure and Applied Mathematics, 1968, p. 1. The one dimensional equations can be written:

$$\frac{\partial u}{\partial t} + u \frac{\partial u}{\partial x} + g \frac{\partial \phi}{\partial x} + g \frac{\partial H}{\partial x} = 0$$

$$\frac{\partial \phi}{\partial t} + \frac{\partial}{\partial x} (\phi u) = 0$$

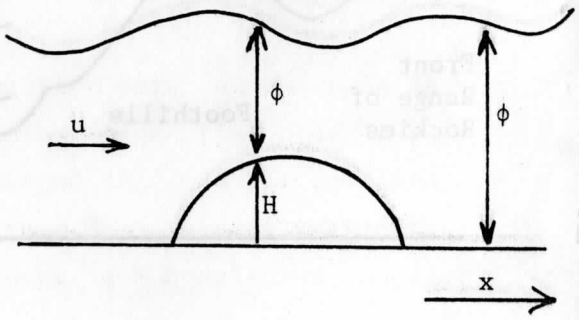

where u is the horizontal velocity
g is the acceleration of gravity
ϕ is the depth of the fluid layer
H is the height of the obstacle

The flow has steady state solutions for a certain range of the depth, horizontal velocity and obstacle height parameters. The conditions can be expressed in terms of non-dimensional parameters derived from the initial fluid velocity and depth distant from the obstacle, u_o and h_o:

$$F_o = \frac{u_o}{\sqrt{g h_o}}$$

$$M = \frac{H}{h_o}$$

Results are as follows:

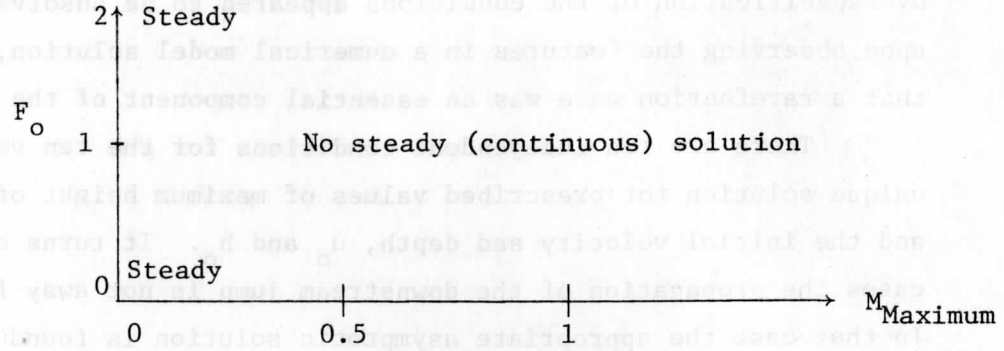

Solutions in the domains called steady are continuous and symmetric with respect to the obstacle. In the middle domain no such steady solution exists. There, however, it is possible to find steady solutions with asymmetric conditions over and to the sides of the obstacle. For the initial value problem, it is possible to connect this steady asymmetric solution to the initial state by adding hydraulic jump discontinuities upstream and downstream of the peak of the obstacle. I felt that the initial value problem approach for this phenomenon was justified because of the unsteady and transitory nature of the Chinook.

The important features of the symmetrical solution for the initial value problem were completely determined by specification of the maximum mountain height, H_c, and the initial velocity and depth, u_o and h_o, at the sides of the mountain. The solution after a period of time, referred to as the asymptotic solution, had values on either side of the obstacle equal to the initial conditions and flow over the obstacle given by conditions derived from the equation of motion and the continuity equation.

The features of the asymmetrical solution required the determination of 10 asymptotic state variables which were independent of time. These were:

h_A the final upstream depth
u_A the final upstream velocity
c_ℓ the propagation speed of the jump upstream of the mountain
ϕ_c fluid depth at the peak of the mountain
u_c final velocity at the peak of the mountain
h_x final downstream depth far from the mountain
u_x final downstream velocity far from the mountain
h_B final downstream depth at the edge of the mountain
u_B final downstream velocity at the edge of the mountain
c_r propagation speed of the jump downstream of the mountain

These are all illustrated in the following two slides. The domain defined by the u_x and h_x was not included in the original study and problem with the overspecification of the conditions appeared to be unsolvable. Then based upon observing the features in a numerical model solution, it became clear that a rarefaction wave was an essential component of the analytical solution.

There are ten independent conditions for the ten variables and thus a unique solution for prescribed values of maximum height of the mountain, H_c and the initial velocity and depth, u_o and h_o. It turns out that in some cases the propagation of the downstream jump is not away from the mountain. In that case the appropriate asymptotic solution is found by assuming that the jump is a stationary feature on the mountain as shown in the next slide. The position of this jump feature replaces its propagation speed as the variable to be determined.

Some of the solutions obtained by the theory are shown. The first diagram gives the final upstream depth and velocity at the edge of the mountain as a function of the initial parameters. All variables have been normalized by the initial depth and its associated linear gravity wave speed, h_o and $\sqrt{gh_o}$. The next diagram gives the solution for propagation speed of the downstream jump feature away from the mountain. For the conditions where it does not move, the mountain height where it remains stationary is given.

The analytical solutions were confirmed by a numerical model simulation. The model was based on the Lax=Wendroff second-order finite difference method. No explicit viscosity effects were needed to handle the large nonlinear situations near the jump features since the numerical scheme has a strong damping effect on the very small wavelengths.

The four different types of asymptotic solution were demonstrated as shown in the next slide. The first (A) was for subcritical flow where the final solution is steady and symmetrical. The second (B), was for conditions where jumps exist in the solution but the downstream jump remains stationary on the mountain. The third, (C) also includes jumps in the solution, however both move away from the mountain. In the fourth, (D), conditions are supercritical everywhere and the final solution is steady and smooth.

Results from the model are shown in a movie made directly from computer output. This allows the nature of the time dependent and steady aspects to be clearly seen. The next slides show the characteristics of the output presentation. The subcritical case is shown first. Height of the fluid surface is shown below the curve for velocity within the layer. Velocity increases over

the mountain. The next diagram shows the supercritical case where flow speed decreases over the mountain. The stationary and moving jump cases are shown in the next two slides. In all of these diagrams and in the movie, the arrow shows the position of a fluid element that was originally at the crest of the mountain.

(One-layer mountain flow movie)

In the second study a two-layer version of the shallow water, hydrostatic model was used to provide a more realistic representation of the atmospheric Chinook situation. Both analytical and numerical approaches were used. Results are in a publication:

Houghton and Isaacson, 1968, Mountain Winds.
Studies in Numerical Analysis, 2, pp. 21-52.

The two-layer case was far more than twice as complicated as the one-layer case. With two-layers, internal as well as external gravity wave modes exist. Furthermore the possibility of a Kelvin-Helmholtz shear instability exists. In order to make simulations for the atmosphere, a third, but passive, layer was added at the top. This allowed the two model layers to be confined to the tropospheric representation. It reduced the phase speeds of the fastest "external" gravity waves which relaxed numerical constraint for the time step and lateral boundary conditions. The passive layer was included only for the final simulation experiments.

The basic equations for the model without the third passive layer are shown below. Primes refer to variables in the upper layer. The symbol r is the ratio of densities between the two layers. Symbols represent the quantities as shown in the sketch.

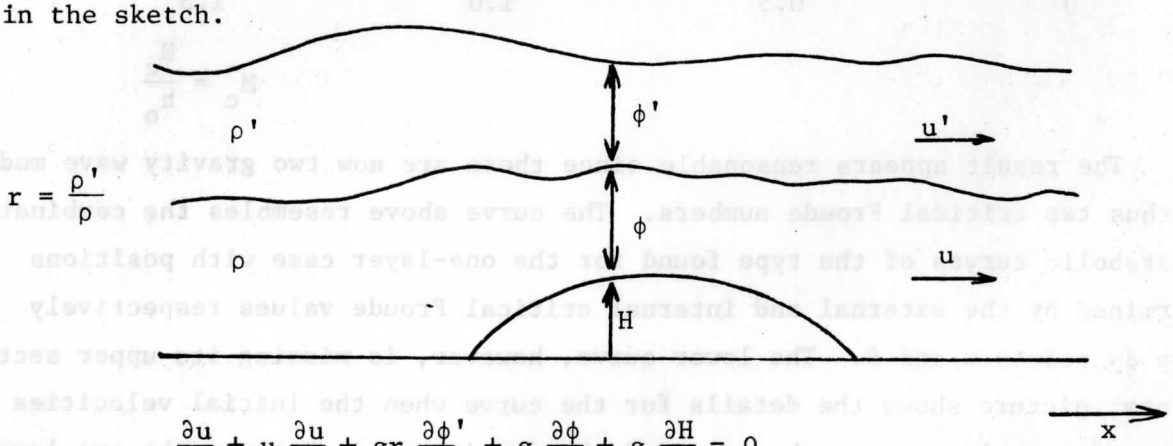

$$\frac{\partial u}{\partial t} + u\frac{\partial u}{\partial x} + gr\frac{\partial \phi'}{\partial x} + g\frac{\partial \phi}{\partial x} + g\frac{\partial H}{\partial x} = 0$$

$$\frac{\partial \phi}{\partial t} + \frac{\partial}{\partial x}(\phi u) = 0$$

$$\frac{\partial u'}{\partial t} + u'\frac{\partial u'}{\partial x} + g\frac{\partial \phi'}{\partial x} + g\frac{\partial \phi}{\partial x} + g\frac{\partial H}{\partial x} = 0$$

$$\frac{\partial \phi'}{\partial t} + \frac{\partial}{\partial x}(\phi' u') = 0$$

Analysis for the analytical solution proceeded as with the one layer model. First the steady, symmetrical and smooth solutions were determined. Mathematically this required solving a ninth degree polynomial derived from equation of motion and mass continuity constraints. Unlike for the one-layer model, it was not possible to find the analytical expression for the curve in initial condition space which defined the limits for existence of this type of solution. However, based on the one-layer solution and two-layer analytical model results, the following description was obtained for no vertical wind shear in the initial velocity specification and equal thickness in the two layers initially. (Depth of lower layer away from the obstacle is equal to h_o.)

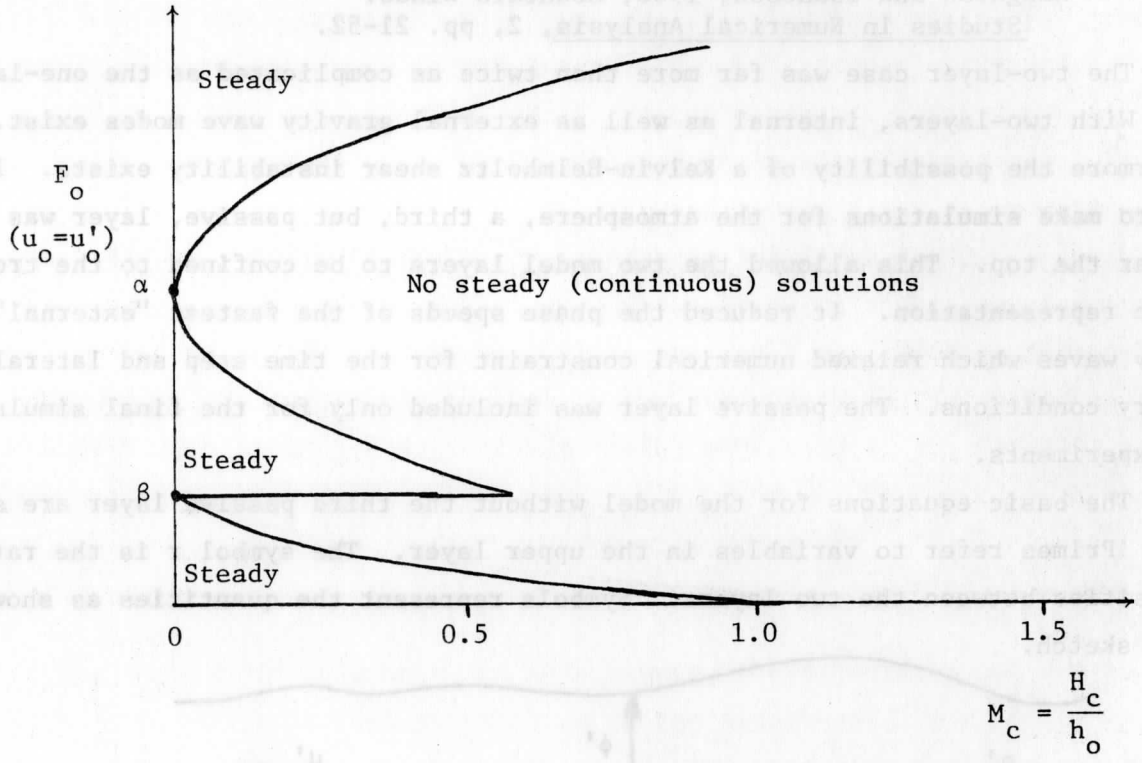

The result appears reasonable since there are now two gravity wave modes and thus two critical Froude numbers. The curve above resembles the combination of parabolic curves of the type found for the one-layer case with positions determined by the external and internal critical Froude values respectively shown as points α and β. The lower curve, however, is missing its upper section. The next picture shows the details for the curve when the initial velocities and depths of both layers are the same and the density ratio between the two layers is 0.8. The next slide shows an example of the solution for heights in Domain A where steady solutions were possible.

Analytical methods were attempted for the jump and asymmetrical solutions that existed for other values of the initial conditions. It was possible to find relationships for the steady parameters that would exist on either side of

the jumps and rarefaction waves that were part of the total solution. However, it was far too complicated to find the total solution by analytical methods.

A numerical model was developed to find the solutions. It was formulated according to the same Lax-Wendroff finite difference scheme used in the one layer model. In some numerical calculations, instabilities arose due to the local amplification of short wavelength features around the jump zones. Thus it was necessary to introduce a very small "pseudoviscosity" term. We used a form that had been designed for hydraulic jump situations. It was applied in the equation of motion only in regions where there was convergence in the horizontal velocity. It was of the form:

$$\left|\frac{\partial u}{\partial x}\right|\frac{\partial u}{\partial x} \quad \text{in layer 1 and} \quad \left|\frac{\partial u'}{\partial x}\right|\frac{\partial u'}{\partial x} \quad \text{in layer 2}$$

for $\frac{\partial u}{\partial x} \leq 0$ or $\frac{\partial u'}{\partial x} \leq 0$

and was equal to zero for $\frac{\partial u}{\partial x} > 0$ and $\frac{\partial u'}{\partial x} > 0$.

where as noted before the prime refers to the upper of the two layers.

This model was used to make calculations for a large number of different initial states. By examining the solutions and relating them to properties of the one-layer model solutions and analytical diagnostics of the two-layer jumps and rarefactions, it was possible to determine the general categories of the solution as shown in the next slide. Numerical solutions were found for the 40 initial conditions shown by the dots.

Characteristics in the various labeled regions are as follows:

A : Symmetrical smooth solutions

B : Stationary internal jump on the lee slope of the mountain

B': Critical flow point forms on the upwind slope of the mountain, the downstream internal jump is either on the lee slopes or it propagates away from the mountain.

C : Two jumps, one external and one internal form on the downstream side of the mountain. In some cases, shear instability forms in the region between the two jumps. An internal rarefaction wave propagates upstream.

D : Symmetrical solutions result

E : Same as C except that only a jump propagates upstream.

The next slides show some examples of the solution to illustrate some of the typical structures found in these regions. The first shows Region B with the stational jump. There is also an upstream propagating jump and

several rarefaction waves. The following slide shows Region B' where the critical flow point occurs on the upwind slope of the mountain. There are some numerical oscillations at this point. The next slide shows Region C. Strong vertical wind shears exist in the region just downstream of the mountain and sometimes a shear instability developes. This has been shown to be a physical and not just a mathematical instability by examining a simple linearized model for the conditions there. The instability does not cause unbounded amplitudes in the model because the fluid parcel remains in the region for only a short time and the damping of the numerical scheme helps to limit amplitudes.

In Regions B, C and E it was possible to determine the entire solution upstream of the mountain by using the analytical relationships for jumps and rerefaction waves. Thus it was possible to check directly those aspects of the numerical solution. Agreement in the region behind the upstream moving jump was excellent with an error of less than 0.7% in all of the cases. Errors for depth of the lower layer behind the upstream moving rarefaction wave were larger being about 5% in Region B and as high as 25% in Region C.

The final test for the study was to attempt a simulation for the specific conditions in the atmosphere. Since the model was incompressible, its stability was made comparable to that in the atmosphere by the following relationship where ρ is density and θ is potential temperature

$$\frac{1}{\rho}\frac{\partial \rho}{\partial z} = -\frac{1}{\theta}\frac{\partial \theta}{\partial z}$$

Model Atmosphere

By specifying density in this manner, the velocities and depths could be made numerically equivalent to those in the atmosphere. A study of typical conditions for the Chinook had demonstrated that there is usually a weak stable layer just above the mountain peak. This was then taken to be the top of the lower layer and the tropopause was taken to be the top of the second layer. Potential temperature values in the lower stratosphere were used to determine the density in the upper passive layer.

The next slide shows the specification of the simple model parameters for the Chinook conditions at Boulder. The topography for a thin band across central Colorado was used at the lower boundary. Ficticious topography was used at either side for the convenience of handling the lateral boundaries.

The next slide shows the nearly steady conditions that developed in the numerical integration for the height field. The pattern resembles conditions in Region B with a stational jump on the lee slopes of the mountains. The

solution for velocity shown in the next diagram shows very high velocities in the lower layer with magnitudes reaching 50 meters per second compared to a final value of 12 meters per second further east.

Finally a model calculation was made for a single case for February 20, 1968 for which special observational data was available. Unfortunately, the day was not one of strong winds but it is interesting to see how the model compared with such details. In the next slide two model solutions for height, shown by the dots and circles, are compared to the potential temperature analysis from aircraft observations. The model does not similate the lee waves but it does show some features of the low level structure on the lee slope of the mountain. However, the velocity observations do not compare so clearly to the model solution for velocity. There are no velocity observations in the area of interest.

The time dependent depiction of the numerical model results for the two-layer case provides considerable appreciation of the features in the solution. I wish to show a movie that first illustrates 10 of the 40 simulations made for the general analysis and then the evolution characteristics in the simulation for the actual Colorado situation.

The movie has the following parts. I was unable to determine by eye all of the specific parameters used in the first 10 cases, but I thought I could tell which domain each one represented.

a. M = .6 Region B
b. M = .6 Region B'
c. M = .6 Region D
d. M = .6 Region E
e. M = .6 Region E
f. M = .8 Region E
g. M = 1.0 Region C with small instability
h. M = 1.0 Region C with small instability
i. M = 1.0 Region E with large instability
j. M = 1.0 Region E with large instability
k. Colorado case heights, large domain shown
ℓ. Colorado case velocities, large domain shown
m. Colorado case heights, local domain shown
n. Colorado case velocities, local domain shown

(Movie for two-layer model results)

Further work on the problem using the approach of this type of nonlinear model would certainly require study of the influence of surface friction and the role of the artificial trapping of wave energy implied by the upper boundary conditions plus many other effects. The complexity of the mathematics for the two layer model suggests that a similar form of analysis would not be possible for a model with more layers. Thus there remains no good reason to stay with such poor vertical resolution. More recent studies have considered models with many layers and models with well formulated linear representations. In other words, research in this area has progressed beyond what I was able to achieve.

B. Gravity Waves

The label of gravity wave is given to a large number of mesoscale phenomena. Sometimes it is clear that the phenomena do involve gravity wave processes. In other cases the gravity wave process is a likely explanation for the phenomena but nothing can be proved easily.

Fundamentally, a gravity wave is a dynamical phenomenon where the acceleration of gravity is essential for producing the basic restoring pressure force for horizontal motions. This effect can be a dominant factor in determining the evolution of atmospheric disturbances for a wide number of space and time scales covering the entire mesoscale range. For lower frequency phenomena the Coriolis parameter becomes important to this direct restoring mechanism and we refer then to gravity inertial or inertial gravity waves.

Like many mesoscale phenomena, observations are usually inadequate to properly define the structure and propagation characteristics of the gravity wave. In many cases we have to rely on surface data alone for quantitative information, but then it can be very difficult to understand the information.

Many theoretical studies have been made for the gravity wave. Vertical propagation, horizontal propagation, resonance and trapping, finite amplitude steady shape cases, nonlinear deformation, instability, critical level phenomena are some of the many aspects that have been investigated. However, application of the theoretical results has been difficult.

In this lecture I wish to discuss several specific studies that I have made to advance our understanding of the role of gravity waves in the atmospheric system. In the first study, an extension of simple dynamical theory to an atmospheric situation was attempted. In the second and third studies, attention was given to isolating the structure and effects of gravity inertial waves using atmospheric observations.

Interaction of vertically propagating gravity waves with the mean state

An important feature of gravity waves is their vertical propagation. In many cases we think only of horizontal propagation effects. However, conditions are rare when the identity of a wave at a given level persists for synoptic time scales because of dispersion, dissipation and the vertical spreading of the wave signal.

As the gravity waves propagate upward, amplitudes of the associated velocity oscillations can frequently increase because of the reduction in mean density. This means that waves which appear small in the troposphere can have important effects on the stratosphere. Topography, convection and jet stream adjustment processes assure the presence of gravity waves in the troposphere which can propagate upwards.

Vertical profiles of wind observations in the stratosphere have shown the existence of a relatively small scale vertical structure and thus large shears in the mean flow. There has been interest in understanding the relative role of small scale gravity waves, the atmospheric tides, and other processes in producing this structure.

In this study the nonlinear interaction of vertically propagating gravity waves with the mean flow was investigated. For simplicity the nonlinear process was limited to the wave-mean flow interaction. The nonlinear interaction between wave modes was ignored. It was felt that this would retain an important form of interaction because of the characteristics of the critical level phenomenon discussed in an earlier lecture. Because of this simplification, it was possible to modify the gravity wave numerical model for vertically propagating waves that I discussed before to represent this nonlinear interaction.

The basic concept is as follows. The presence of a vertical shear in the mean flow can cause a critical layer effect for a vertically propagating gravity wave. At a critical level, the wave propagation is blocked and large gradients in the vertical flux of wave momentum can develop. This momentum flux gradient implies that an acceleration in the mean flow, u_o, will occur which can change the critical layer. The expression for this acceleration is approximately

$$\frac{\partial u_o}{\partial t} = -\frac{1}{\rho_o}\frac{\partial}{\partial z}(\rho_o \overline{u'w'})$$ where primes refer to wave variables.

A series of model simulations were performed to determine some of the possible results of this interaction.

Results are presented in two publications:

Jones and Houghton, 1971. The coupling of momentum between internal gravity waves and mean flow: A numerical study, J. Atmospheric Sciences, 28, 604-608.

Jones and Houghton, 1972. The self-destructing internal gravity wave. J. Atmospheric Sciences, 29, 844-849.

The basic model is of the same form as described in a previous lecture. Rotation is ignored, there are no variations in the y direction, the wave is periodic in the x direction and there is no viscosity effect up to the height of 100 km except in the last experiment. The basic state is isothermal. Retaining this very simplified system made it possible to extend directly the previous modeling study. The intent was to suggest the importance of certain mechanisms rather than to try to make a complete representation of an atmospheric phenomenon.

In order to best understand the final nonlinear simulations, the problem was approached in stages. The interacting system investigated can be represented schematically as follows:

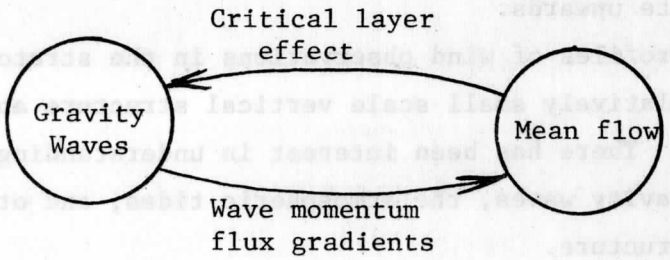

This cycle was considered in parts.

a. Critical layer effect with mean flow fixed

b. Critical layer effect with mean flow a prescribed function of time

c. Full non-linear cycle.

It was important to study the situation in part b to make additional checks on the model performance and to better understand the final solution.

The details of the theoretical considerations will not be presented here. However it was possible to separate the effects of shear in the mean flow from acceleration of the mean flow on the wave.

The following two frequency definitions need to be used:

ω : the frequency as observed in the fixed reference system.

ω' : the intrinsic frequency or the frequency as observed from a frame of reference moving with the local mean velocity of the fluid, u_o.

The following relationship exists between these two quantities.

$$\omega' = \omega + k u_o$$

where k is the wavenumber for the x direction variations. The critical layer effect occurs at the point where $\omega' \rightarrow 0$ and this happens when the gravity wave propagates up through a layer with a mean shear $\frac{\partial u_o}{\partial z}$. On the other hand,

the local acceleration of the mean flow changes the frequency approximately according to the expression $\frac{\partial \omega}{\partial t} = - k \frac{\partial u_o}{\partial t}$ and thus the intrinsic frequency is not changed by this process and local mean flow acceleration alone cannot cause a critical layer effect.

It can be concluded that the mean motion accelerations affect critical layer phenomena only by altering the shear zone through which the waves subsequently propagate. Once mean accelerations have occurred, critical zones can no longer be determined by the relationship of the mean winds to the fixed coordinate system. Thus a time-varying mean state results in a zone instead of a single level for the critical effects for a wave forced with a given frequency and horizontal wavenumber at the lower boundary. This would tend to lessen the vertical gradient of wave momentum flux and thus to cause acceleration of the mean flow over a deeper layer.

In the first test with a full nonlinear version of the numerical model, the constant shear profile of the mean flow with a critical level at 56 km height was used for the initial state. Then wave energy was introduced at the lower boundary at a constant rate and the subsequent results observed.

The slides show the results. In the first slide is the solution when the mean flow was held fixed. Note the critical level and the very large gradients of wave momentum flux at the critical level. In the nonlinear case the solution as shown in the next diagram resulted. The critical level now appears to be a zone, the vertical gradients of wave momentum flux are less at this level than in the previous case and the mean flow has been accelerated at this level. The next slide shows the details of the changes in the mean flow. Note the creation of the very large vertical shears which could result in subsequent shear instability.

Six numerical solutions shown in time lapse by a movie help to highlight the properties of the gravity waves in this study. I must apologize in advance because the images came out very faint and are hard to see. I will explain what to look for to help offset the poor pictures. The u components of the wave and mean flow are shown as a function of height in the same manner as in the slides. The movie has six parts as described.

a. Linear model with no mean flow and constant forcing at the lower boundary. The development of the basic constant amplitude wave discussed in an earlier lecture is seen. Note the downward phase propagation even though the energy is moving upward.

b. Linear model with fixed critical level and constant forcing at the lower boundary. The development of critical level characteristics as shown in the first slide is observed.

c. Linear model with fixed critical level and forcing at the lower boundary for only 3 hours. The movement of a wave packet which gives the group velocity is easier to follow.

d. Linear model with initial critical level and with subsequent specified acceleration of the mean flow to remove the critical level for later wave energy to reach the 56 km height but not for the waves already near the 56 km height.

e. Same as part d except that forcing at the lower boundary is stopped after 3 hours, so the effects of the mean velocity acceleration on the group velocity can be more easily observed.

f. Nonlinear case with an initial critical level at 56 km.

(Gravity wave ensemble movie)

Two additional calculations were made with the nonlinear model to investigate situations more relevant to the stratospheric situation. A small eddy viscosity term was added to represent turbulent effects and to control numerical oscillations. In the first case, a wave packet was sent up through the atmosphere with initially no mean wind flow. This could represent a situation where gravity waves produced for a short time in the troposphere propagate upward into the upper stratosphere where vertical shears of the mean wind are not a significant feature. The transitory nature of the gravity wave system creates vertical gradients of wave momentum flux even without a critical layer present initially. The numerical model simulation showed the subsequent acceleration of the mean flow, the development of a critical layer and then the blocking and eventual dissipation of the wave system by the diffusion effect. The end result was that about one third of the original wave energy was converted to mean flow energy and the remainder was lost to dissipation. Results are shown in the next slide.

In the second experiment a random continuous forcing was applied at the lower boundary. The model simulation showed the development of a vertical structure in the mean flow similar in very general terms to that sometimes observed. Results are shown in the next slide and then for both experiments in movie form.

(Gravity wave movie)

Observations showing horizontal propagation of an internal gravity wave

Reference, a paper by one of my students,

Eom, 1975. Analysis of the internal gravity wave occurrence of 19 April 1970 in the Midwest. Monthly Weather Review, 103, 217-226.

In this study the problem of identifying and describing the gravity wave phenomenon using routine atmospheric observations was considered. Even though we feel that gravity waves are common in the troposphere, it is often difficult to identify and analyze them, especially those which are large enough in horizontal scale to affect weather conditions.

Satellite images have shown cloud structures that act like horizontally propagating gravity wave systems. Sometimes this motion is very striking in time lapse pictures. Nevertheless, most of our quantitative observations of the gravity waves come from surface instruments such as the barograph. At Wisconsin there has been a high interest in the surface pressure fluctuations with a period of several hours. We now have a half dozen accurate pressure change recorders in the Madison area to describe more completely the characteristics of such pressure oscillations.

On April 19, 1970 a very large pressure change was observed in Madison. The pressure dropped 11.5 mb within 2 1/2 hours and then rose slightly. Noticeable changes in the surface wind occurred at the same time which were not related to any precipitation or convective activity. We attempted to identify and understand this event. It was likely a horizontally propagating internal gravity wave and the case was good for demonstrating several diagnostic methods.

The barogram traces and hourly surface observational data from 44 stations were studied. The analysis focused on the variations of surface pressure, wind and cloudiness, all of which showed short-period oscillations and changes during this time. At Madison, it had been noted that the stronger winds at the surface were associated with lower pressure and decreased cloudiness.

The basic synoptic situation is summarized in the next slide. A weak surface low existed in the central part of the United States with warm frontal conditions in much of the Upper Midwest area. Thus wind flow was easterly at low levels and the air was very stable. At higher levels a jet stream of moderate strength coming out of the southwest existed to the west of the area where the gravity wave phenomena occurred. No significant precipitation was occurring in the region of interest. The next slide shows the vertical structure of temperature along the path of the disturbance. Note the very stable layer at lower levels.

The following diagram shows the barogram traces for surface pressure for stations along a southwest-northeast line going through Madison. The propagation of the primary impulse is clearly shown. Also subsequent oscillations are evident. Synoptic surface pressure analyses were made to determine the horizontal structure. It showed well defined features which were circular in shape. It was possible to show the track of the low pressure center and a center for maximum surface wind speed deviation. Both were closely correlated and moved to the northeast at about 50 meters per second.

In an effort to apply dynamical principles to the analysis, a simple internal gravity wave model was formulated to represent this situation. The two-layer model treated the low stable layer as the lower layer and the rest of the troposphere as the upper layer. Rotation was ignored, justified on the basis of the short period of oscillation and propagation in one horizontal direction was assumed. The incompressible version of the model used the same two layer equations as in the mountain flow study except that the equations were linearized.

The model provided not only predicted phase speeds which could be compared to the observed wave, it also gave eigenfunctions which related variations in the important dynamical parameters, surface pressure, horizontal wind speed and the vertical displacement of the layer boundaries. By specifying one parameter such as the surface pressure, the value of all the others were determined. The vertical displacement at the top of the lower layer was assumed to correlate directly with the low level cloudiness. In this way a quantitative relationship of low level wind speed to the surface pressure change way predicted and the relationship to cloudiness estimated. The schematic of the model gravity wave structure is shown.

Results from the model were used to study station data for cloudiness, wind speed and surface pressure. The next slide shows the comparison for cloudiness. Changes in cloudiness at the time of the primary pressure decrease appeared to be consistent with the model but it was not possible to see such a clear correlation at other times. The correlation for wind speeds was good. The following slide shows the quantitative determination of wind speed determined from the surface pressure measurements using model eigenfunctions for both a pressure coordinate and an incompressible height coordinate formulation. These are shown with the dashed lines. The observed wind speed deviations are shown in the solid lines.

There were numerous approximations made in this analysis and it is unwise to claim that the actual structure of the phenomenon corresponds well

to the two layer model. Nevertheless, this analysis has demonstrated how basic dynamical considerations can be combined with multivariable analyses to give stronger evidence of a gravity wave type phenomenon in the atmosphere. The dynamical approach would be greatly helped if information on the vertical structure of the phenomenon was available. In this study vertical structure was assumed to be related to characteristics in the synoptic scale thermodynamic structure of the atmosphere.

Isolation of the Gravity Inertial Motion component for general tropospheric conditions

In the previous study a specific case was analyzed where the gravity wave effects were unusually large and where other scales of motion could be rather easily ignored. It is appropriate to consider diagnostic techniques that can isolate the gravity inertial motion component in more general synoptic situations even when the synoptic scale features may be intense. This is a basic problem for mesoscale meteorology.

The gravity wave isolated in the last study is probably not the most important type to analyse. The gravity inertial component associated with the extratropical cyclone development and jet stream maxima is probably much more relevant to the problem of mesoscale precipitation characteristics. It would be related to adjustment processes in the jet stream. I want to suggest some possibilities for this type of diagnostic analysis. Current observational data may not have the accuracy and consistency for this form of analysis but it would be feasible to use on numerical prediction model output.

It is possible to think of atmospheric motions as consisting of two components. One is the quasi-geostrophic or balanced state which describes the general evolution of large scale features. The other is the fundamentally unbalanced gravity inertial mode which relates to adjustment processes of the large scale and to structures with smaller scale energy sources. The separation of these components is clear in simple linear models such as those which have been used for adjustment studies.

However, for the general situation, definition of the gravity inertial component is not so easy. Isolation of this component according to frequency is confused due to Doppler shift effects and to the continuous nature of the energy spectrum in frequency. The ageostrophic component alone will describe the gravity inertial component but it also includes aspects of the large scale situation as shown by solutions for filtered equation systems such as the quasigeostrophic, balanced and, more recently, the semi-geostrophic system.

The analyses approach suggested here is to subtract the fields defined by the filtered systems from the total variable field in order to define the gravity inertial component. The multiplicity of filtered models than can be used means that the gravity inertial component so defined will not be unique.

This method was tested on the output from a simple two layer primitive equation model. Both quasigeostrophic and balanced equation systems were used to determine the filtered data fields. The quasigeostrophic variables were determined both from the pressure field in the primitive equation solution and from a prediction model run in parallel with the primitive equation model. In this way two estimates of the quasigeostrophic variables were made.

The balanced model variables were determined from either the pressure field or the streamfunction in the primitive equation model results. Then which ever of the two was not so prescribed was then determined from the balance equation, $\nabla^2\phi = f\,\nabla^2\psi + 2\,J\left(\frac{\partial\psi}{\partial x}, \frac{\partial\psi}{\partial y}\right)$

The vertical motion was then computed from these values of stream function and pressure using a complicated set of equations that had to be solved iteratively. Thus there were two fields of vertical motion that could be determined for the balanced system, according to which variable in the primitive equation output was used to specify the system.

Schematics for the various methods to obtain filtered model vertical motions as shown below:

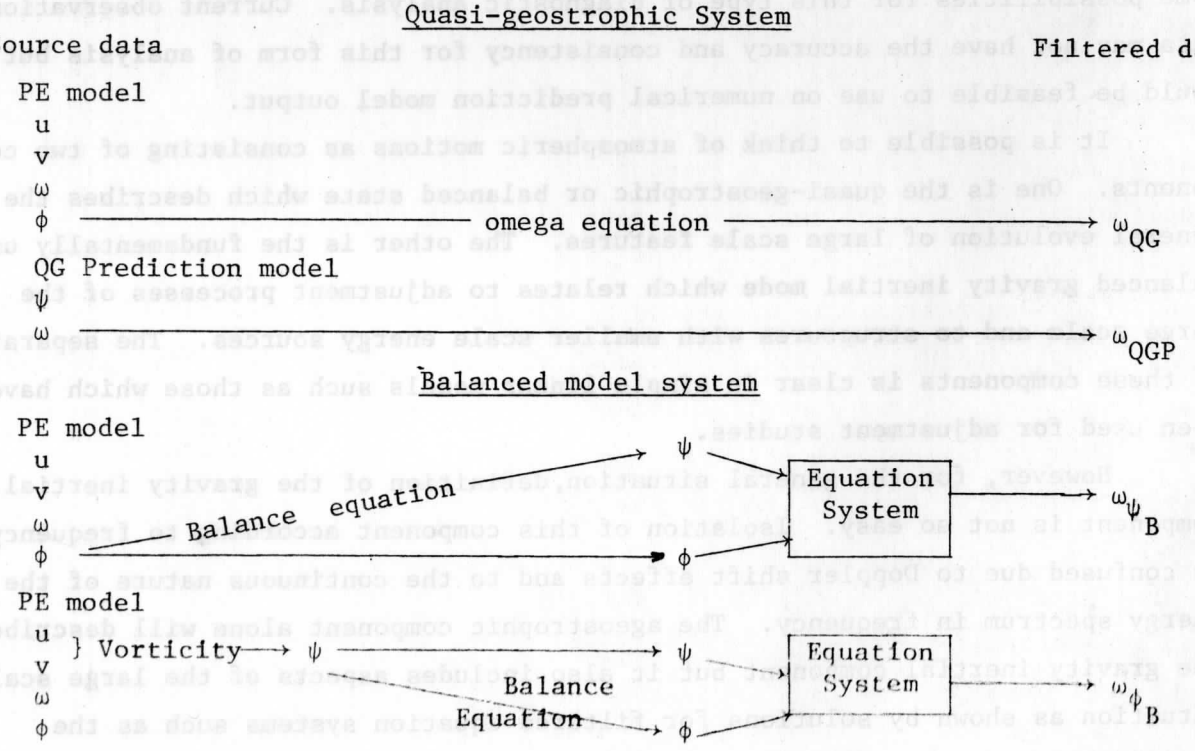

The four filtered model vertical motion fields were subtracted from the primitive equation model vertical motion, ω_{PE}, to give the estimate for the vertical motion associated with the gravity inertial waves.

These analyses were performed on the output of the two layer model for the simple case of the propagation of a jet maximum in a channel with a constant Coriolis parameter. The first slide shows the initial conditions with the isotachs for the u component and the vertical motion. The initial vertical motion was specified using the quasigeostrophic relationships. The next slide shows the primitive equation model results after 24 hours for the vertical motion field. The jet maximum center has moved to the position shown by X. The vertical motion shows the classical 4-cell pattern consistent with quasigeostrophic theory for the circulations about a propagating jet core. The horizontal structure of this circulation is shown by the meridional ageostrophic velocity component at the upper level in the model in tenths of meters per second.

The vertical motions computed by prognostic quasigeostrophic model and quasigeostrophic vertical motion equation using the primitive equation pressure field, panels A and B respectively, are shown in the next slide. They both show the 4-cell pattern. These fields were then subtracted from the primitive equation vertical motion for the same times and the results are shown in the next figure. These should have some relationship to the gravity-inertial waves. An oscillation is observed resembling a standing oscillation about the jet core position.

The two vertical motion fields obtained by the balanced method are shown next. Differences between these and the primitive equation vertical motions are shown. Again an oscillation with about a twelve hour period is observed.

These are very preliminary results and I do not mean to imply that new insights into the dynamics of a propagating jet or gravity inertial waves has been obtained. It is encouraging that there was consistency between the results using the four different filtered model values. I just wanted to suggest a type of analysis that could be used to objectively determine the features of the gravity inertial component in model output and someday perhaps in the atmospheric observations.

C. Precipitation Characteristics (Radar Echo Studies)

One of the most important problems of mesoscale meteorology is the forecasting and understanding of precipitation. Even though precipitation can be related to synoptic scale features in the atmosphere, the occurrence and intensity characteristics of precipitation are clearly at the mesoscale.

The development of radar sensing techniques during and after World War II has given us the capability to observe the three dimensional characteristics of precipitation. The radar technology has been advanced to include doppler and dual doppler systems which by determining the horizontal motion components of the precipitation drops can provide some information on the horizontal velocities in the storm. This technique has been particularly useful for studying vortex motions in severe thunderstorm and relating them to the occurrence of tornadoes.

Determination of quantitative precipitation rates is still a problem. The use of a surface observing network is difficult because of the sampling problem. Radar signal returns are not linearly related to rainfall rate. Calibration factors can be estimated for individual radar systems but it is not always safe to use the same calibration factors for different systems without verification checks. There has been some success in correlating satellite visible image brightness with convective rainfall rate in Florida but the general determination of quantitative precipitation rates from satellite data is not yet feasible. The use of microwave sensing from satellites is another possibility for this determination.

At the present time, the entire eastern two thirds of the United States is covered by a National Weather Service weather radar network. The slide shows the positions of stations. Their spacing is close enough so that a 250 mile or 400 km range would overlap. However, for many situations of active precipitation, the 125 mile or 200 km range is considered to be a realistic range for useful data in which case there is very little overlap.

National summaries of radar data including information on radar echo tops are transmitted frequently on the facsimile communication system in the United States. These show areas of radar echoes outlined subjectively from individual radar scope images. In late 1971 an experiment was made to provide objective digital radar data that would be easily transmitted and analyzed. This was called the Digitized Radar Experiment, D/RADEX. Resolution of the data transmitted for operational forecasting purposes has not been sufficient for detailed studies of the information. With the development of video and data transmission systems such as AFOS and McIDAS, the access to current radar information should improve.

An important problem is to utilize all of this radar information in weather prediction methods. There has been very little progress in merging the radar data with automated weather prediction systems including numerical

weather prediction. This involves two basic considerations. First is the use of radar information for general initial data specification. The second is to determine the aspects of radar data which could be used as explicit forecast parameters in numerical and deterministic prediction methods. Many of the detailed features in the radar data would not be expected to be represented in the prediction model. In the current operational models, precipitation is an output parameter that involves parameterization formulations.

There are, at least, two possible uses for the radar data in the specification of the initial state. The first involves the analysis for the moisture parameters. Currently relative humidity is determined from radiosonde observations and cloud data from sources such as surface observations and satellites. Such analyses might be improved by including the radar data. Analysis for cloud water and precipitation liquid water content would be greatly improved with the radar information; however, these are not input parameters for current operational prediction models. The second possible use for radar data is to help specify the initial vertical motion fields. This requires having direct relationships: between radar information the quantitative precipitation rate, between precipitation rate and the vertical structure for latent heating, and then between the latent heating profile and the vertical motion fields at the scale resolvable in the model. At the Numerical Weather Prediction Conference last October in Silver Springs, Maryland, a paper was presented by the numerical modeling group at The Pennsylvania State University concerning a test of this approach for a mesoscale numerical model (Tarbell, Warner and Anthes).

For the last few years I have been investigating radar information to determine how useful it would be as an explicit forecast variable in prediction schemes. This involved studying its predictability characteristics and its relationship to other variables that would be part of the prediction scheme.

The first study involved a comprehensive statistical analysis of radar precipitation data over part of the United States. It is discussed in the publication:

> Mielke and Houghton, 1977. An Analysis of radar echo systems for the Upper Midwestern United States. Journal of Applied Meteorology, 16, 833-843.

Radar echo structure includes very small elements that may have a lifetime less than an hour and larger echoes that can persist for hours. In order to focus on echo characteristics that have a chance to be resolved in mesoscale models, only the largest scale of organization that could be found was considered. Many descriptive studies of radar echo characteristics have looked at

smaller scale aspects. Organization and evolution of radar echoes have been observed and discussed for many years. The characteristics of the bands and circular shapes have been described in terms of spacing, movement orientation to synoptic features, and development and decay processes.

In this study groupings of echo patterns were identified that moved as a unit retaining a similar structure characteristic in time. These were referred to as echo systems and were assumed to be dynamically linked. The envelop of the system was the basic parameter for the study. Original radar scope photographs were used in order to have the most complete form of the data. However, this meant that the analysis was subjective and very tedious.

The data from 8 radar stations in the Upper Midwest of the United States from 1974 were analyzed. A total of 203 radar echo systems were tracked and described. The next slide (a repeat of the first slide) shows the area of the data. It is from a region where there is plenty of extratropical cyclone activity. Thus frontal and air mass precipitation situations were well represented in the data. The next slide shows the distribution of the data according to the time of year. Most of the cases were from Spring and early Summer and from the late Fall. Each echo system was classified as a warm front, cold front or air mass type depending upon its relationship to the features National Weather Service surface analysis. The following slide gives further details on the characteristics of echo groupings that were included and excluded from the analysis.

Basic results of the study are now shown. The next slide shows the frequency distribution for the echo systems of the three basic categories (warm front cold front and air mass) according to the maximum area observed for the system over its lifetime. For circular shapes the area of 10,000 km^2 is equivalent to a radius of approximately 55 km. The maximum area statistics can be summarized as follows:

Echo type	Equivalent radius	
	Mean	Standard deviation
Warm (65 cases)	75 km	68 km
Cold (85 cases)	58 km	57 km
Air mass (53 cases)	32 km	30 km

The mean radius for the frontal type systems is large enough so that they could be resolved by mesoscale models with a grid spacing less than 30 km.

Of course, since many of the shapes are not circular, perhaps we should not be quite so optimistic. On the other hand there are some precipitation systems which were significantly larger. It is reasonable to expect operational numerical prediction models to have this kind of resolution in the not too distant future.

The next slide summarizes the other key factor, the lifetime of these echo systems. As expected from physical considerations, the warm frontal types have the longest average lifetimes and the air mass type the shortest. The mean lifetimes for the three types are 8.1, 5.6 and 3.9 hours respectively for the warm front, cold front and air mass cases. The differences were statistically significant to the 99% confidence level.

The lifetimes of the frontal category echo systems are long enough to warrant their inclusion in mesoscale prediction models as dependent variables. This possibility for deterministic predictability was not evident in the short lifetimes of individual radar echoes. Methods of simple extrapolation for predicting the movement of radar echo areas have shown skill for periods as long as three hours. Longer periods for prediction should be possible for some aspects of the radar echo distribution based on the results obtained in this study. Of course this will require specifying the proper prognostic and diagnostic equations.

The analysis showed a direct relationship between duration of the echo system and its area. The next slide shows the scatter diagrams and fitted quadratic curves for each of the three echo categories. The life cycle of the echo systems in terms of area of coverage was relatively symmetric with maximum area being obtained about half way through the life cycle for all three echo categories. The next slide shows the frequency distribution for the ratio of the time to reach maximum area to the total lifetime.

In order to incorporate the radar echo or radar echo system into a model as a regular dependent variable, it is necessary to formulate the appropriate prognostic and diagnostic relationships to the other variables of the model. This study with the echo systems was extended to determine some relevant correlations.

Distance from the surface frontal position was examined for 106 of the frontal category echo systems. The frequency distribution for distance of the initial echo location was determined. For the warm frontal case, the average position was 80 km ahead of the surface frontal position with a standard deviation of 67 km. A large number occurred in the 80-120 km range. The cold front

echo systems occurred much closer to the surface frontal position with a mean distance of 19 km ahead of the front. Even though the standard deviation for this statistic was 45 km, nearly half of all the system started within 16 km of the front.

The relationship of the radar echo movement to the upper level winds has been examined in a large number of studies. Not only are the mean differences in speed and direction important, but also the correlation coefficient and the regression equations comparing the two velocities are useful. These relationships were determined for the echo systems analyzed in this study.

The direction of movement of the echo system was compared to the wind directions for the following levels, 700, 500, 400-850, 400-700, and 300 mb levels. The layer quantities were the average of the value at the top and bottom of the layer. In general as summarized in the next slide, the mean direction of motion was to the right of the wind direction except for the air mass cases. The means ranged from 2.5° to 15° to the right for the frontal cases but from 5° to the right to 4° to the left for the air mass case. The diagram shows the frequency distributions for the two categories for each echo system class for which the correlation was the best.

The following table summarizes results for the better correlation cases.

Echo type	Wind level	Mean departure from observed wind	Linear regression equation	Correlation coefficient
Warm	500	8.2°	$D_{Echo} = .86\ D_v + 39°$	.86
	300	2.5°	$D_{Echo} = .79\ D_v + 53°$	.84
	4-700	4.5°		.77
	4-850	12.9°		.66
	700	9.2°		.62
Cold	300	6.9°	$D_{Echo} = .86\ D_v + 40°$	.94
	4-700	8.5°	$D_{Echo} = .85\ D_v + 44°$	.92
	700	12.1°		.91
	500	7.1°		.89
	4-850	14.6°		.89
Air mass	700	-4.1°	$D_{Echo} = .87\ D_v + 35°$	.86
	4-700	-2.3°	$D_{Echo} = .81\ D_v + 56°$	.83
	4-850	5.1°		.82
	500	-1.9°		.79
	300	-1.1°		.75

where D_{Echo} and D_v are the direction of movement of the echoes and wind respectively

A further analysis on the direction of movement was done to determine the dependence of these statistics on the size of the system. Each echo type category was divided into two equal samples according to size and the statistical analysis repeated. Results for the wind levels which had the best correlations in the last analysis are presented.

Echo type	Wind level	Size	Mean departure from observed wind	Correlation Coefficient
Warm	500	Small	2.5°	.92
		Large	13.1°	.74
Cold	300	Small	3.5°	.96
		Large	9.9°	.93
Air mass	700	Small	-1.0°	.76
		Large	-7.6°	.92

In the frontal categories, the larger echo systems move more to the right than the smaller ones. This was consistent with earlier studies which showed that small echoes tend to move to the left and large echoes to the right of mid-tropospheric wind directions. It is the opposite for the air mass systems.

A similar analysis was done comparing propagation speeds of the echo systems to the wind speeds in the various levels and layers. The 300 mb level speeds were not included because the large horizontal gradients in speed at that level due to the proximity of the jet stream caused large interpolation errors when finding the echo area conditions from the rawinsonde station data. Speed correlations were much less satisfactory than direction correlations, a result that has been obtained in other studies. Results are summarized below:

Echo type	Wind level	Mean departure from wind speed ($m\ s^{-1}$)	Correlation Coefficient
Warm	4-700	-7.8	.62
	700	-3.7	.56
	4-850	-6.9	.50
	500	-8.2	.43
Cold	500	-9.1	.56
	4-700	-8.5	.53
	4-850	-6.5	.46
	700	-3.8	.38
Air mass	4-700	-7.8	.60
	700	-2.9	.59
	500	-7.1	.56
	4-850	-6.5	.56

The next slide summarizes these results in vector form. The labels W, S and L refer to the mean wind, small systems and large systems respectively.

In a second study focus was given to examining the relationships between properties of the radar echoes and variables defined at the surface. This is reported in a paper which has just been published:

Thomas and Houghton, 1979. The relationship between cold-frontal radar echoes and selected surface kinematic parameters. Monthly Weather Review 107, 1589-1599.

This study considered relationships of variables with precipitation which would be expected to have a direct physical relationship. Such parameters would be likely variables for prognostic and diagnostic relationships to determine precipitation forecasts. Surface data is also available at mesoscale scale resolution due to the density of the surface observing system. To limit the scope of the study, only echoes associated with cold frontal situations were considered.

Radar echo data from the three stations Pittsburgh, Pennsylvania; Kansas City, Missouri; and Monett, Missouri for the years of 1977 and 1978 were used. These stations are part of the D/RADEX network, so their data was available for 12 minute intervals in digital form on magnetic tape. Thus it was possible to use the McIDAS system for an accurate and rapid determination of echo area, peak intensity, average intensity and movement. The average intensity was given by the average rainfall rate using a prescribed calibration curve for the R/RADEX data.

The frontal cases used were generally well defined cold fronts where the radar site was, at least, 500 km south of the intersection with the warm front. Quasistationary fronts were not used, nor fronts with evidence of a wave near the radar site. A total of 30 cases were identified; however, it was possible to analyze the data from only 11 of them. For these cases the properties of specific echoes that lasted at least 24 min and which remained within a given radar site area were determined. Note that actual echoes were used and not echo systems as considered in the previous analysis. Their average radius was about 24 km. The final data set contained 99 echoes. These were distributed in time as shown in the next slide.

The following variables were used in the correlation analyses.

For the radar echoes:

Area coverage
Change of area coverage in 24 minutes
Maximum intensity
Change of maximum intensity in 24 minutes
Average intensity (henceforth referred to as average rainfall rate)
Change in average rainfall rate over 24 minutes

Only the maximum intensity, average rainfall rate and change in average rainfall rate correlated significantly with the surface parameters, so these only will be discussed further. For the surface kinematic parameters:

Divergence

Divergence in region one hour before echo was there

Change in divergence over the one hour period ending at echo time

Divergence relative to the mean for a 9° latitude and 9° longitude square domain centered on the radar site

Divergence relative to this mean in region one hour before the echo was there

Change in divergence relative to the mean over the one hour period ending at echo time.

Divergence of moisture flux for the same 6 categories listed for divergence above

Relative vorticity for the same 6 categories listed for divergence.

These 18 surface parameter fields were determined from grid point values of u, v, and the mixing ratio on a 0.5° grid objectively analyzed from surface station reports using a modified Cressman analysis technique.

Examples of the detail in the radar echo and surface parameter fields analyzed are shown in the next three slides. The first shows surface divergence and the radar echo positions for 1500 GMT April 18, 1976 at Monett, Missouri. The second shows the divergence of moisture flux at the samt time. The third shows relative humidity for the same case.

As stated before, only three of the six radar parameters showed significant correlations with the surface parameters. The significant correlations are summarized for each of these radar parameters in turn.

a. Maximum intensity of radar echo

Correlations with maximum intensity of radar echo ranked in order of highest correlation coefficients for those cases significant to the 95% confidence interval (correlation magnitude of .23) are listed

.40 Relative vorticity relative to the grid mean at the echo location 1 hour before the echo was there

.40 Relative vorticity relative to the grid mean

-.38 Divergence of moisture flux relative to the grid mean at the echo location 1 hour before the echo was there

.35 Relative vorticity at the echo location 1 hour earlier

.34 Relative vorticity

-.34 Divergence of moisture flux 1 hour earlier

-.33 Divergence relative to grid mean 1 hour earlier

-.27 Divergence one hour earlier

.24 Divergence of moisture flux relative to grid

Thus we see that 9 of the 18 surface parameters had significant correlations. The relative vorticity and one version of the divergence of moisture flux were the best variables. Divergence itself was less satisfactory.

b. Average rainfall rate

Thirteen of the 18 surface parameters correlated significantly with the average rainfall rate estimated by the radar. Here again relative vorticity was the best variable and divergence or moisture flux was second best. Correlations tended to be slightly higher than those for the last radar echo variable compared to the correlation magnitude for significance at the 95% confidence confidence level (.23). The top five specific parameters are listed:

.53 Relative vorticity relative to the grid mean 1 hour earlier

.50 Relative vorticity 1 hour earlier

.47 Relative vorticity relative to the grid mean

-.43 Divergence of moisture flux relative to the grid mean 1 hour earlier.

.42 Relative vorticity

c. Change of average rainfall rate over 24 minutes

Only seven of the 18 parameters correlated significantly with the change of average rainfall rate over 24 minutes. Here the divergence of moisture flux was the best variable for correlation with divergence being second best. Correlation levels were about the same as for the maximum echo intensity parameter. The critical correlation coefficient magnitude for significance at the 95% confidence interval for this case was .24. The top 5 parameters are listed.

.42 Change in divergence of moisture flux over 1 hour

.41 Change in divergence of moisture flux relative to the grid mean over 1 hour

.38 Change in divergence over 1 hour

.37 Change in divergence relative to the grid mean over 1 hour

.29 Divergence of moisture flux

The scatter diagrams for the best correlated case for each of the three radar echo parameters are now shown. The first shows the maximum echo intensity correlation to the relative vorticity relative to the analysis grid means at the echo position 1 hour before the echo was there. The next shows the correlation between the average rainfall rate and the same relative vorticity variable. The third shows the correlation between the 24 minute change in average rainfall rate and the one hour change in the divergence of moisture flux.

For these three best cases, analyses were made for subcategories according to characteristics of the radar echoes. Varying degrees of significance

were found for the sub categories of

Midwest echoes (Pittsburgh excluded)
Postfrontal echoes
Line echo structures
Banded echo structures
Nonbanded echo structures
Larger area echoes
Smaller area echoes

The slides show correlation values for each of the statistically significant correlation cases shown respectively in the scatter diagrams.

Many separate statistical relationships have been presented here. I'll now try to summarize the more important conclusions of the study. The maximum intensity and average rainfall rate of the radar echoes showed significant correlation with many of the surface parameters tested, particularly the relative vorticity. These correlations were improved by using values of the surface fields for the area covered by the echo one hour before the echo arrived there, and also by using the value of the variable relative to the average over a local area grid. Banded echoes had much better correlations than nonbanded ones. The divergence of moisture flux correlated better than the divergence itself.

It is not practical yet to consider applying these results directly to operational forecasting. In the first place, only the properties of existing echoes were considered and not the development of echoes not initially present. Secondly, the relationships shown here would at best account for only 25% of the variance. Future work will have to consider the importance of the life cycle of the radar echoes on the correlations with other variables. Also correlations with additional variables in the atmosphere need to be considered.

Nevertheless, this study has provided hope that it will be possible some day to relate precipitation characteristics to other variables in such a way that they can be more completely included in deterministic prediction systems.

D. Wind Data from Satellite Images

The wide range of meteorological information that can be obtained from satellites by remote sensing methods has been discussed. At the University of Wisconsin there are numerous projects concerning the processing and analysis of this satellite data. With the McIDAS it has been possible to study quantitatively the cloud displacement rates that can be determined from geosynchronous satellite images. The determination of wind information from cloud motion data is of great

importance to meteorology. Wind data is urgently needed for the analysis and model initialization of the synoptic scales in subtropical and tropical latitudes and for the mesoscale at all latitudes.

Today I wish to discuss results of my research from the last five years on the mesoscale wind field information obtained from satellite cloud images. These studies were concerned with the computation techniques and accuracy of satellite mesoscale wind data, the correspondence of such winds with rawinsonde data and other indicators of mesoscale velocity fields, and with the utilization of such information in mesoscale numerical models.

Computation techniques and accuracy of satellite mesoscale wind data

There are two basic techniques used to determine the displacement vectors from the satellite images. Both require the accurate navigation of the images so that a precise relationship exists between coordinate positions of the data points in the two-dimensional display to positions on the spherical coordinate system of the earth. Very accurate navigation methods have been developed so that the allignment accuracy is better than the dimensions of a single element or pixel of the satellite data.

The first tracking technique is referred to as the single pixel method. Here the brightest point or other distinguishing feature of a cloud is located in each image. This requires being able to identify the same cloud in each image. For mesoscale fields, the highest resolution satellite image area used has a pixel element size of approximately 1 nautical mile by 1 nautical mile at the sub satellite point. The feature tracked has to have a lifetime long enough to be observed in, at least, three consecutive images for quality control reasons. The normal observing interval for the geosynchronous satellite is 30 minutes so the cloud must have a lifetime of 1 hour or more. Many of the smallest features in the high resolution data do not last this long. Thus to obtain much of the mesoscale wind information, it is necessary to have shorter time intervals between satellite images.

The U.S. satellites can be programmed to provide images at shorter intervals ranging from 15 minutes down to as short as three minutes. This requires restricting the latitude belt that is covered since the basic spin scan speed is fixed. By this means, the time frequency of observations becomes more consistent with the space scale of the observations for mesoscale wind determination.

The second tracking technique is referred to as the correlation method. In this approach the brightness data distribution in a small area of the image

at the first time is correlated to the brightness data distribution in the subsequent image in the region where the cloud is expected to be. The location of the center of the area is found for which the correlation coefficient is the greatest.

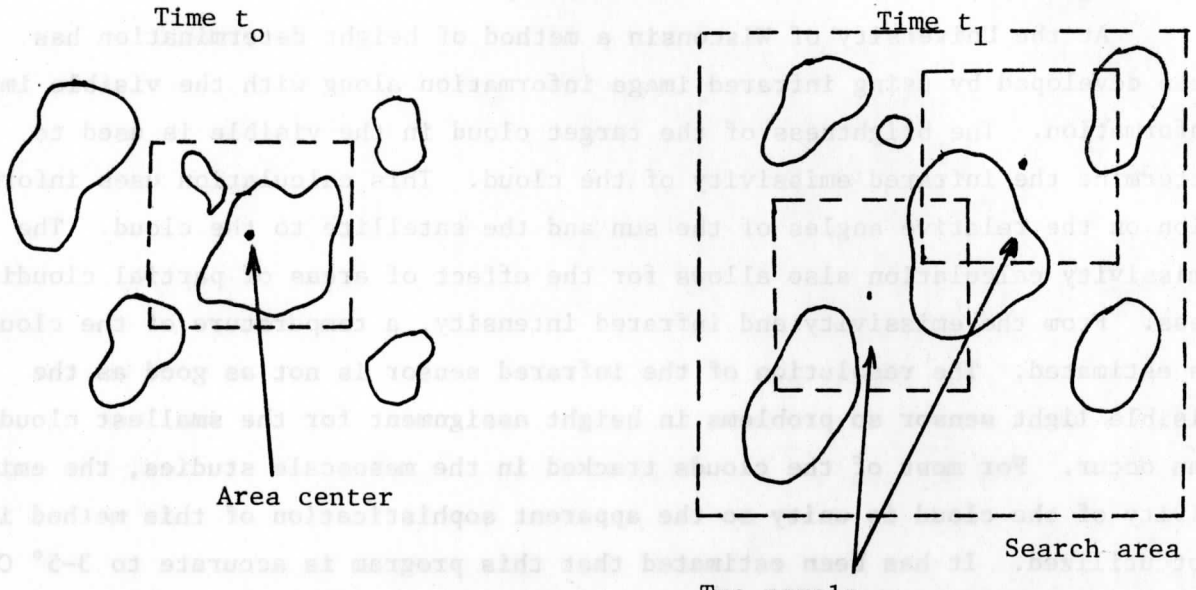

This method gives the average displacement of all of the features within the small area considered. This method has several advantages. First it is less sensitive to small irregularities in the data and second it could be used more easily in an automated cloud tracking procedure than the single pixel method. On the other hand, the correlation method is not so satisfactory in situations where clouds in the same area are at different levels and moving in different directions. In that case it requires a person viewing the time sequence to determine which cloud in the second image corresponds to the one chosen in the first image.

For tropical data sets including the mesoscale, the correlation method has been found preferable. Frequently, the clouds are at a single level especially in the trade wind circulation. However, for mesoscale wind data sets over continental areas in the middle latitudes, the single pixel tracking approach has been found to be more satisfactory.

An important aspect of the cloud tracking technique is to determine the height at which the velocity should be assigned. Many clouds are associated with convective motions thus there is always the problem that the cloud motion observed is not the same as the motion in the environment at the same level.

For tropical area measurements, it has been possible to find by statistical comparisons with rawinsonde data levels of "best fit" for winds from clouds of a well defined type such as trade wind cumulus to the radiosonde winds. However, in the middle latitude mesoscale situations, the variability in the height characteristics of the cloud system makes this method of satellite wind height specification not as satisfactory.

At the University of Wisconsin a method of height determination has been developed by using infrared image information along with the visible image information. The brightness of the target cloud in the visible is used to determine the infrared emissivity of the cloud. This calculation uses information on the relative angles of the sun and the satellite to the cloud. The emissivity calculation also allows for the effect of areas of partial cloudiness. From the emissivity and infrared intensity, a temperature of the cloud is estimated. The resolution of the infrared sensor is not as good as the visible light sensor so problems in height assignment for the smallest clouds can occur. For most of the clouds tracked in the mesoscale studies, the emissivity of the cloud is unity so the apparent sophistication of this method is not utilized. It has been estimated that this program is accurate to 3-5° C. Finally, the cloud temperature must be assigned a height. For mesoscale studies it is preferable to use pressure-temperature relationships derived from local radiosonde data instead of a standard atmosphere relationship.

The height error implied by the error in cloud temperature is in the range of 50 to 100 mb. This has important implications for error in the wind value for horizontal maps since with a large vertical wind shear in the atmosphere a height error results in a large error for the velocity vector. Vertical wind shear is often an important aspect of middle latitude mesoscale weather events.

A very important part of the cloud tracking procedure is the internal consistency check. A cloud is tracked for an entire sequence of images. For large scale studies, three consecutive images have been used. For mesoscale studies this has been increased to four or five as shown.

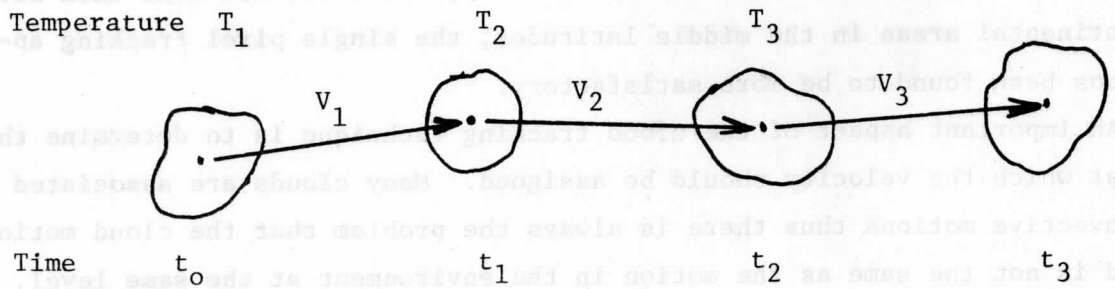

In this way several velocity and height determinations are made for the same cloud. It can normally be assumed that the cloud should have the same velocity and height over this time. Thus consistency of the velocities and temperatures for each element in the series can be checked. Irregularities in either suggests that the accuracy of the velocity determination is questionable. The final velocity and height is obtained by averaging the elements of the series.

The overall accuracy of mesoscale satellite wind data is discussed in the following reference:

Wilson and Houghton, 1979. Mesoscale wind fields for a severe storm situation determined from SMS cloud observations. Monthly Weather Review, 107, 1198-1209.

Quantitative estimates were made for 24-minute averaged wind vectors for a middle latitude baroclinic situation. The following error estimates were obtained:

Error type	RMS vector error magnitude ($m\ s^{-1}$)
a. Navigation	0.4
b. Image resolution	0.6
c. Single pixel tracking	1.1
d. Height assessment	2.5
e. Nonrepresentative cloud motions	3.7

If all except the first are considered to be random effects, then their combined RMS error is about 4.7 $m\ s^{-1}$. The analysis of the nonrepresentative cloud motion error required comparison with nearby rawinsonde reports which also can be nonrepresentative. Thus the magnitudes presented above especially for d and e should be used with some caution; however, the relative importance of the error types is probably quite realistic.

Correspondence of satellite mesoscale wind data with rawinsonde data and other indicators of mesoscale velocity fields

Regardless of how accurate the satellite wind data is claimed to be, its usefulness is strongly dependent on its correspondence and consistency with other forms of velocity data. Satellite wind data will never be able to give a complete three dimensional coverage, thus requiring its merging with other forms of information. Since at the current time, other forms of mesoscale velocity data are not readily available, they have been deduced from other sources in order to make initial tests of the mesoscale satellite wind data fields.

Even with the rapid processing capability of McIDAS, the production of a research quality mesoscale data set for areas as small as 360,000 square kilometers and containing only 300 wind vectors has taken up to 15 hours of time, mostly on the computer. This fact plus the need for extensive diagnostic analyses has limited the number of cases that have been studied. Results from the specific case studies should not be considered as general conclusions.

A comprehensive analysis was performed on data for May 6, 1975 which illustrates the correspondence of satellite wind fields to rawinsonde data, vertical motion fields implied by convective activity, and to a preliminary numerical model simulation of the situation based on conventional data input. Results appear in the following conference paper:

> Houghton and Lee, 1977. Mesoscale wind fields for the May 6, 1975 Omaha Tornado situation derived from SMS cloud observations. Preprint Volume, Tenth Conference on Severe Local Storms. Oct. 18-21, 1977. Omaha, Nebraska. Published by the American Meteorological Society, pp 16-21.

The general synoptic situation for the case study is shown in the diagram. A surface low pressure system existed in the Northern Great Plains area. A rapidly occluding frontal system extended eastward and southeastward out of this system. The cold front was also a dry line front marking the leading edge of dry air coming out of the Rocky Mountain region. At the upper levels a jet stream was located over the occluded front. A ridge at upper levels is shown by the dashed line.

The shaded area is the region considered for the study. A damaging tornado formed at the western edge of this area soon after this time. It takes the full screen of the video display to show all of the high resolution visible satellite data for this area.

The next picture shows the visible satellite image for this time for the central U.S. area. Information has been sacrificed to show all of this on the video screen at one time. Note the intense convective activity along the dry line cold front. The green outlines the area for analysis of the high resolution data. The next picture shows the infrared image at the same time. This emphasizes the active convective clouds along the dry line and the high clouds over the warm front. The next slide shows the high resolution visible data in the area for study. Note the large number of individual features that can be tracked. This covers an area roughly 600 by 600 km. The image for the infrared component at the same scale reveals its poorer resolution. It shows that high clouds

exist on the western and eastern sides of the region with generally lower clouds in the middle. The following diagram shows the positions of the surface fronts superimposed over the infrared image in black and white.

The basic synoptic features with the location of the main infrared cloud images, and with the location of special analysis areas and cross sections is shown. The high clouds to the east prevented obtaining an adequate three dimensional data set for determination of kinematic parameters such as vertical motion in that region. The vertical structure of the wind data was illustrated by considering a cross section through both frontal zones and a cross section just ahead of the cold front that passed through several areas of active convection.

The basic wind data obtained is shown in the next slide. Here it is easy to compare the data coverage for the upper air network, the surface hourly reporting stations and the mesoscale satellite data. The satellite data has been grouped into four layers according to characteristics in the vertical structure of radiosonde observations. The need to do vertical grouping emphasizes the relatively poor vertical resolution obtained in the satellite winds. A total of 310 wind vectors was obtained. The satellite wind data density is better at low level than high levels. However, the high level winds still have better resolution than the rawinsonde network. The image correlation tracking method yielded about half as many wind vectors.

The next slide shows the number of satellite wind vectors as a function of height. The basic height parameter is a cloud temperature which corresponds approximately to the pressure heights as shown according to local radiosonde data. The layers into which the data was groups are also shown. For comparison, the vertical distribution of satellite winds over an area about the same size but over Texas is shown. This is presented in the paper by Wilson and Houghton referred to earlier. The vertical distribution is more even. The horizontal coverage in the four layers used for analysis is rather inhomogeneous.

Returning to the first data set, a detailed comparison was made between the satellite wind data in a one degree radius region and the rawinsonde reports at the center for the level where data coverage was best. The satellite data was considered both in the original form as shown here and also after interpolation to a 0.5° latitude-longitude grid. Unfortunately rawinsonde data for the satellite image time of 1800 GMT was not available and the rawinsonde data taken before and after had to be averaged. The next slide summarizes the results. The RMS differences are in the same range as the error estimate for the

satellite winds. The differences are reduced when considering the mean of the satellite wind values and when using gridded satellite wind data.

The divergence and vorticity computed from the satellite winds for the 800-600 mb layer were compared to the synoptic features as shown in the next slide. Note the convergence centers near the cold front but the general tendency for divergence along the warm front. The vertical distribution of satellite wind data in the western two thirds of the study domain allowed rough estimates for vertical motion to be made. These were adjusted to satisfy a condition of zero vertical motion at 210 mb using an objective scheme proposed by O'Brien. The next slide shows the computed values at the midlevels in the troposphere. Vertical motion tends to be upward east and along the cold front with a pattern consistent with the active convective systems. Motion is upward in the shaded areas. Some weak upward motion exists ahead of the warm front. However, downward motion exists over the surface warm front which is consistent with the relatively inactive clouds there.

In order to further evaluate the three dimensional velocity fields derived from the satellite winds, comparisons of the fields were made with the output of a mesoscale numerical model and the satellite winds determined by NASA for the same case. The numerical model data was from a 6 hour forecast made with the Drexel University - NCAR model discussed before. It had a 70 km horizontal resolution and was initialized from standard observations six hours before the satellite wind data time. It was hoped that the model would develop some realistic mesoscale features since there appeared to be important synoptic scale forcing of the mesoscale.

The horizontal fields of the u and v components from the satellite winds and model are compared in the next diagram. There is some similarity in the general patterns with the v component field being more similar than the u component field. The gradients in the model wind data are larger in both the horizontal and vertical, at least, along the north-south cross section as shown in the next slide. Correspondence for divergence and vorticity does not appear to be close although some similarities can be observed. On the other hand comparison of the vertical motion fields is surprisingly good as shown next. The east-west and north-south cross sections for divergence, vorticity and vertical motion are not very good.

The next figure shows a comparison between the model, satellite winds and NASA satellite wind data for divergence at the 800-600 mb level. Correspondence is noted. Finally a comparison of the satellite and model vertical motions with the observed cloud features is presented.

The comparison with the model data served as much to reveal the deficiencies in the model simulation as it did to give any measure of the validity of the satellite wind information. Perhaps this type of analysis was premature.

A larger number of short interval satellite image data sets have recently become available as part of an ongoing mesoscale research program in the United States. This project is called SESAME. The availability of mesoscale rawinsonde reports will make direct verification of the satellite wind data possible. The next slide shows the augmented rawinsonde network that made 3 hourly observations for special observing periods. An even smaller scale rawinsonde network existed in the Oklahoma area. Data from these will be valuable for additional research on mesoscale satellite data including the derived winds and for research involving mesoscale modeling. The last analysis showed that help is needed for both areas.

The 35 km model covered the region outlined in green. Low level satellite wind data was obtained in the small outlined region in the center of the model domain where the high cirrus clouds did not obscure the lower clouds. One of the high resolution visible satellite images used is shown in the next slide. I showed the wind field obtained in my lecture on objective analysis. You'll recall that there was great sensitivity to the objective analysis scheme. The Barnes method was chosen to produce the grid point data for initialization. The next slide shows the initial fields in terms of divergence and vorticity with and without the satellite wind data. Note that the satellite wind data adds considerable small scale features to the initial data.

Experimental design is outlined on the board.

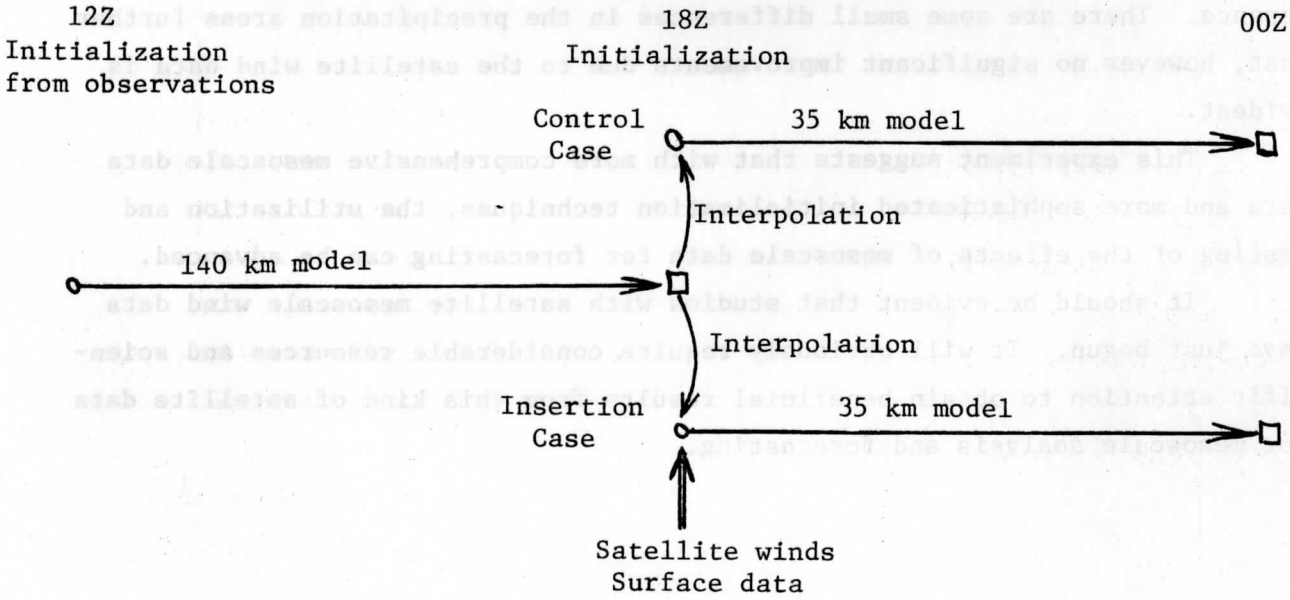

Very simple assimilation and initialization techniques were used since this was designed as an exploratory experiment to help design a valid Ph.D. case study. Initial vertically integrated mass divergence was prescribed to be zero.

Results of the model experiment are shown in terms of the derived parameters of divergence and vorticity. These highlight the adjustment and evolution phenomena in the model better than the velocity components themselves. The slide shows the results for divergence and vorticity after one hour. The divergence difference magnitudes have become smaller and outward gravity inertial wave propagation has started. The vorticity difference field remains contained within the insertion area and its boundary zone. After 6 hours, the divergence difference fields have reached the model boundaries especially along the direction of the upper level jet flow. Large vorticity differences remain in the original insertion area. Error fields for both divergence and vorticity reveal a structure similar to the mesoscale structure that develops in the control case.

Details of the evolution in the divergence difference fields in the insertion area is shown next. Even though there appears to be many small features, there is a low frequency component suggesting that some of the divergence information of the satellite wind data has been accepted by the model in terms of realistic features as well as noise. The details of the vorticity difference patterns show very clearly that a low frequency and realistic mode of evolution has been activated by the satellite data. However, the precipitation forecast of the model showed little effect of the satellite wind data. The next slide shows the predicted convective precipitation rate at 6 hours for both cases. The precipitation structure over Oklahoma and eastern Texas shows little difference. There are some small differences in the precipitation areas further east, however no significant improvements due to the satellite wind data is evident.

This experiment suggests that with more comprehensive mesoscale data sets and more sophisticated initialization techniques, the utilization and testing of the effects of mesoscale data for forecasting can be advanced.

It should be evident that studies with satellite mesoscale wind data have just begun. It will obviously require considerable resources and scientific attention to obtain beneficial results from this kind of satellite data for mesoscale analysis and forecasting.

E. Local Weather Prediction

The ultimate test for meteorology is the ability to make local weather predictions. This is what most of the general public needs and can use. Thus it is important that our observation, analysis and prediction technology and research address this matter. My discussion today will cover some aspects of this problem and summarize some methods that are used in the United States.

The problem facing local weather prediction is the extreme spatial and temporal variation in atmospheric conditions that can exist at the surface of the earth. This includes the variables of temperature, wind, sunshine and precipitation. The slide shows the dramatic effect that topography can have on growing conditions. This valley is from an area in Northern Wisconsin and it is referred to as a "frost pocket" because nighttime temperatures are generally much lower than in the surrounding area increasing the incidence of frost. The variations in the local climate affects the growth of the evergreen trees.

Local temperature variation is of practical importance to agriculture in Wisconsin. The next slide shows frost damage to a corn field that occurred in June. The local nature of the effect and sensitivity of the corn to the temperature is demonstrated by the sharp boundaries to the damage area shown in the next slide. Providing a local forecast that would be of value to this farmer is certainly a major challenge.

The mix of observational data available for local weather prediction is large. The next slide shows some of the main forms of data routinely available. The vertical, horizontal and temporal resolution characteristics are shown in schematic form. Surface data can provide more detail than suggested in this slide. Also satellites can provide more descriptive detail. The next picture shows a view of Florida taken by an astronaut from space. Satellite technology is approaching the point where this type of resolution will be routinely available.

Local weather prediction is of two forms, climatological and short range in time. Microclimatological information can identify many of the important spatial variations in weather conditions. Such information can be of great use to agriculture, transportation and even architectural design. Crop planting, the placement of surface transportation lines and the design of buildings to take the best advantage of solar and wind effects are some of the applications where the meteorology profession needs to show more clearly the benefits of using microclimatological data.

In the discussion today I wish to focus on the short time range aspects of local weather prediction. Here there is need for improving deterministic

prediction. Currently in the United States, precipitation forecasts for the 0 to 48 hour forecasts are given in terms of probability. This actually may be a more realistic method of presenting a forecast. However I would like to believe that some day short range forecasts would be able to give the time of beginning and time of ending of precipitation and a measure of its intensity instead of only a probability of occurrence.

There are four general approaches to local weather forecasting. Three of these are shown in the National Weather Service automated prediction system in the next slide. These are the dynamic prediction model, limited dynamic and kinematic models and the statistical model. The fourth is the subjective method used by the forecaster who has a familiarity with weather conditions in a given area.

The dynamic prediction approach to local forecasting involves the development of higher resolution primitive equation models. The National Weather Service has a model with 60 km horizontal resolution. Regional mesoscale models are being tested that have a horizontal resolution of 35 km. As noted before, there remains serious problems with the parameterization and initialization of such models. The time intervals for which useful forecast information can be expected is summarized in the following diagram.

Mesoscale forecasts from numerical models

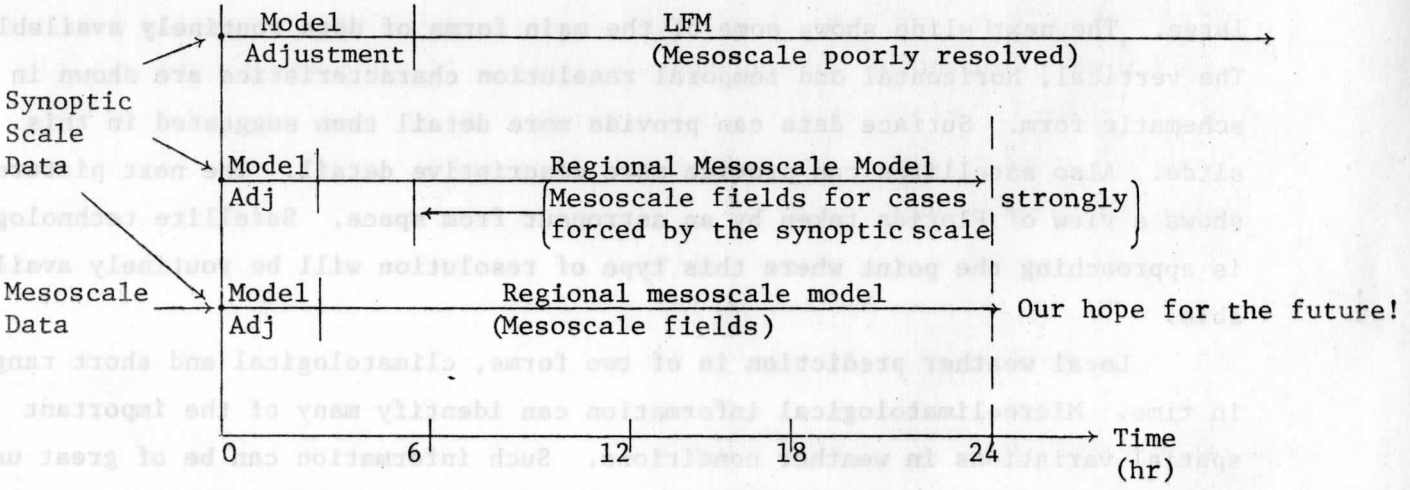

Regional mesoscale models have been shown to produce mesoscale fields. However, these are situations where the synoptic-scale has strong baroclinic activity which causes mesoscale structure to develop. Consistent performance for simulating mesoscale phenomena would not be expected until initial mesoscale

data becomes available. The prediction models cannot represent the initial time interval well because of model adjustments resulting from the initial state specification. It is likely that other forecast model approaches will give more useful information for the first few hours of the forecast period.

Several limited dynamic numerical prediction models were discussed earlier. These included the sea breeze model developed by Pielke where the synoptic scale motions were prescribed, and the boundary layer model where conditions at the 1.6 km level were prescribed.

Trajectory or advection model

The trajectory or advection model has been found useful for forecasts of mesoscale structure. In this method the large-scale advecting velocity is a prescribed parameter in the model and scalar quantities are then determined by the advection equation

$$\frac{\partial s}{\partial t} = - V_3 \cdot \nabla s + \frac{ds}{dt}$$

where V_3 is a given function of x,y,z,t and $\frac{ds}{dt}$ is a source or sink term.

Advantages of this approach are realized when the advecting velocity is relatively independent of the scalar being advected, and thus small scale structure in the scalar field can be retained. A good example of this is the motion of small cumulus clouds. Details of the cloud structure prescribed at the initial time can be found at a later time if the advecting velocity just acts to move it and not change it.

The advection model formulation is linear for the advection process which represents a major mathematical simplification. Also a Lagrangian formulation of the equation can be used which further reduces numerical truncation effects. In the Lagrangian formulation, the coordinates and magnitude of an element in the scalar field are the dependent variables. Gradients of the scalar field do not appear explicitly in the governing equations eliminating a source of truncation error.

$$\frac{dx}{dt} = u \qquad \frac{dy}{dt} = v \qquad \frac{dz}{dt} = w$$

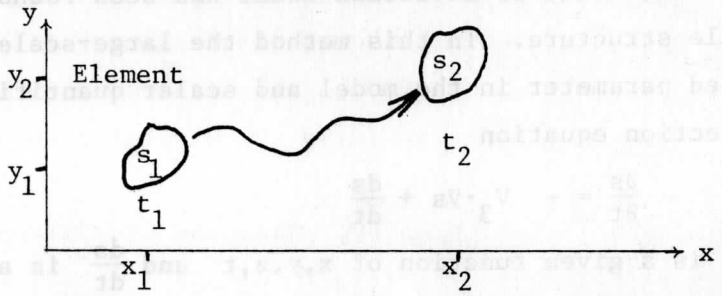

By using a trajectory model with adequate initial data, the National Weather Service has been able to make forecast maps that show considerable small scale structure. The next slide is an example of a 24 hour forecast for dew point obtained in this manner.

The U.S. Air Force makes cloud and precipitation forecasts by using the trajectory model approach. I will describe it briefly. A high resolution cloud analysis is obtained from satellite and surface observations in a five layer representation of the troposphere. The percent of cloudiness for each grid volume is then converted to a relative humidity parameter by using empirically derived functional relationships. The next slide shows the function which differs according to height. The relative humidity parameter is the CPS or condensation pressure spread which is the difference between the pressure of the air parcel and the pressure at which saturation would be reached by an adiabatic cooling process.

The CPS field is then advected in space according to the three dimensional velocity field from a primitive equation prediction model. The value of CPS in each air parcel is changed according to the pressure change of the parcel. If saturation occurs, the excess is removed as precipitation and the moisture content of the parcel is reduced. The forecast cloud cover is then obtained from the forecast relative humidity field be using the same functional relationships.

Statistical prediction

Statistical prediction models are becoming increasingly important for local weather forecasting in the United States. I wish to present a brief discussion of the method currently employed by the National Weather Service. A recent reference for this method is

> Carter, Dallavalle, Forst, Klein, 1979 Improved Automated Surface Temperature Guidance, Monthly Weather Review, 107, 1263-1274. (October issue).

References given in this paper lead to other informative material.

The statistical scheme is called the MOS or Model Output Statistics technique. The basic concept is illustrated in the slide. Here is shown how it compares to other formulations for statistical forecasting that have been used in meteorology. The so-called classical approach utilizes correlations derived between atmospheric variables and correlations for a single variable over time. The perfect prog (perfect prognostic) approach uses correlations between different variables at the same time. A perfect prediction assumption for one allows the scheme to be used to obtain the forecast for other variables.

The MOS scheme involves correlations between variables at a given time. However, predictor variables are derived from model output. By appropriate statistical methods it is possible to incorporate allowances for deficiencies in the model forecast into the statistical relationships. Every time the model is changed, the statistical relationships have to be changed to correct for model induced biases.

The basic statistical relationships are determined by a stepwise screening regression procedure to derive linear regression equations. The equation is of the form:

$$Y = a_o + a_1 X_1 + a_2 X_2 + a_3 X_3 + a_4 X_4 + \ldots . \quad a_{10} X_{10}$$

Here Y is the variable to be predicted. The a's are the multiple regression coefficients and the X's are the predictors selected by the screening procedure.

The screening technique selects the predictor which yields the highest reduction of variance in the predictand ($Y_{observed} - Y_{predicted}$) when combined with the existing terms in a multiple-regression equation. In the analysis, a large number of possible predictors are tested. They include observed weather elements, climatic factors and numerical model forecast parameters. The predictand is the observed value of the variable of interest. The predictor that

gives the largest reduction in variance becomes X_1. Then the program scans the list of predictors remaining to determine the one which results in the largest reduction in variance when used in conjunction with the terms already determined. This procedure is followed until all 10 predictors and their multiple-regression coefficients have been selected. Research has shown that 10 predictors is close to the optimum number of predictors for this application of the statistical method. The set of predictors and multiple regression coefficients vary according to the numerical model used, the variable being predicted, the location for which the prediction is being made, and the length of the forecast.

MOS forecasts are produced from output of both the PE and LFM prediction models. The LFM results are available sooner and determine the "early" guidance statistical forecasts, the PE data gives a "final" guidance statistical forecasts. These local area forecasts are being extended to periods as long as 60 hours.

Operational statistical forecasts are being made for a large number of variables as shown on the next slide. I will give the meaning of the abbreviations used.

PoP Probability of precipitation

PoFP(P) Probability of frozen precipitation

PoT Probability of thunderstorms

PoST(T) Probability of severe thunderstorms

PoPA I am not sure of this one (later determined to be probability of precipitation amount)

PoSW I think this is the probability of snow showers.

An example of the type of model predictors that have been selected in the regression equation for predicting maximum and minimum temperature is shown in the next slide. Note that both PE model and TM (trajectory model) output is used and a large number of difference variables are involved. Examples of the ten predictors used in the prediction equation for forecasts for a specific city are shown in the next slide. They include model results from both the PE and TM, surface synoptic observations (SS) and climatological or astronomical data. The predictors are ordered according to their effect on the reduction of variance for forecast error. Notice that variables from different times are used. The RV (%) refers to the reduction in variance as each predictor is added. The S.E. (°F) gives the standard error in the forecast estimates as each term is added.

The next slide shows the frequency of selection and average number of PE model predictors used in MOS forecasts for surface wind prediction.

The specific predictors and the values of the multiple regression coefficients that have been used in probability of precipitation forecasts for the Eastern part of the United States are shown in the next slide. I don't know why 12 instead of 10 predictors are shown. Notice that the variables are not continuous functions in this case. The predictor is either 1 or 0 depending on the magnitude of a specified variable. Note that the variables are averaged over a number of grid points, either 5 or 9 in this case.

Predictors and their contribution to the probability are shown for severe thunderstorm prediction and severe thunderstorm prediction in the next slides. In this case the predictors generally seem to be physically related to the predictand. This is not always so obvious in the statistical relationships.

I have shown examples of the MOS equations that have been used. These are subject to change, so I do not want to indicate that these are the equations in use today.

The paper I referred to earlier gave information on the recent formulations used for LFM MOS forecasts. For many years, the LFM MOS were considered only preliminary with the best results coming from the PE MOS forecasts. However, this paper suggests that the accuracy of the LFM MOS forecasts are now approaching those from the PE MOS.

I will now discuss the statistical forecasts for surface temperature. Operational statistical forecasts for temperature have been provided in the United States since 1965. Until 1973 these were based on the "perfect prog" approach. Since 1973 the MOS technique has been used. For many years the early guidance LFM MOS results were from 0.1 to 0.3°C less accurate than those from the final guidance PE MOS.

A new LFM MOS routine was introduced in 1978 based on the higher resolution version of the LFM. This routine provides estimates for temperature for every three hours out to 51 hours from initialization time and also maximum and minimum temperature forecasts for the days and nights extending out to two days after the initialization time or approximately 60 hours into the future.

The standard error from the maximum and minimum forecasts and the 3-hour forecasts are summarized below for the warm and cold seasons respectively.

Max-Min

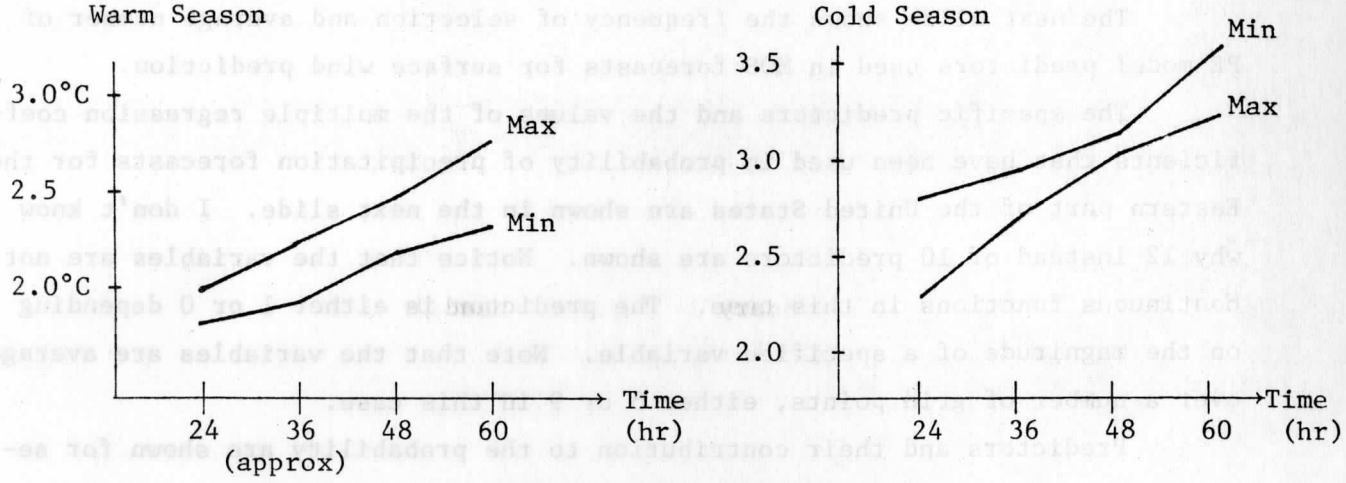

3 hour Projections

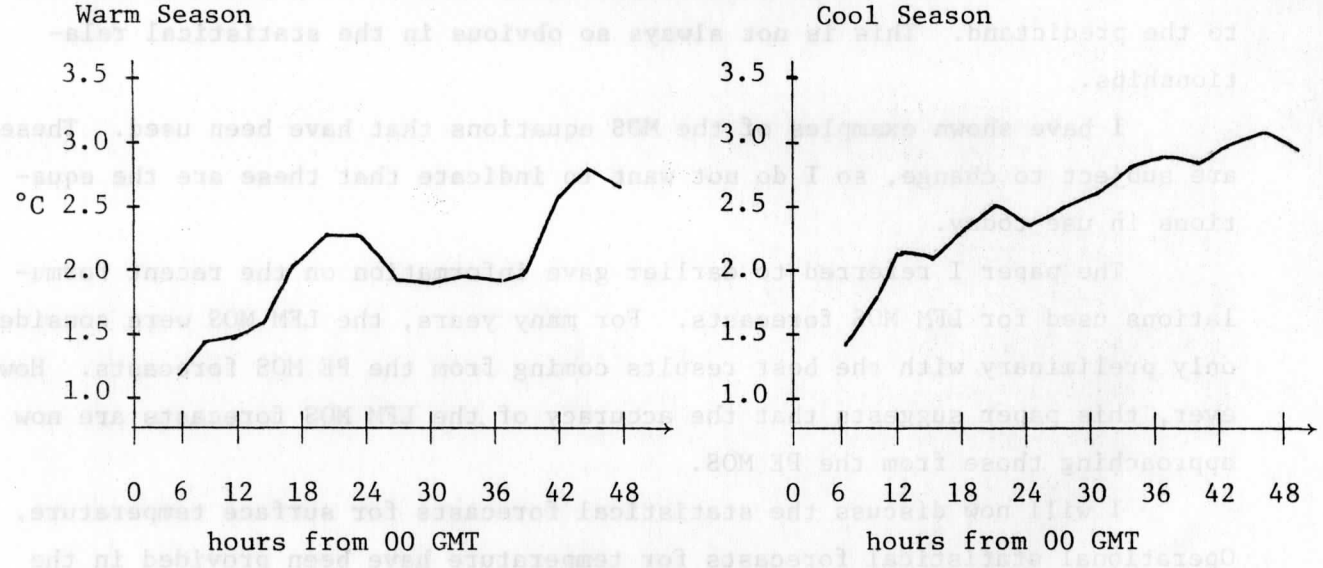

In the first two diagrams both the maximum and minimum temperatures are defined at the approximate 12 hourly intervals since forecasts are made with both the 00 GMT and 12 GMT initial time data so for instance the 24 hour period forecast can be either for a maximum or a minimum.

Just before coming to China, I obtained information on the actual equations used currently for the LFM MOS maximum and minimum temperature forecast for Madison from Dr. Wash who is teaching our synoptic laboratory course this semester. In order to make sure I have included enough specific detail in this lecture I will give the formula used for the 24 hr minimum temperature in Madison in March based on information obtained from the 12 GMT observational cycle.

Minimum temperature in °F equals

- 295.06°F
+ .19929 X Observed temp at 15 GMT in °F
+ .24314 X LFM 24 hr 850-1000 mb thickness in meters
+ .05617 X LFM 18 hr 1000 mb dew point in °K
+ .0025384 X Observed temp at 12 GMT in °F
+ .19736 X LFM 24 hr boundary layer wind speed in m s^{-1}
- 6.6256 X cosine of $(\frac{2\pi}{365}$ X day of year)
- .016093 X LFM 12 hr forecast 850-1000 mb thickness in meters
+ .041919 X LFM 12 hr mean relative humidity in the lower three layers of the model in %
+ 3.597 X (1 if snow cover at 12 GMT is less than 1 inch)
(0 if snow cover is greater than this)
+ .31159 X (1 if the cloud ceiling at 12 GMT is less than 10,000 feet)
(0 if the ceiling is greater than this)

This has a multiple correlation coefficient of .901 and a reduction in variance of .812 comparing $T_{observed}$ to $(T_{observed} - T_{forecast})$.

It is clear that statistical methods will always be an important component of the United States automated weather prediction system in order to provide local forecast information. It puts the numerical model forecast into terms that are very useful to the local weather forecaster.

This brings me to the end of my lecture series. I hope that the material has been presented in a form that was easy to understand without too many mistakes in the details. I also hope that some of the material will be of value to your specific area of work in meteorology. At least, I hope that the lecture material may help you to search out additional references to work in my country for your area of interest.

In order to complete the documentation for the lecture series, I am leaving at Nanjing University a copy of every publication of mine (except one which I forgot) that was referred to in the lectures. Some of the information was not yet published and I will not be able to leave complete reference material for it.

The most important aspect of this lecture series has been the help you have given me for the projection of slides and movies and the translation of my words into Chinese. I wish to thank the slide projectionists and the movie projector operator for their excellent service. I also want to thank the translators: Jin Han-Liang, Bao Cheng-Lan and Dang Ren-Qing for their excellent work. I know that they worked as hard as I did during this lecture series.

END